Accepted Manuscript

Journal of the Geological Society

Is plate tectonics a post-Archean phenomenon? A petrological perspective

Michael Brown, Julian A. Pearce & Tim E. Johnson

DOI: https://doi.org/10.1144/jgs2024-091

To access the most recent version of this article, please click the DOI URL in the line above. When citing this article please include the above DOI.

Received 6 May 2024
Revised 3 July 2024
Accepted 5 July 2024

Supplementary material at https://doi.org/10.6084/m9.figshare.c.7348948

Is plate tectonics a post-Archean phenomenon? A petrological perspective

Michael Brown[1*], Julian A. Pearce[2,3] and Tim E. Johnson[4]

[1] Department of Geology, University of Maryland, College Park, Maryland, 20742-4211, USA

[2] School of Earth and Environmental Sciences, Cardiff University, Cardiff, CF10 3AT, UK

[3] LODE, Natural History Museum, Cromwell Rd, South Kensington, London SW7 5BD, UK

[4] School of Earth and Planetary Sciences, Curtin University, Perth, WA 6845, Australia

ORCID: MB, 0000-0003-2187-616X; TEJ, 0000-0001-8704-4396; JAP, 0000-

*Correspondence: mbrown@umd.edu

Abstract: The petrogenesis of contemporary igneous and metamorphic rocks is commonly explained by plate tectonics, but how far back in time does this relationship hold? Here we investigate whether the distinctive petrological features of recent ocean crust, subduction-related magmatism and regional metamorphism can be unambiguously identified in the Archean geological record. From an igneous perspective based on geological relationships and Th–Nb systematics, it is difficult to claim that any Archean 'ophiolite' was part of a global plate system rather than deriving from a plume ascending through attenuating lithosphere. Furthermore, the rarity of subduction-related rocks, particularly their plutonic equivalents which have good preservation potential, is consistent with the concept of local convergence and short-lived subduction. From a metamorphic perspective, the appearance of orogenic eclogites in the Paleoproterozoic, the widespread occurrence of blueschists and ultrahigh pressure metamorphic rocks since the late Neoproterozoic, and a change from a unimodal to a bimodal distribution of metamorphic *T/P* during the Proterozoic, are responses to secular cooling and the evolution of tectonics since the Archean. Our petrological perspective is that plate tectonics analogous to that on Earth today is probably a post Archean phenomenon.

Supplementary material: Supplementary figures and tables are available at

Received

Earth today is a plate-tectonic planet, in which its outer shell, the lithosphere, is fragmented into numerous plates separated by a globally continuous network of boundaries that are the foci of magmatism, deformation and metamorphism. How and on what timescale plate tectonic behaviour emerged after the last magma ocean is unknown (Harrison 2024), with proposals ranging from the Hadean (>4.03 Ga) to the Neoproterozoic (<1 Ga) (Korenaga 2013). Earth has been cooling on average by 50–100°C/Gyr since 2–3 Ga (Labrosse and Jaupart 2007; Herzberg *et al.* 2010; Herzberg 2022), although before c. 3 Ga it is unclear whether heat loss was in balance with the remaining internal (primordial and radiogenic) heat or whether the mantle was warming to a peak at c. 3 Ga (Labrosse and Jaupart 2007; Herzberg *et al.* 2010). These uncertainties make forward modelling of geodynamics challenging and Earth's early tectonic evolution uncertain (O'Neill *et al.* 2016).

For silicate bodies in the Solar System, heat loss is mainly driven by mantle convection and is manifest at the surface (lithosphere) by one of several potential global tectonic modes (Lenardic 2018): stagnant lid, sluggish (or squishy) lid, mobile (or active) lid, and an episodic or transient mode comprising alternating behaviours. Which mode operates is largely a function of ambient mantle potential temperature (T_P; the temperature the convecting mantle would have at the surface if extrapolated along an adiabat without melting). In a sluggish lid mode operating at higher ambient mantle T_P than today, the lithosphere tends to be 'squishy' because a larger volume of melt is generated and trapped within the lithosphere during ascent (Sizova *et al.* 2015; Lourenço *et al.* 2020). Plate tectonics is an active lid mode because the lithosphere participates in convection via formation of weak plate boundaries, allowing it to sink (subduct) into the mantle. To a first order, in plate tectonics the lithosphere drags the interior and drives mantle flow (Coltice *et al.* 2019). By contrast, in a sluggish-lid mode the velocity of mantle flow exceeds that of the lithosphere and the interior drags it, although drip-like subduction associated with lithospheric mobility may occur (Foley 2018; Fuentes *et al.* 2019; Foley 2020).

As active lid, sluggish lid and episodic modes all involve subduction, evidence of subduction does not uniquely identify Earth's tectonic mode (Lenardic 2018). Estimates of ambient mantle T_P in the Archean are higher by at least 100 °C and possibly as much as 250 °C compared to today (Herzberg *et al.* 2010; Putirka 2016; Aulbach and Arndt 2019; Brown *et al.* 2022; Herzberg 2022) such that plate tectonics might not have been possible (van Hunen and van den Berg 2008; Sizova *et al.* 2010; Gerya 2014; Chowdhury *et al.* 2020). In that case, plate

tectonics evolved from some precursor tectonic mode (1981; Höink *et al.* 2013; Kankanamge and Moore 2016; Fuentes *et al.* 2019).

Earth's tectonic mode during the Precambrian is controversial because it is unknown and probably unknowable (Şengör 2001). One school argues that plate tectonics started in the Hadean (essentially since crystallization of the last magma ocean) and has probably operated continuously since (Harrison 2020; Seales and Lenardic 2020; Windley *et al.* 2021), whereas another school considers Earth's tectonic mode prior to the Proterozoic to have been different due to a higher ambient mantle T_P that precluded stable subduction (van Hunen and van den Berg 2008; Sizova *et al.* 2010; Gerya *et al.* 2021; Bédard 2024). Lastly, there is a view that plate tectonics emerged in the Paleoproterozoic, shut down during the Mesoproterozoic, then restarted in the Neoproterozoic (Stern 2020, 2023). Arguments against this last hypothesis have been presented by Spencer *et al.* (2021) and Roberts *et al.* (2022), while Sobolev and Brown (2019) and O'Neill *et al.* (2022) argued for a Mesoproterozoic slowdown rather than shutdown of plate tectonics.

Since there is a higher degree of melting at higher T_P, in the past the oceanic lithosphere would have comprised a thicker crust and a thinner underlying depleted mantle than today, and overall could have been both thinner and more buoyant (Crameri *et al.* 2019). Such a lithosphere would have been weaker and more susceptible to breakoff (van Hunen and van den Berg 2008; Sizova *et al.* 2014; Gerya *et al.* 2021), and the style of subduction could have been more like that described by Davies (1992) or thought to occur currently on Venus (Crameri *et al.* 2019; Perchuk *et al.* 2019). At present, the global variation in ambient mantle T_P may be up to ~150°C (Dalton *et al.* 2014). Thus, for a warmer ambient mantle with a similar variation in T_P, subduction could have occurred locally where mantle T_P was cooler, but a globally linked network of plate boundaries may not have been able to form (van Hunen and van den Berg 2008; Sizova *et al.* 2010; O'Neill *et al.* 2018). Consequently, subduction could have occurred at some localities on Earth since the late Hadean, but global plate tectonics may not have emerged for another 1 to 3 Ga (Bercovici and Ricard 2014; Sizova *et al.* 2015; Brown *et al.* 2020a; Dewey *et al.* 2021; Stern 2023). In this case, the precursor mode could have been sluggish lid (Fuentes *et al.* 2019) or, possibly, a stagnant lid (O'Neill *et al.* 2016), in the latter case perhaps transitioning via a mixed mode lid-and-plate regime to plate tectonics (Capitanio *et al.* 2019b). No matter the precursor tectonic mode, estimates of T_P in mantle rising as plumes from a lower hot thermal boundary

layer in the Archean are higher than ambient mantle T_P (Herzberg *et al.* 2010; Putirka 2016) and represent a complementary mechanism of heat loss that could have been more dominant on a non-plate tectonic Earth (Tomlinson and Condie 2001).

As far as we know, Earth's Hadean rock record is limited to a few 10s of square kilometres of c. 4.03 Ga gneiss at the western margin of the Slave craton (Bowring and Williams 1999; Reimink *et al.* 2016). However, zircon grains that have survived since the early Hadean (up to c. 4.4 Ga) have been used to argue for a subduction-related petrogenesis for their igneous hosts and to characterize surface conditions then (Wilde *et al.* 2001; Valley *et al.* 2002; Watson and Harrison 2005; Trail *et al.* 2017; Boehnke *et al.* 2018; Harrison 2020; Turner *et al.* 2020). Although Hadean zircons may allow us to draw conclusions about their petrogenesis, whether they are representative of the global tectonic mode operating in the Hadean is uncertain.

The characteristic geological features of plate tectonics include: large-scale rigidity of lithosphere plates, evidenced by dyke swarms; distinctive tectonic settings for sedimentation, including passive margins and foreland basins; distinctive styles of divergent and convergent plate boundary magmatism, as discussed herein; distinctive styles of subduction- and collision-related metamorphism, as discussed herein; and lithospheric mobility with differential displacement between cratons and/or terranes, as evidenced by paleomagnetic data and the supercontinent cycle (Hawkesworth *et al.* 2024). However, plate tectonics recycles most of the evidence of its past existence by subducting oceanic lithosphere, although ophiolites are interpreted as evidence of past oceans and some fragments of ocean lithosphere may be preserved as tectonic slivers in orogenic belts (Agard *et al.* 2023; Condie and Stern 2023). Our understanding of plate tectonics is based on its contemporary characteristics, and the geological features associated with plate tectonics are largely based on the past 200 Myr for which we have a largely complete oceanic record. However, ambient mantle temperature was warmer in the past, so differences with increasing age are to be expected and are seen in the geological record and in numerical models of tectonics (Sizova *et al.* 2014; Sizova *et al.* 2015; Capitanio *et al.* 2019a; Capitanio *et al.* 2019b; Holder *et al.* 2019; Brown *et al.* 2020b; Chowdhury *et al.* 2020; Dewey *et al.* 2021; Spencer *et al.* 2021; O'Neill *et al.* 2022; Gunawardana *et al.* 2024).

Here we investigate whether those distinctive petrological features of magmatism and regional metamorphism that are widely inferred to express plate tectonic processes can be unambiguously identified in the Archean geological record. From an igneous perspective, we

search for evidence for oceanic crust and volcanic arcs in the Archean rock record using comparisons with the chemical composition of younger counterparts from known plate-tectonic and plume settings. Next we compare the recent metamorphic record with that for the Precambrian, assess the development of bimodality in thermobaric ratios (*T/P*) as a characteristic feature of plate tectonics, and compare the unimodal distribution of *T/P* in the Archean with values from numerical models of geodynamics. Then we address whether the petrological archive is reliable in relation to potential biases. Based on petrology, we conclude that plate tectonics has been operating on Earth since at least the early Paleoproterozoic.

The igneous perspective

At the present day, magmatism linked to plate tectonics takes place in a range of settings: at divergent plate boundaries; at convergent plate boundaries; at 'pull-apart' sites at transform plate boundaries; and in collision zones (both syn- and post-collision). The principal way to determine whether plate tectonics analogous to today operated in the Archean has been to recognize divergent and convergent plate boundary magmatism in the crustal archive. However, this is not a simple task as the criteria used to fingerprint igneous rocks formed in present-day plate tectonic settings may not apply to an evolving Earth given the expected higher ambient mantle T_P in the Archean (Herzberg *et al.* 2010; Aulbach and Arndt 2019; Brown *et al.* 2022; Herzberg 2022). Moreover, it is not just a question of recognizing the products of potential plate margin magmatism, but also showing that they can be distinguished from the range of igneous rocks that might be generated in non-plate tectonic settings, where magmatism was likely dominated by mantle plumes (Fischer and Gerya 2016). Here, we test claims for Archean plate tectonics based mainly on the petrology and geochemistry of volcanic rocks, examining in turn evidence related to divergent margins (the 'search for Archean oceanic crust') and convergent margins (the 'search for Archean volcanic arcs').

Methodology

The methodology for identifying volcanic indicators of plate tectonics is not straightforward and is represented here in the form of a flow chart (Fig. 1). The chart highlights three routes to plate

tectonics: the first (the 'green route') leads to oceanic divergent plate margins or oceanic off-axis settings; the second (the 'red route') leads to convergent plate margins; and the third (the 'purple route') leads to intraplate basalts derived from lithosphere carrying inherited subduction signatures. The 'blue routes' lead to basalts from intraplate settings that do not require a role for plate tectonics.

Each of the divisions on the flow chart have been termed a decision point (DP) based on geochemistry and/or geology (Table 1). Geochemistry focuses primarily on the crustal proxy, Th/Nb, a well-tested plate tectonic setting discriminant, either in that form (Pearce 2008; Pearce *et al.* 2021), its reciprocal (Nb/Th: Condie 2003, 2005) or its petrogenetic equivalent (Th/Ta: (Wood 1980). In this study, Th/Nb forms the diagonal on the Th/Yb v Nb/Yb 'crustal proxy diagram' (Figs 2–5). The first level of subdivision (DP1) separates suites of mafic (basic and basic–intermediate) volcanic rocks with low-high Th/Nb from those with consistently high Th/Nb (DP1a) and those with consistently low Th/Nb (DP1b). In this context, 'high' means 95% of compositions fall within the volcanic arc basalt (VAB) array in Figs 2–5, 'low' means they fall within the oceanic basalt (OcB) array on these plots and 'low-high' means they cross the boundary between the OcB and VAB arrays. DP1a has already been used by Smithies *et al.* (2018) and Mole *et al.* (2021) in their two-fold subdivisions of Archean greenstones, and the terminology here is equivalent in concept to the 'variable v constant Th/Nb' discriminator of Smithies *et al.* (2018), but with the added incorporation of the precise 95% OcB–VAB discriminant boundary (Th/Nb = 0.15: Pearce et al., 2021). DP1b was the focus of Pearce (2008) in his 'search for Archean oceanic crust'. For both DP1a and DP1b, the high and low Th/Nb (red, purple and green) routes carry most of the potential plate tectonic indicators.

The second level of subdivision incorporates indicators other than Th/Nb geochemistry, in order to re-locate any exceptions to the first-order interpretations that (1) high Th/Nb is the route to subduction, (2) low-high Th/Nb is the route to a continental intraplate setting, commonly a plume-related large igneous province (LIP), and (3) low Th/Nb is the route to oceanic crust. For this, there are four decision points (see Table 1 for details). DP2 transfers from the subduction route to the intraplate route any high Th/Nb suites that may be inferred to be unrepresentative (crust-rich) samples of what is actually a low-high Th/Nb suite; DP3a transfers from the intraplate route to the subduction route any low-high Th/Nb suites that may be inferred to have a back-arc or forearc origin with variable subduction input and hence variable Th/Nb; 3)

DP3b transfers from the intraplate to the oceanic route any low-high Th/Nb suites that can be shown to be oceanic crust modified by metasomatism during high-temperature metamorphism; and 4) DP4 transfers from the oceanic crust route to the intraplate route any low Th/Nb suites that can be shown to have belonged to a continental intraplate setting but to have appeared oceanic due to limited crustal interaction.

The third level of subdivision deals with distinctions within the resulting 'cleaned up' three-fold (subduction, intraplate and oceanic crust) classification. Decision point DP5 on the high Th/Nb route in Fig. 1 separates the red route to active subduction from the purple route to inherited subduction. This could involve, for example, geologically distinguishing the arc setting of the former from the intraplate setting of the latter, geochemically distinguishing the mantle wedge source of the former from the lithospheric source of the latter, or isotopically identifying the significant time difference between subduction input and melting in the latter. Along the low-high Th/Nb (intraplate) route, the key third level decision point (DP6) is between plume–crust and plume–SZLM interaction, where 'plume' in this context means intraplate magma derived from upwelling mantle asthenosphere and 'SZLM' refers to sub-continental mantle lithosphere modified by subduction zone derived melts and fluids. Both plume–crust and plume–SZLM interactions have similar intraplate settings and so geological criteria are unlikely to be effective. However, on the crustal proxy diagram, the plume–crust trend typically lies between the OcB array and continental crust, while the plume–SZLM trend lies typically between the OcB array and volcanic arc compositions. However, this is not always diagnostic, requiring, for example, isotopic characterization to better distinguish continental crust and subduction end members.

It should be noted that this flow chart (Fig. 1), including the decision points, has been chosen to be as robust as possible in its applicability to the Archean. Thus, for the oceanic (green) route, higher ambient mantle T_p will increase the degree of melting, which will decrease dispersion along the OcB array. However, Th/Nb is unlikely to be affected owing to the similarity in mineral–melt partitioning between Th and Nb. Moreover, there is no indication that Th/Nb of the mantle has changed significantly with time, except perhaps in the earliest Earth as discussed later. As a consequence, the Phanerozoic OcB array should apply to all except perhaps some Eoarchean magmas. An important geological consideration is that higher ambient mantle T_P may have led Archean ridge-generated oceanic crust to resemble the crust of ridge-centric Phanerozoic oceanic plateaux in its structure, thickness (up to ~25 km; (Tetreault and Buiter

2014) and geological characteristics (Moores 2002). Higher ambient mantle T_P also likely limited the thickness of Archean oceanic lithosphere and this, combined with higher Archean mantle plume T_P, may have enabled Archean off-axis mantle plumes to start to melt well below the base of the lithosphere with potentially high degrees of melting leading to fewer OIB-like compositions and further thickening of pre-existing oceanic crust.

For the intraplate route, higher magma temperatures during the Archean might have increased the extent of plume–crust interaction, although higher magma fluxes may have created channelways with reduced access to unreacted crust. Moreover, the small difference between Phanerozoic felsic continental crust (FCC) in Figs 2 and 4 and Archean felsic continental crust (A-FCC) in Figs 3 and 5 (Rudnick and Fountain 1995) should produce similarly diagnostic trends from low to high Th/Nb. For the active subduction (red) route, it has been argued that warmer Archean slabs might have a reduced Th/Nb owing to a greater proportion of basaltic to sediment-derived melt in the subduction component (Van Hunen and Moyen 2012). However, while most subducted sediment has significantly higher Th/Nb than subducted altered oceanic crust, experimental melting of MORB-like basalts under hot (>1000 °C) subduction conditions (Rapp *et al.* 1999) still generate melts that will react with the mantle wedge to produce primitive arc magmas that plot in the VAB array. Such experiments are supported by the Phanerozoic VAB array in Fig. 4 that contains numerous arc magmas from ridge-subduction, subduction initiation and plume-proximal settings, which are believed to record zones of hot subduction. Thus, although the 95% probability tramlines for an Archean VAB array cannot be known precisely, it is likely that the Phanerozoic discriminant boundaries are a reasonable approximation.

Finally, for the plume–SZLM interaction (purple) route, there is no reason why any Archean subduction should not metasomatize mantle lithosphere in a similar way to Phanerozoic subduction, although the depth of the metasomatized 'layer' may decrease because of the shallower intersection of the lithosphere geotherm and the solidus of the invading melt. However, an important question is: when did mantle lithosphere become sufficiently stable to allow the resulting SZLM to be preserved as a mantle source reservoir? The answer does not affect the methodology, but is does mean that an absence of SZLM characteristics does not necessarily equate to an absence of subduction, with profound consequences for the oldest (c. 3 Ga) SZLM signature detected, as discussed later.

In practice, the principal questions of applicability relate less to the continuation of existing (albeit hotter) processes into the Archean, and more to the significance of non-uniformitarian processes (i.e. those restricted to the Archean) that might yield false subduction signals. We have added this possibility to the flow chart as dashed blue lines with a decision point DP7 that needs to be addressed before potential active subduction (at DP7a) or potential inherited subduction (at DP7b) can be treated as a definitive plate tectonic indicator. In reality, as non-uniformitarian processes are poorly defined, so is the decision process at DP7 (Fig. 1). Notwithstanding, we consider two main non-uniformitarian processes that might give false subduction signals: crustal delamination as an alternative to plate subduction; and relict primitive (Hadean) mantle sources as an alternative to subsequent (at least Paleoarchean to Recent) mantle sources.

Crustal delamination as a subduction alternative is primarily based on geochemical and geophysical modelling. For example, Bédard (2006) argues that delamination of lower crust following plume activity can refertilize otherwise hot, residual mantle from preceding plume events and so lower the mantle solidus and promote further melting. Johnson *et al.* (2014) use geodynamic models to argue that delamination of overthickened primary crust by Rayleigh–Taylor instabilities provides a alternative to subduction in the Archean. Identifying the potential subduction setting in question as plume-related and using a full range of isotopes and trace elements to fully define the enrichment source (for example, identification of lower crustal sources that fit delamination better than subduction components) are among the most promising approaches to demonstrate non-uniformitarian processes.

The second possibility is whether primitive mantle and magma-ocean cumulates in the mantle could act as subduction-like sources in Eoarchean settings. These materials, if predating crustal growth, can have higher Th/Nb than Phanerozoic equivalents so giving their melting products apparent (i.e. 'false') subduction signatures. The availability of these sources and involvement of minerals that can fractionate Th from Nb may, it is argued, be assisted by 'ultra-deep melting in a heat pipe Earth' (Webb *et al.* 2020; Rollinson 2022).

The search for Archean oceanic crust I: Post-Archean comparators

Background

Most studies have equated the search for oceanic crust with the identification of Archean ophiolites (Moores 2002; de Wit 2004; Kusky 2004; Kusky *et al.* 2004; Dilek and Furnes 2011; Furnes *et al.* 2014; Furnes and Dilek 2022). This has usefully furnished the community with a list of potential exposures of oceanic crust in the geologic record and for some, though by no means all (Condie and Stern 2023), has provided definitive evidence for plate tectonics through Earth history. Some of the opposing arguments are detailed and involve specific interpretations of outcrops and their structural settings. However, two more general criticisms, articulated well by Hamilton (2007), seem to be particularly important. The first is the somewhat arbitrary expansion of the original definition of ophiolite which, while having the benefit of allowing many more ocean crust outcrops to be identified, also allows at least some potential continental crustal outcrops unrelated to ocean basins to be classed as ophiolites. The second is that many interpretations of outcrops as representing oceanic crust seemingly have not considered whether non-plate tectonic interpretations also provide viable explanations. Below, we address these criticisms for the subset of ophiolites interpreted as having formed in major ocean basins unrelated to subduction.

Ophiolite complexes have long been informally described as 'oceanic lithosphere emplaced on land', a description that forms the basis for its role as a plate tectonic indicator. The formal definition remains that provided by the Penrose Field Conference participants as 'layered sequences, some 6-km thick on average, comprising deep-sea sediment overlying submarine (commonly pillowed) lavas, sheeted dykes, cumulate rocks (isotropic gabbros, cumulate gabbros and cumulate ultramafic rocks) and tectonized peridotites' (Anonymous 1972). Most diagnostic are the sheeted dykes (>95% dykes by volume, some with one-way chilled margins) and tectonized peridotite. This formal definition also allows for the fact that few on-land exposures retain an original stratigraphy and/or have all these characteristics, in which case they may be described as 'fragmentary' and/or 'incomplete' ophiolites, respectively. However, even if the ophiolite stratigraphy and/or these features are absent, this need not negate an ophiolite interpretation, as oceanic lithosphere produced in (very) slow spreading systems can lack sheeted dykes and have more complex internal structures (Cannat *et al.* 2006).

'Post-Penrose' ophiolite studies have also considered the fact that oceanic crust can form in a range of settings, many of which also have non-Penrose structures. In these cases, the

principal subdivision is into mid-ocean ridge (MORB or MOR) type and supra-subduction zone (SSZ) type (Pearce *et al.* 1984), or non-subduction and subduction type (Dilek and Furnes 2011). Both types essentially subdivide ophiolites according to whether or not the oceanic lithosphere in question relates to divergent plate boundaries (mainly mid-ocean ridges, ridge-centred oceanic plateaux, and the oceanic parts of ocean–continent transition zones) or convergent plate boundaries (mainly forearc and backarc spreading centres). In this section, we focus on MOR-type ophiolites.

As emphasised above, the search for Archean oceanic crust also has to consider the alternatives. In an Earth without plate tectonics, most igneous rocks might be expected to be part of continental Large Igneous Provinces (LIPs; (Ernst 2014), many of which are related to continental rifts. Like oceanic crust, continental LIPs typically comprise volcanic sequences, dyke and sill swarms and underlying mafic–felsic cumulate sequences. If erupted in regions of lithospheric thinning, pillow lavas can be common. Therefore, methods of distinguishing oceanic from continental magmatism are critical in the search for Archean oceanic crust. Geologically, such methods include the search for autochthonous continental basement and relict continent-derived xenoliths and xenocrysts.

In summary, past oceanic crust can potentially be identified using the following non-geochemical criteria (Kerr *et al.* 2000; Kusky 2004). (1) Formation in an oceanic setting, as identified by the absence of intercalated terrigenous sediments, autochthonous continental basement and older, inherited continental crust-derived zircons, and, if underlain by continental crust, a basal thrust fault. (2) If formed at a ridge axis, the presence of the full Penrose ophiolite sequence including a fully sheeted dyke swarm with one-way chilled dykes and the presence of mantle tectonites, or, if these features are not present, then a significant number of components of the ophiolite stratigraphy. (3) If formed in deep water (at a ridge axis or the lower part of an oceanic plateau), the presence of pillow lavas and indicators of low vesicularity, an absence of extensive pyroclastic rocks, and the presence of chert and deep-water sediments, sea-floor metamorphism and black smoker deposits. (4) If formed as part of an oceanic plateau on ocean crust basement, the absence of continental indicators as in (1), together with the absence of sheeted dykes, few interbedded sediments and pyroclastic units, predominantly submarine magmatism, and predominantly basaltic composition, although komatiites may also be present.

We focus here on putative Precambrian ophiolite localities. Moores (2002) compiled the original list of pre-Rodinian 'ophiolites and possible ophiolites' based on stratigraphy, rock type and, to a lesser extent, composition, noting that they cluster in age at 1.0–1.5 Ga, 1.8–2.3 Ga, 2.5–2.7 Ga and c. 3.4 Ga. Nine of those listed by Moores (2002) are Archean in age, at: Dongwanzi, China (c. 2.5 Ga); Wind River, Wyoming (c. 2.6 Ga); Kalgoorlie and Norseman, Australia (c. 2.7 Ga); Cameron–Beaulieu, Yellowknife and the Point Lake in the Slave Province, Canada (c. 2.7 Ga); and the Jamestown and Pietersberg complexes, South Africa (c. 3.4–3.5 Ga).

Detailed descriptions of many of the proposed Precambrian ophiolites and a synopsis in the volume on 'Precambrian Ophiolites and Related Rocks' (Kusky 2004) laid out the evidence for and against each being a fragment of ancient oceanic crust. In the same volume, de Wit (2004) made a list of Archean ophiolites, largely matching that of Moores (2002), but also making the case for preservation of oceanic crust in mélanges such as those reported from the East Pilbara Terrane and Isua Supracrustal Belt (Komiya *et al.* 1999; Komiya *et al.* 2004). In examining "four billion years of ophiolites", Furnes *et al.* (2014) expanded the list of potential Archean ophiolites to include, for example, the c. 2.7 Ga Wawa sub-province in the southern Superior Province, concluding that "half the Archean greenstones originated as oceanic crust". All potential outcrops of non-subduction type oceanic crust, which form a significant thread of the argument in favour of plate tectonics on the early Earth, are evaluated in the upcoming text by attempting to follow the 'green' routes to oceanic crust in Fig. 1, either via decision points DP1b and DP4 or, if metasomatized at high temperature, via DP1b and DP3b.

Phanerozoic comparators

Before carrying out the search for potential Archean oceanic crust, we examine the dispersion of Phanerozoic analogues on the Th/Yb–Nb/Yb diagram (the crustal proxy projection) to facilitate interpretations. For the purpose of finding plate tectonic indicators, we define oceanic crust in its broad sense to include both the crust formed at ocean ridges and any off-axis edifices and intrusions subsequently built on and within it. In this context, ocean crust is made up of three tectonically defined magma types: mid-ocean ridge basalts (MORB), oceanic plateau basalts (OPB) and ocean island basalts (OIB). Each can be subdivided according to source depletion into D (depleted), N (normal) and E (enriched) and into tholeiitic (th) and alkalic (alk). The Th/Yb–

Nb/Yb crustal proxy projection based on the combination of all these magma types from the known plate tectonic (Phanerozoic) Earth is shown in Fig. 2a, on which the 95% probability density limits of the combined MORB–OIB–OPB data give the boundaries of the resulting oceanic basalt (here labelled 'OcB') array (see Pearce *et al.* (2021) for the data points). Averages of some of the main oceanic magma types plotted within the OcB array are plotted to highlight the along-array variability and the key fact that their Th/Nb ratios (the diagonal on this projection) are all broadly similar. An exception, not relevant here, is a subset of alkali basalts with EMII enriched sources that define a separate EM–OIB field at the upper edge of the OcB array.

The boundaries of the volcanic arc basalt (VAB) array are also based on 95% probability density limits, in this case based on the combination of oceanic and continental arc rocks of mafic (basic and basic-intermediate) compositions. Coincidentally, its lower boundary is almost the same as the upper boundary of the OcB array and so this also defines the discriminant boundary. However, the VAB array is not restricted to volcanic arcs, as Th/Nb is a crustal proxy rather than just a subduction proxy. Thus, it also contains the vast majority of continental crust compositions (felsic continental crust (FCC) has been plotted in Fig 2a) and therefore also mafic volcanic rocks from other settings with a clearly detectable crustal input or with a subduction-metasomatized lithospheric mantle (SZLM) source. On this basis, we expect any oceanic crust formed at a major divergent plate boundary, or off-axis within the resulting oceanic basin, to plot between the 95% probability OcB tramlines on the crustal proxy projection, and this is the main potential oceanic crust-based plate tectonic indicator. The projection in its older form (Pearce 2008) has already been used for this purpose (Dilek and Furnes 2011; Furnes *et al.* 2014).

However, as already emphasised, the crustal proxy projection only provides a geochemical indicator that is *consistent with* an oceanic crust origin. To be definitive, their composition must be distinguished from their possible alternatives, primarily compositions from continental intraplate LIPs. As Fig. 2b shows (see Pearce *et al*. 2021 for data points), a significant part (almost 50%) of the continental LIP basalt field lies within the OcB array, with the remainder occupying the VAB array by virtue of have been derived from, or contaminated by, subduction-metasomatized lithospheric mantle (SZLM) and/or continental crust. Many of these continental LIPs in the OcB array can be distinguished from oceanic LIPs and other oceanic basalts based on data dispersion, the continental LIPs typically having a component of variation

from the OcB array to continental crust. Nonetheless, a small number of continental LIPs do form trends entirely within the OcB array. It is these suites that can be most easily mistaken for oceanic basalts.

Fig. 2c gives some examples of Phanerozoic oceanic plateau basalts that might be considered the most useful comparators with proposed Archean oceanic crust. The key feature of oceanic basalts is that they lie almost entirely within the OcB array tramlines. Variations along the OcB array are mainly a function of mantle enrichment and depletion coupled with degree of melting if in the garnet facies. Oceanic plateaux such as those from the Colombia–Caribbean LIP (CLIP) (Kerr *et al.* 1997) and the various components of the Greater Ontong–Java plateau (OJP) (Tejada *et al.* 1996; Tejada *et al.* 2013; Golowin *et al.* 2017; Golowin *et al.* 2018) experience the greatest variations, which can be summarized as: (1) most mafic lavas from oceanic plateaux cluster close to the average OPB composition and reflect broadly similar plume compositions that underwent a high degree of melting; (2) depleted sources are not uncommon and lead to a separate cluster around the D-OPB composition, which here includes the well-known Gorgona komatiites from the CLIP; (3) a subset of data typically plots towards enriched compositions as a result of local mantle enrichments and/or lower degrees of melting; and (4) mantle heterogeneity can cause compositions to plot near the top (and base) of the array, as in the case of the main Mahihiki EM-rich sourced basalts in Fig. 2c.

The difficulty in distinguishing between the oceanic crust plate tectonic indicator and continental plume-derived magmas with no plate tectonic connotations is highlighted in Fig. 2d. The contrast between the two options is best seen in the typical example of a transition from continental to oceanic plume magmatism in the North Atlantic Igneous Province (NAIP) (Fitton *et al.* 2000). Here, the pre-rifting stage, where plume-derived magmas penetrate and erupt over thick continental lithosphere, gives rise to trends extending from the OcB array towards continental crust compositions and hence well into the VAB array. With continuing lithospheric extension, which here includes the main East Greenland dyke swarm (Hanghøj *et al.* 2003) and their offshore equivalents (Fitton *et al.* 2000), a higher proportion of compositions plot in the OcB array and hence fewer reach the VAB array. Compared to the oceanic plateau basalts, represented here by Iceland (Kokfelt *et al.* 2006), the continental basalts plotting in the OcB array do have a discernible crustal input represented by increased Th/Nb. However, that input is minor and only seen because both types of composition are available for comparison. It is thus

likely that the large volumes of magma that rapidly traverse highly attenuated continental lithosphere experience limited interaction and hence a limited increase in Th/Nb. Moreover, as already noted, such localities may have some ophiolite characteristics such as pillow lavas, abundant dykes, and basic intrusions. Thus, continental rifts that experienced considerable extension and magma flux, but which never extended sufficiently to form true oceanic crust, can be misidentified as oceanic plate tectonic indicators without careful integration of geochemical and geological criteria. Making this distinction is represented in the flow chart by decision point DP4.

How the cluster of NAIP (and other continental LIP) data can be explained by a combination of two components is summarized in Fig. 2e. The first component, the plume-derived endmember, lies along the OcB array at a point defined in particular by the degree of melting and degree of source depletion or enrichment. The second component, the continental crust contaminant (here represented by average felsic continental crust; FCC), typically lies in the upper right part of the VAB array. The interaction between the two endmembers is defined here by assimilation and fractional crystallization (AFC) trends that simulate the observed 'plume–crust' trends. The compositions of the endmembers and the relative rates, r, of assimilation to fractional crystallization (based on the equations of DePaolo (1981) are most influential in defining the AFC trend. The degree of fractional crystallization, F, determines the degree of displacement from the plume endmember composition. The trends shown in Fig. 2e are based on $r = 0.3$. Other forms of interaction, such as direct mixing of mafic and felsic magmas and migration of evolving magmas through crustal hot zones, give alternative (but not greatly dissimilar) pathways between intraplate magma and crust.

An important caveat in the search for oceanic crust, especially for Archean rocks, is the effect of high temperature (upper amphibolite or granulite facies) metasomatism, which can give misleading interpretations of basalts (Fig. 2f). This process is easy to recognise as it is characterised by significant variations in Th/Nb on length-scales that are much shorter than those expected, for example within single lava units. In the absence of external fluids, the amphibolite to granulite facies transformation typically leads to significant loss of Th due to loss of supercritical fluids and melt. The liberated fluids and melts can infiltrate and react with rocks along their fluid pathways, commonly leading to Th-rich metasomatism and an increase in Th/Nb. Fig. 2f focuses on the Catalina schist on Catalina Island in Southern California and the

Shuksan metamorphic suite in the North Cascades (Sorensen and Grossman 1989; Sorensen and Grossman 1993). Both represent Jurassic MORB metamorphosed to amphibolite facies during accretion under hot (subduction initiation) conditions. In both cases, the compositions are displaced to variably higher Th/Nb that, without other information, might misleadingly imply a continental intraplate setting and the misidentification of rocks that actually are oceanic plate tectonic indicators. However, the similar trend followed in Fig. 2f by the non-oceanic, eclogite–amphibolite facies continental margin metabasalt sills from the Chinese CCSD borehole in the Sulu UHP belt (Xiao *et al.* 2011), Yang and Pearce, unpublished) demonstrates that low-high Th/Nb amphibolites that have undergone metasomatism cannot be assigned an oceanic crust setting without more detailed investigations.

Palaeoproterozoic comparators

In Fig. 3a, we plot three well-documented Paleoproterozoic ophiolites, which are the oldest non-subduction ophiolite types described as having clear geological and geochemical indicators of an oceanic provenance. At 2 Ga, the Purtuniq ophiolite, from the Cape Smith fold belt in Northern Quebec, is arguably the oldest ophiolite to have all the crustal members of the Penrose ophiolite sequence, including a sheeted dyke complex, although no mantle tectonite has been found (Scott *et al.* 1991; Scott *et al.* 1992; Scott *et al.* 1999). In Fig. 3a, the lavas and dykes plot in the OcB array and are closer to E-MORB than N-MORB, which might also be due to a plume-proximal oceanic setting.

Jormua was chosen as a type-example of a ‘continental margin ophiolite’ by both Dilek and Furnes (2014) and Pearce (2014) based on geological reconstructions and its OIB to E-MORB geochemistry (Peltonen *et al.* 1996). In detail, the Jormua ophiolite is typical of ocean–continent transition zones such as the present Iberian margin, with some of the terrane having continental characteristics (inherited Archean zircons and exhumed continental lithosphere) and some having the full Penrose ophiolite sequence, including both the sheeted dykes plotted here and mantle tectonites (Peltonen *et al.* 2003; Finlayson *et al.* 2023). In Fig. 3a, the ophiolite basalt data plot in the OcB array despite the proximity to a continent and are more similar to E-MORB than N-MORB, which (as noted earlier) is characteristic of incipient ocean formation.

The third example is a set of lavas from the Amisk Collage (an accretionary complex) in the Flin Flon Belt, Canada, described as having N-MORB, E-MORB and OIB characteristics and interpreted as oceanic crust (Stern *et al.* 1995; Babechuk and Kamber 2011). After filtering out the recognized effects of Th- and Nb-metasomatism, these characteristics are confirmed by the dispersion of data within the OcB array from E-MORB and tholeiitic OIB to D-OPB in Fig. 3a. As seen in Figs 2c and 2d, data dispersion of this type is typical of Phanerozoic oceanic plateaux such as the Ontong–Java Plateau (Golowin *et al.* 2017) and Iceland, where mantle plume melting within the garnet facies coupled with complex mantle flow give mantle depletions and enrichments that can lead to a wide range of Nb/Yb ratios.

These studies are important from an igneous perspective and in the context of the theme of this paper as they show that, by 2 Ga, oceanic crust compositionally similar to that formed at the present day was being formed during the plate tectonic 'Wilson Cycle' period of ocean opening and closing that led to the first major supercontinent (Nuna/Columbia). Between this time and the Archean (2.5 Ga), evidence for oceanic crust is more ambiguous and controversial, such that the search for subduction might be more definitive.

The search for Archean oceanic crust II: Results

We present the results of our search for Archean oceanic crust in four parts: (1) proposed cases of Archean greenstones described as non-subduction type ophiolites but which classify as continental intraplate basalts based on decision point DP1b in Fig. 1; (2) proposed examples of Archean 'MORB-OIB' and 'ophiolitic' complexes that could be interpreted in several other ways based on Fig. 1; (3) examples of mafic volcanic rocks affected by high-temperature metamorphism used to support Archean plate tectonics, but where metasomatism may have masked the true interpretation; and (4) proposed examples of Archean oceanic crust that satisfy the low Th/Nb criterion (at decision point DP1b) but then need further assessment (at DP4) to determine whether they are truly oceanic.

Archean 'ophiolites' as attenuated continental crust

The Yellowknife greenstone belt (Southern Slave Province, Canada) is potentially the most significant of the proposed ophiolites as the lowermost (Kam) formation contains the only example of sheeted dykes reported from Archean greenstones (Baragar 1966; Helmstaedt *et al.* 1986). In Fig. 3b, the lower Kam lavas from this belt plot on OcB-FCC trends, placing them clearly on a low-high Th/Nb, non-oceanic, trajectory at DP1b. An oceanic crust interpretation was similarly rejected by Bickle *et al.* (1994), who pointed out that the 'sheeted dyke swarm' was described as 'closely spaced dykes with interspersed pillowed and massive basalts', which is different from the 95% cross-cutting dykes with one-way chilled margins characteristic of 'Penrose ophiolites'. Moreover, the dykes are not rooted in underlying gabbros as in 'Penrose ophiolites', but instead appear to intrude underlying continental basement. These authors also emphasized evidence for xenocrystic zircons in felsites from the same formation. The counter argument, advanced by Corcoran *et al.* (2004), is that the lower boundary is tectonic and that the greenstones were part of an oceanic plateau that was thrust over the basement. However, Northrup *et al.* (1999) questioned this hypothesis by showing that the dykes cutting the gneissic basement were contemporaneous with the 'sheeted dykes', an observation consistent with their continental intraplate interpretation based on Nd isotopes. Therefore, the Yellowknife 'ophiolite' has a very high probability of having formed as a LIP focused on attenuated continental crust, as deduced by Cousens (2000).

Several other Neoarchean greenstones, albeit without sheeted dykes, have been listed as examples of possible or probable fragments of accreted oceanic crust, but similarly plot on low-high Th/Nb trends towards continental crust in Fig. 3b which, when combined with geological criteria such as those of (Bickle *et al.* 1994), lead to a continental intraplate setting based on Fig. 1. This group includes other parts of the Slave craton (Corcoran 2001) as well as greenstones elsewhere that have also appeared on ophiolite lists, such as the c. 2.7 Ga Belingwe greenstones from the Zimbabwe craton (Shimizu *et al.* 2005), the c. 2.7 Ga Norseman and Kambalda greenstones from the Yilgarn craton (Said *et al.* 2010; Said *et al.* 2012), and the c. 3.47 Ga lower Onverwacht volcanics in the Kaapvaal craton (Robin-Popieul *et al.* 2012). Notably, like Yellowknife, the Belingwe greenstones have a well-defined autochthonous granitic basement (Bickle *et al.* 1994) with lavas containing continental xenoliths (Shimizu *et al.* 2004), while Norseman and Kambalda greenstones have intercalated terrigenous sediments (Said *et al.* 2012).

Archean 'MORB–OIB-bearing' mélanges misinterpreted as oceanic crust

Mélanges interpreted as chaotic fragments of oceanic crust (and mantle) accreted during subduction have also been used as evidence for plate tectonics (Kusky *et al.* 2020). If the fragments are restricted to volcanic upper crust with MORB–OIB characteristics, they are commonly termed 'MORB–OIB' mélanges. If they also contain sufficient members of the Penrose ophiolite stratigraphy, they are commonly termed 'ophiolitic mélanges'. Here we evaluate the three examples that make up the most detailed claims for demonstrating Archean plate tectonics from the Mesoarchean to Eoarchean: Cleaverville (c. 3.1 Ga) and North Pole (c. 3.5 Ga) from the East Pilbara Terrane; and Isua, SW Greenland (c. 3.8–3.7 Ga).

The Cleaverville greenstones in the West Pilbara Terrane (part of the Regal Formation; (Sun and Hickman 1999) have been interpreted by Ohta *et al.* (1996) as an accretionary mélange comprising intercalated sediment and pillow lavas, with the lava compositions described as 'A-MORB' (Archean MORB). However, the crustal proxy diagram (Fig. 3b) shows the compositions to lie just above the OcB array due to their relatively high Th/Nb ratios, a point made by Sun and Hickman (1999). On the flow chart in Fig. 1, these follow a poorly defined low-high Th/Nb route. A back arc basin origin was an option but, at decision point DP3a, inter-lava sedimentation did not support an oceanic crust origin (Kiyokawa *et al.* 2019), making plume–crust interaction the more probable explanation. In any case, there is little to support the 'MORB–OIB' interpretation.

The 'MORB–OIB mélange' from the North Pole region of the East Pilbara craton has been identified and mapped in detail by Komiya *et al.* (2002) who provided significant data in support of their interpretation, later augmented by additional trace element analyses (Nakamura *et al.* 2020). However, the GSWA (Geological Survey of Western Australia) mapped and sampled the whole Northern Pilbara craton and concluded that the various greenstones (including the c. 3.5 Ga terrane mapped by Komiya et al (*op. cit*.) were not part of an accreted mélange but were volcanic formations successively erupted onto a continental basement (Hickman 2016) to create a long-lived volcanic plateau (Van Kranendonk *et al.* 2015), an interpretation supported by the common presence of inherited zircons and crustal enclaves. Unfortunately, the ICP-MS data in Komiya *et al.* (2002) suffers from incomplete dissolution in sample preparation, so we have matched the units they sampled with equivalent units (North Star Basalt and Mt Ada Basalt) in

the GSWA dataset (Smithies *et al.* 2007) for the Th/Yb–Nb/Yb projection (Fig. 3c). This low-high Th trend from the OPB endmember in the OcB array does not support an oceanic crust origin, instead favouring plume–crust interaction in a continental setting (cf. Fig. 2b), the preferred interpretation of Smithies *et al.* (2005b).

The 'MORB–OIB mélange' from the Isua Supracrustal Belt is similarly controversial, unsurprisingly given its tectonic complexity. Komiya (1995) and Komiya *et al.* (2004) claimed that their age and geochemistry defined them as "the oldest MORB and OIB in the world". However, this description is confusing because the MORB and OIB assignments do not match present-day classifications. Specifically, the 'OIB' lacks the high Nb/Yb (residual garnet) characteristic of present-day OIB and (if oceanic) best resembles present-day OPB (cf. Fig. 2a). In addition, the 'MORB' has very low Nb/Yb indicative of a mantle source depleted in residual garnet, and hence not typical of a mid-ocean ridge setting. They also exhibit a small but significant enrichment in Th that causes the data to plot in the lower left-hand part of the VAB field. Following the flow chart, the sample set classifies as 'high' Th/Nb, following the 'red route' to subduction and so will be re-examined in the next section. Thus, while it is true that Isua compositions are potentially significant in terms of plate tectonics, there is no clear evidence for the proposed MORB–OIB bimodality.

Proposed Archean ocean crust masked by high-temperature metamorphism

Using the simple but effective criterion of significant, small length-scale Th/Nb variations (Table 1), it is evident that many amphibolite-facies volcanic rocks of Archean age have experienced Th enrichment or depletion relative to Nb during metamorphism, which can likely be ascribed to interaction with Th-rich supercritical fluids or melts. Figures 3d, e gives examples of outcrops cited as representing Archean oceanic crust from (i) the end of the Archean (North China Craton, 2.6–2.5 Ga) and (ii) the beginning of the Archean (SW Greenland and Northern Canada, c. 3.8–3.7 Ga), all of which emphasise the need to test for mobility of so-called immobile elements before interpreting Archean amphibolites.

The Wutaishan and East Hebei amphibolites from the North China craton have been used by a number of authors to infer the presence of oceanic crust and hence plate tectonics towards the end of the Archean (2.6–2.5 Ga), despite Th/Nb exhibiting short length-scale variations

indicative of metasomatic Th enrichment. For Wutaishan, Wang *et al.* (2004) subdivided amphibolites from the Wutai complex into MORB-like, island arc tholeiite (IAT)-like and adakitic. As Fig. 3d shows, the classification fits the geochemistry in the sense that data plotting in the OcB array classify as MORB, whereas those plotting above it (in the VAB array) could classify as island arc tholeiite (IAT). However, in the absence of stratigraphic control, this is only one interpretation (Option 1). If all the data are treated instead as a single group, two further interpretations are possible. In Option 2, the amphibolites are all MORB but experienced variable metasomatism and hence variable Th enrichment (as in the accreted Jurassic MORB in Fig. 2f). In Option 3, the amphibolites underwent variable metasomatism combined with pre-existing magma–crust interaction (as in the Sulu Belt continental rift amphibolites in Fig. 2f). Options 1 and 2 favour plate tectonics whereas Option 3 does not. Moreover, if the plate tectonic interpretation is correct, Option 1 provides evidence for both MORB and arc (divergent and convergent margin) magmatism, while Option 2 favours MORB (divergent margin) only.

The same problems arise from the work of Ning *et al.* (2022) on amphibolites from two other complexes of similar age from East Hebei: the Zunhua ophiolitic melange and the Shangyin MORB–OIB-type mélange. They also form OcB–VAB trends (some Shangyin gabbro samples also showing some scatter best explained by cumulation), which could be explained in these three different ways. In the flow chart (Fig. 1), these samples follow low-high Th/Nb route to decision point DP3, whereby they can potentially sub-divide into 'oceanic crust' (at DP3b), 'SSZ oceanic crust' (at DP3a) or continue along the intraplate route to plume-lithosphere interaction. However, at present, there is insufficient information to make this decision. Thus, a more sophisticated interpretation and sample selection is needed to ascertain whether these really are plate tectonic indicators.

Eoarchean (c. 3.8–3.7 Ga) amphibolites from Isua (SW Greenland) and Nuvvuagittuq (northern Quebec) provide other well studied examples of metasomatized amphibolites, in this case representative of some of the Earth's oldest volcanic rocks. In particular, Frei *et al.* (2002) and Polat and Hofmann (2003) demonstrated Th mobility relative to Nb during metamorphism of amphibolite facies submarine lavas from Isua. Their data (plotted in Fig. 3e) form a similar trend to the Phanerozoic amphibolites in Fig. 2e and Wutaishan amphibolites in Fig. 3d and face the same ambiguities. For Nuvvuagittuq, O'Neil *et al.* (2011) and Turner *et al.* (2014) identified three lava units, and interpreted the lower two ('high-Ti' and 'unenriched low-Ti') as potential

subduction initiation MORB-like and boninite-like oceanic crust related to subduction initiation; these precede an upper unit interpreted as arc-derived as discussed later. However, short length-scale variations make it clear that Th has been mobilized, thus complicating evidence for the true tectonic setting. In Fig. 3, their trends resemble those of Isua (Fig. 3e), the North China Craton (Fig. 3d) and Phanerozoic accreted amphibolites (Fig. 2f), with further work needed to confirm or reject a plate tectonic origin.

Archean greenstones most similar to oceanic crust

Of the many proposed examples of Archean oceanic crust, only a small subset satisfies even the first criterion of the flowchart in Fig. 1, that of low and constant Th/Nb at decision point DP1b. This subset is plotted in Fig. 3f. However, to be considered true oceanic crust and therefore potential plate tectonic indicators, they also need to 'pass' decision point DP4, which is based on criteria needed to distinguish oceanic crust basement from highly attenuated continental crust.

The c. 2.7 Ga Superior Province greenstone belts located in the southern Superior craton provide some of the most convincing claims for having formed in an oceanic Archean plate tectonic setting. In particular, a significant body of work (Fan and Kerrich 1997; Kerrich *et al.* 1999; Polat and Kerrich 2000; Polat 2009) has been used to argue that the Wawa sub-province is fully oceanic and made up of two parts, an older part best explained as oceanic crust and a younger part best explained as an (oceanic) island arc and back-arc basin (discussed in the next section). In their model, the Tisdale group represents an oceanic plateau and ocean islands and the Schreiber–Hemlo group is an accretionary complex containing komatiites and tholeiites of oceanic crust provenance.

Unlike the greenstones described in the previous sections, there has been less controversy over these interpretations, and even Bédard and Harris (2014), who favour a different overall tectonic model driven by mantle flow rather than plate tectonics, treat these Superior Province greenstones as oceanic-like tracts between separating cratonic fragments. However, although Kerrich *et al.* (1999) considered that there is no evidence for continental crust associated with these greenstones (Thurston 2002), the geochemical test is much less clearcut (Fig. 3f). The data for the 'plateau' units plot within the OcB array but with a greater scatter to high Th/Nb values than is normal for oceanic crust. Thus, the Th/Nb geochemistry is a better match for, say, the East

Greenland continental margin than Iceland in Fig. 2d. This could also be explained by analytical variance, especially as Th concentrations are low, but the reported data quality makes this interpretation unlikely. Moreover, subsequent work by Ayer *et al.* (2002) and Thurston (2002) supported an autochtonous continental basement for rocks of this age based on the presence of zircon xenocrysts and other geochemical indicators. On this basis, the route to oceanic crust in Fig. 1 would fail to pass decision point DP4 and eventually be assigned a continental intraplate setting.

More detailed investigation of the full range of sub-provinces in the SE Superior craton (including Th/Yb–Nb/Yb plots for each) has been made by Mole *et al.* (2019), whose interpretation of a continental rift system driven by plume magmatism prior to c. 2.7 Ga matches previous work better than an oceanic basin. Of course, this does not negate the possibility that oceanic crust had formed but was not preserved, and so it need not negate the tectonic model of craton breakup and re-assembly as proposed, for example, for the Wawa subprovince (Polat 2009) and the Wabigoon superterrane (Bjorkman *et al.* 2024).

The c. 2.8 Ga Kostomuksa and c. 2.9 Ga Sumozero–Kenozero greenstone belts in the NW and SE Baltic Shield (Puchtel *et al.* 1998; Puchtel *et al.* 1999) have been interpreted as having lower units with oceanic plateau characteristics and have been cited by Kerr *et al.* (2000) and others as examples of Archean oceanic plateaux. Specifically, Kostomuksa has been interpreted by Puchtel and co-workers as a partially accreted oceanic plateau, and Sumozero–Kenozero as a partially accreted plateau subsequently overlain by arc-like upper units. They report a lack of field evidence for continental basement and a lack of geochemical features such as low εNd that are typically associated with interaction with continental lithosphere. Moreover, the compositions plot entirely, and uncommonly, fully within the OcB array on the crustal proxy projection (Fig. 3f). Despite a 100 Ma age difference, the two Baltic Shield greenstones have a narrow data dispersion near present day average OPB with no clear vector towards continental crust. Of all the proposed examples of Archean oceanic crust, they are the most convincing, as demonstrated by a comparison between Fig. 3f and Figs 2c, d. The principal caveat is that key supporting studies, such as a search for inherited zircons, have yet to be carried out.

The c. 3.3 Ga Kromberg mafic–ultramafic sequence in the Barberton Mountain Belt was claimed to represent accreted oceanic crust based on evidence from structures (an allochthonous interpretation), geology (an absence of inherited zircons) and geochemistry (juvenile εNd and

oceanic Th/Nb ratios) (Grosch and Slama 2017). These authors also used the Th/Nb–Nb/Yb projection to demonstrate the similarity between the Kromberg sequence and the Abitibi/Wawa and Somozero greenstones, a feature also evident in Fig. 3f. In detail, however, Th/Nb is still somewhat higher than expected for oceanic crust, which was attributed to a primordial (higher Th/Nb) mantle source. However, this seems unlikely as both older and younger parts of the Barberton greenstone belt include lavas with normal mantle sources (Fig. 3b). Thus, although the decision at DP4 in Fig.1 is not definitive, a continental intraplate setting would seem more likely.

The search for Archean volcanic arcs I: comparators

Background

As with the 'search for oceanic crust', there have been many attempts to identify subduction-related igneous rocks in the Archean and to use these as evidence for plate tectonics. These studies have also proved controversial with interpretations ranging from pan-Archean arc magmatism (Polat and Kerrich 2006; Sotiriou *et al.* 2022), through intermittent periods of arc magmatism (Van Hunen and Moyen 2012) to an absence of arc magmatism (e.g. the "snArc" of Bedard *et al.* (2013)). As with the previous section, the aim here is to make an independent assessment based on geochemical proxies, notably Th/Nb, which (as already discussed) is one of the most robust in circumventing the likely temporal global variations in heat flow and continental crustal inputs.

Volcanic arc rocks may be defined as those derived from magmas generated above zones of active subduction of oceanic crust. One obvious problem in interpreting past subduction-related magmas is that present day studies have revealed they can be highly variable within and between arcs (Schmidt and Jagoutz 2017). Two principal variables are the nature of the lithospheric basement (oceanic or continental) and the geodynamic status of the subduction system. For the former, continental arcs are typically marked by less partial melting, less mantle depletion, and greater interactions between magmas and lithosphere (SCLM and crust) compared with oceanic arcs. For the latter, geochemical compositions change during the evolution of single arcs, from subduction initiation through a period of steady-state subduction interspersed by

transient events such as ridge subduction and flat subduction, and ending with continental subduction in their final (syn-collisional) stage.

Volcanic arc magmas that erupt at the present day principally follow the basalt–andesite–dacite–rhyolite (BADR) sequence with basalts dominating oceanic arcs and andesites dominating continental arcs (Gill 2012). They can also be subdivided according to potassium content (at a given silica value) into a (low-K) tholeiitic series, calc-alkaline series and high-K calc-alkaline series (Peccerillo and Taylor 1976) — or, more rigourusly, into separate classifications based on K-content (high-, medium- and low-K) and iron enrichment (tholeiitic and calc-alkaline or low-, medium- and high-Fe) (Arculus 2003), where low-K and high-Fe characterize the majority of oceanic arcs, whereas medium- to high-K and medium- to low-Fe characterize the majority of continental arcs (Garcia 1978). Ultrahigh K magmas (shoshonitic series and lamproites) are also significant as indicators of particularly high slab fluxes into the mantle wedge or of highly metasomatized SCLM, as, for example, in continent–arc collisions, rear-arc settings and areas of slab-failure (Morrison 1980). Adakite-related volcanic rocks with their definitive high Sr/Y (Defant and Drummond 1990; Castillo 2012) have been found to characterise specific volcanic arc settings such as ridge subduction, flat subduction and slab edges.

Despite this wide variation in volcanic arc magma types, some geochemical features are characteristic of virtually all subduction zones. These include the element inputs and fractionations that take place in subduction zones to create high ratios of the more subduction-mobile large ion lithophile elements (LILEs) relative to the less subduction-mobile high field strength elements (HFSEs) which are evident in such features as high Th/Nb (the main subject of this study), negative HFSE anomalies on MORB-normalised plots and the decoupling of isotope values such as εNd and εHf. Also ubiquitously important are the consequences of added subduction fluids that include the high oxygen fugacities that influence the behaviour of redox-sensitive elements such as V during melting, so leading to distinctive Ti/V (Shervais 1982), as well as the sequence of phase appearance related to factors such as melt depolymerization and the enhanced role of hornblende crystallization. Geological criteria are also an integral part of the search for subduction. Criteria used for volcanic arcs (Garcia 1978) include: compositional peaks of basic to basic-intermediate rocks if oceanic but andesitic if continental; abundant andesitic pyroclastic rocks; highly vesicular lavas for their composition and (if oceanic) assumed depth of

eruption; abundant volcanogenic clastic sediments; associated underlying plutons including batholiths if sufficiently long-lived; and porphyry-type ore deposits.

However, as in the search for oceanic crust, any significant deficiency in the correct recognition of plate tectonics via subduction-related magmatism in the Archean may lie less with the identification of potential subduction signatures in the igneous rocks and more with whether the same signatures can also be created in a plume-dominated Earth without plate tectonics. The methodology here with its focus on the Th/Nb crustal proxy is the same as that used to search for oceanic crust, but is now applied to the search for volcanic arcs and related subduction indicators which require finding volcanic suites that follow the 'red and purple' routes on Fig. 1. As before, we first examine comparator examples from the consensus plate tectonic Earth (the Phaneozoic), then find, as another comparator, the oldest consensus volcanic arc system, before finally carrying out the search for Archean volcanic arcs based on existing lists of potential Archean volcanic arcs, notably that of Polat and Kerrich (2006).

Phanerozoic comparators

The Th/Yb v Nb/Yb plot for oceanic basalts in Fig. 2a is duplicated in Fig 4a but with more information on the compositions of mafic volcanic arc lavas (basalts and basaltic andesites) in the VAB array. The dashed fields distinguish the broad areas occupied by oceanic (Oc-VAB) and continental (Cont-VAB) compositions (see Pearce 2021 for data points) and the red squares give the average compositions. The distinctive difference is that, overall, Cont-VAB have higher Nb/Yb than Oc-VAB at similar Th/Nb, which can be attributed in part to less depleted (higher Nb) mantle sources in continental settings, and in part to a suite of other factors that include more terrigenous sediments undergoing subduction, more continental crust to assimilate and lower degrees of deeper melting. Note, however, that these fields apply only to subduction of oceanic lithosphere, as even Oc-VAB can have high Nb/Yb once continental lithosphere is subducted in a syn-collision environment.

Fig. 4b repeats the large igneous province (LIP) basalt field from Fig 2b but with the aim of highlighting the overlap between the VAB and mafic LIP fields. This overlap results because Th/Nb is a crustal proxy rather than a subduction-specific proxy, as high grade metamorphism and plume–lithosphere interactions can also lead to subduction-like signals. In the flow chart

(Fig. 1), decision point DP1a separates most subduction-related mafic volcanic rocks, which follow the red and purple route based on consistently high Th/Nb (i.e. >95% plot within the VAB field), from most mafic, intraplate volcanic rocks, which follow the 'blue route' based on their low-high Th/Nb. As already covered, decision point DP2 then transfers out of the subduction route and into the intraplate route any high Th/Nb suites that can be shown to extend into the OcB field by extrapolation back to primitive magmas. Decision point DP3a transfers into the subduction route low-high Th/Nb suites that might have transitional subduction (marginal basin) compositions. In Fig. 4c–f , we provide some type examples of Phanerozoic volcanic rocks to highlight the similarities and differences between those indicative of subduction with those having no subduction connotation. Where possible, we combine mafic compositions (basalts and basaltic andesites) with felsic compositions (andesites, dacites and rhyolites) to provide complete BADR trends.

Plume–crust type interactions

The increase in Th/Nb due to interaction between continental intraplate magmas and crust is highlighted in Fig. 4c showing the full BADR trends. The Yellowstone LIP (Hildreth *et al.* 1991) is a classic example of a bimodal (basalt and rhyolite) suite, made up of a basaltic plume-derived magma undergoing extensive interaction with the crust. Hildreth and coworkers recognised the extensive basalt–rhyolite mixing and basalt contamination and explained the rhyolites as the products of crustal melting in the lower crust aided by basalt injection followed by accumulation in upper crustal reservoirs. The products of these plume–crust interactions are the diagonal trends in Fig. 4c.

The British Tertiary Province, part of the North Atlantic Igneous Province (NAIP), contains several examples of BADR series formed by plume–crust interaction that have been confirmed by isotope studies. A simple example is Ardnamurchan (Geldmacher *et al.* 1998), where the evolving compositions have been interpreted in terms of fractional crystallization coupled with shallow assimilation of ambient Precambrian metamorphic rocks. It differs from the Yellowstone trend in having a lower Nb/Yb plume endmember (closer to the average OPB) but a similar crustal endmember (close to FCC) which results in a shallower plume–crust interaction trend.

The Etendeke LIP, represented by the c. 132 Ma picritic Spitzkoppe dyke swarm in Namibia, provides a further example of well constrained plume–crust interaction (Thompson *et al.* 2007). These authors find evidence for 'limited interaction' with metasomatized lithosphere' before interaction with Damaran crust, although Fig. 4c does not allow the two to be distinguished. The plume and crustal endmembers are similar to those of the NAIP example, but more interaction was required to reach evolved compositions, a possible consequence of the more picritic (magnesian) plume-derived inputs.

Plume–SZLM type interactions

Although plume–crust interaction is unrelated to plate tectonics, plume–mantle lithosphere interaction may carry a 'hidden' record of past subduction if the lithospheric component in question is subduction-modified lithospheric mantle (SZLM). However, identifying plume–SZLM interaction can be difficult as the plume-derived magma is interacting with continental crust as well, resulting in a complex spread of data.

The examples shown in Fig. 4d are distinct from plume–crust interaction in that they typically extend from the OcB array towards the centre of the VAB array rather than towards continental crust. If the OcB endmember has an E-MORB or tholeiitic OPB composition, they can form trends with negative slopes. This is the case with the upper units of the Siberian Traps (Lightfoot *et al.* 1990), the Bunbury basalts (Olierook *et al.* 2016) and the Durham Basin from the SW part of the CAMP LIP (Grossman *et al.* 1991). The latter forms a complicated cluster rather than a simple trend which emphasises the potential difficulty of identifying plume–SZLM trends. However, if they can be identified in the Archean, they may provide useful additional indirect evidence for subduction.

Active arc volcanism

Some of the different types of volcanic arc formation that make up the VAB array, extended to include the more evolved rocks, are highlighted in Fig. 4e. In each case, as already noted, the most basic composition depends on the degree of depletion of the mantle source and the composition and relative input of the subduction component. The length and orientation of the mafic to felsic trend depends on the crystallizing assemblage (particularly the incoming of hornblende with low Th/Nb), as well as on the composition of the continental crust and extent of

crustal contamination. The set of examples in Fig. 4e have been chosen to facilitate the interpretation of proposed Archean arc BADR series in the next section.

For normal oceanic arcs, Candlemas (Scotia Arc) and Soufrière (Montserrat, Lesser Antilles arc) represent oceanic arc BADR series. For Candlemas, a low-K tholeiitic series, parent magma derived from a depleted mantle wedge crystallized an olivine–clinopyroxene–plagioclase assemblage with no significant crustal input (Pearce *et al.* 1995). In Fig. 4e, this magma exemplifies a depleted arc endmember characterized by intermediate Th/Nb, very low Nb/Yb ratios and little mafic–felsic dispersion. For Soufrière, a medium-K calc-alkaline volcanic suite with a significant sediment-dominated subduction flux and an amphibole–plagioclase crystallization assemblage (Zellmer *et al.* 2003), amphibole fractionation together with interaction with older arc crust explain the greater spread of compositions from mafic to felsic. For 'hot oceanic subduction', Simbo (New Georgia Group, Solomon Islands) provides an example of picrites and high-Mg andesites (HMA) from a site of ridge subduction (König *et al.* 2007). Like the other oceanic arcs, they are characterised by high Th/Nb BADR trends.

The majority of continental arcs have medium-K calc-alkaline character, and so are broadly similar to Soufrière which (although oceanic) has developed on an oceanic plateau, lacks an actively spreading back-arc basin, and is proximal to sources of continent-derived sediment. Thus, on Fig. 4e we have plotted Vulcano from the South-central Aeolian arc (Francalanci *et al.* 2007; Peccerillo *et al.* 2013) to illustrate features of the high-K (shoshonitic) continental arc series. The setting of Vulcano is complex, on a continental rise on the edge of the Tyrrhenian Sea above a retreating oceanic plate, and the high Th and K contents causes it to occupy the upper right corner of the VAB array. As an example of 'hot subduction' in a continental arc setting, we have chosen Shasta (Southern Cascade arc), a continental medium-K calc-alkaline arc volcano incorporating high-Mg andesites and associated with subduction of very young crust (Grove *et al.* 2002; Grove *et al.* 2005). The reduced subduction flux (and hence low, though still arc-like, Th/Nb) combined with extensive interaction with continental crust gives a steeper BADR trend than most arc volcanoes. Some of this trend may also relate to the presence of two separate parental magma sources, namely from the rear-arc and mantle wedge (Streck *et al.* 2007). As will be seen, this steeper trend has analogues in the Archean crustal record.

Inherited subduction signatures

Arc-like magmas can result not only from active subduction but also reactivation of sub-continental lithosphere enriched by past subduction events. Fig. 4f highlights some type examples of inherited subduction-modified magmas: a continental LIP (the Ferrar LIP); an oceanic LIP (the Great Benham Rise); a post-collision volcano (Mt Ararat); and a zone of continental extension (the Basin and Range).

The continental Ferrar LIP (FLIP) is an elongate belt of Jurassic age some 3000 km long mainly made up of hypabyssal intrusives of SHMB and high-Mg andesite composition which were emplaced over a very short time interval at c. 183 Ma. It is one of the best-known, consensus examples of magma derived from a 'fossil subduction zone' (Choi *et al.* 2019). Its precise context is debated, though most publications ascribe it to a subduction-modified sub-continental mantle lithosphere source (Hergt *et al.* 1991). Interestingly, there is no plume-derived magma in the region, though the far-field effect of the near-contemporaneous Karoo plume may be important from a tectonic and thermal perspective. In Fig. 4f, basic compositions plot near the centre of the VAB array.

The Great Benham Rise (GBR) refers to a series of related, mainly Eocene, oceanic plateaux in the Philippine Sea linked to the upwelling of the Ancestral Manus mantle plume (Yeh *et al.* 2021). The initial impact was with Cretaceous oceanic arc lithosphere resulting in extension and eruption of arc-like lavas in a rift-basin setting (Hickey-Vargas *et al.* 2013). For this study, the key point is that these lavas plot in the field of oceanic VAB magmas in Fig. 4f (cf. Fig. 4a), demonstrating that inheritance can also be chemically dependent on the setting of the original subduction system.

The Basin and Range volcanic province in SW USA and NW Mexico provides a good example of post-subduction magmatism, in this case likely resulting from extension and mantle upwelling related to the change from a subduction to a transform (proto-San Andreas) plate boundary rather than a mantle plume (Putirka and Platt 2012). The high-K, calc-alkaline, lithosphere-sourced volcanic rocks from New Mexico plotted in Fig. 4f characterize the early stages of magmatism (c. 40–30 Ma), after which time asthenosphere-sourced magmas took over (Davis and Hawkesworth 1994). In Fig. 4f they plot in the centre of the arc array parallel to the discriminant boundary, within the range of active continental volcanic arc magmas.

Mt Ararat (eastern Turkey) is another example of post-subduction melting of lithospheric mantle, but here the setting is post-collisional and the lithsopheric enrichment in the province can

be spatially related to subduction prior to the collision (Pearce *et al.* 1990). The time interval from the end of arc activity to the start of post-collision magmatism is about 35 Ma. However, the compositions of the resulting magmas are similar to those of the preceding continental medium- to high-K, calc-alkaline arc magmas, which plot in the centre of the VAB field in Fig. 4f.

Comparison between Fig. 4e and 4f highlights the fact that distinguishing inherited from active arc signatures (decision pont DP5 in Fig. 1) can be difficult unless there are clear geological criteria that can be applied. As noted earlier, one obvious difference is that mantle enrichment for active arcs is usually synchronous with eruption, whereas for inherited arc signatures there may be a significant time difference between the two. Mantle xenoliths from the regions of proposed lithosphere-sourced magma, especially if characterized using the Re–Os isotope system (Walker *et al.* 1989), may also provide useful information.

Palaeoproterozoic comparators

The oldest, well documented and largely undisputed post-Archean subduction events took place between 1.96 and 1.81Ga during the formation of Laurentia by accretion of Archean terranes during the Palaeoproterozoic period (Hoffman 1988). Of these events, the best-preserved in terms of volcanic stratigraphies and accompanying geochemical data are in the Trans-Hudson Belt of Northern Canada, which may be considered part of a larger terrane extending from Wyoming through Canada, Baffin Island and Greenland to the Baltic Shield. It is believed to result from opening, and subsequent closure though subduction, of the so-called Manekewan ocean. Corrigan *et al.* (2009) concluded that ocean opening initiated at c. 2.17 Ga, that it began to close at c. 1.92 Ga, and that closure was complete at by c. 1.80 Ga. It is the volcanic arc magmas erupted during the c. 120 Ma of closure that provide us with an opportunity to test methodologies and to act as a comparator for proposed Archean arcs.

Fig. 5a focuses on the Flin Flon Belt in Northern Manitoba–Saskatchewan (Canada) (Stern *et al.* 1995), which can be divided into an oldest ‘boninite–tholeiite’ suite (c. 1904–1900 Ma), followed by a ‘calc-alkaline’ suite (c. 1900–1890 Ma) and finally a ‘more potassic calc-alkaline’ suite (<1890 Ma). In Fig 5a, each volcanic unit plots within and along the VAB field accompanied by an increase from relatively low Th/Nb in the oldest suite through arc-average

Th/Nb in the middle suite to still higher Th/Nb but also higher Nb/Yb in the youngest suite. Stern *et al.* (1995) interpreted this sequence as representing an oceanic arc that evolves from subduction initiation through to a mature arc, a sequence observed elsewhere in the Trans-Hudson Belt (Leybourne *et al.* 1997) and in many present-day arc systems. Continental arc systems are also present, as exemplified in Fig. 5a by the volcanic rocks of the LaRonge Belt, which lies north of the Flin Flon Belt and include the Lynn Lake and Rusty Lake greenstone belts (Chauvel *et al.* 1987; Watters and Pearce 1987; Thom *et al.* 1990). As with present-day continental arcs, these plot within the VAB array, but with higher Nb/Yb compared to their oceanic equivalents and also follow a trend indicative of crustal interaction as well as fractional crystallization.

Overall, therefore, there is evidence here for a full subduction cycle from birth to death of a subduction zone, with geochemical characteristics not obviously distinguishable from Phanerozoic subduction cycles. In the flow diagram (Fig. 1), most of the magmas may be assigned to active subduction at decision point DP5 given the high Th/Nb characteristics and the abundant geological evidence for a subduction rather than an intraplate setting. However, some of the youngest magmas may be the product of post-collision subduction inheritance due to melting of mantle lithosphere enriched during the preceding subduction episode, a common feature of Phanerorozoic subduction systems (Pearce *et al.* 1990). Thus, plate tectonics resembling the present day likely was possible back to at least 2 Ga. Our evaluation strongly supports the assertion of Thom *et al.* (1990) that processes and compositions have probably not changed much over the past 2 Ga. However, we are not aware of any comparable subduction systems in the Archean in terms of longevity and compositional range.

The search for Archean volcanic arcs II: Results

We present the results of our search for Archean subduction-related rocks in five parts: (i) examples of Archean greenstones described as volcanic arcs but which classify as having continental intraplate settings; (ii) examples of Archean greenstone suites with likely inherited subduction signatures; (iii) an example of an Archean greenstone suite with possible evidence for plume–SZLM interaction; (iv) examples of Archean greenstone suites with likely Archean active

subduction signatures; (v) examples of Archean amphibolite suites with potential subduction signatures.

*False Archean subduction signatures: plume–crust interaction*s

There are many examples of Archean plume–crust interactions that follow the 'blue (plume/intraplate) route' through the flow diagram in Fig. 1, and several were reported in the section on ophiolites (Fig 2b). A wide range of further examples have been published by Barnes *et al.* (2012) and Smithies *et al.* (2018) from the Yilgarn and Pilbara cratons (Australia) and by Mole *et al.* (2021) from the Superior craton. Here we have highlighted three of their best examples of BADR sequences resulting from plume–crust interaction rather than plate subduction: the Agnew Greenstones (2.7 Ga) from the Kalgoorlie Terrane in the Yilgarn Craton (Barnes *et al.* 2012); the Duffer and Panorama groups (3.46–3.43 Ga) from the East Pilbara Terrane (Smithies *et al.* 2005b); and Frotet–Evans greenstone belt from the Opatica sub-province from the Superior craton (Boily and Dion 2002; Mole *et al.* 2021). We also added a fourth well-studied example, the Belingwe greenstones (2.7 Ga) from the Zimbabwe craton (Shimizu *et al.* 2005).

These examples are very similar, all forming a trend between two endmembers: a plume endmember close to average OPB composition in the OcB array and a crustal component close to Archean felsic continental crust (A-FCC) in the upper right segment of the VAB array. All four exhibit a bimodal distribution on Fig. 5b, a mafic mode comprised predominantly of komatiite, basalt and basaltic andesite compositions, and a felsic mode predominantly of andesite to rhyolite compositions. This bimodality differs from the unimodal distribution with an andesitic peak that is common in Phanerozoic continental volcanic arc terranes, a distinction further indicative of an intraplate origin.

Inherited subduction-like signatures

Some well documented examples of high Th/Nb volcanic rocks that follow the 'purple route' to inherited subduction (Fig. 1) are shown in Fig. 5c. As the aim is to investigate inherited Archean subduction, the volcanic rocks themselves need not be of Archean age, though the metasomatism

of the lithosphere, by definition, must be. Two of the chosen examples of this type are Palaeoproterozoic and both plot in the centre of the VAB field in Fig. 5c. The youngest example (2.06 Ga) comprises the Bushveld B1 'chills' (Maier *et al.* 2016) and the penecontemporaneous Dullstrom Volcanics (Buchanan *et al.* 1999). A key feature in these, and many other Archean lithosphere-sourced magmas with subduction-like signatures, is their boninite–HMA, or SHMB–HMA signatures, the likely result of melting of highly depleted and refertilized lithospheric sources. The second example is the Matachewan LIP dyke swarm (2.48–2.44 Ga) in the Superior province Canada (Ernst and Bleeker 2010). As one of the world's largest dyke swarms, it clearly has a plume-related LIP origin. However, unlike the Bushveld example, these are not boninitic, implying that the lithosphere was less depleted prior to refertilization.

Pearce and Reagan (2019) found that there are many examples of magma from depleted and refertilized sources within the period 3–2 Ga, all of which link to LIP or non-plume continental rift settings. The Mallina Basin (Smithies *et al.* 2004) contains what are possibly the oldest clear examples of inherited subduction signatures. Like many other Archean and Palaeoproterozoic examples in this age range, they mainly classify as SHMB–HMA suites and form a trend on Fig. 5c within the centre of the VAB array. The setting (within a sedimentary basin) and composition (SHMB) both support an inherited subduction component within depleted continental lithospheric mantle.

The final example is the (enriched) Paringa Basalts from the Kalgoorlie Terrane, Australia. In their compilations of volcanic rocks from the Yilgarn Block in Australia, Said and Kerrich (2009), Barnes *et al.* (2012) and Smithies *et al.* (2018) all found the Paringa basalts, and notably the 'enriched' suite, particularly distinctive with 'unusual' features such as low Ba/Th. In Fig. 5c, their data plot entirely within the VAB array. Thus, according to Fig. 1, they follow the 'red' potential subduction route with active arc and inherited arc both options until decision point DP5 is reached. There, even apart from geological indicators, their 'unusual' geochemical features (negative anomalies of P, K, and Ba, in particular) are readily explained by melting of metasomatized lithosphere with residual phlogopite and apatite.

The examples cited above are not the only occurrences of inherited subduction in the Archean record. Most Archean cratons appear to have refertilized lithospheric sources which continue to provide sources of magmas through to at least 2 Ga. However, whether they can be regarded as plate tectonic indicators will depend on decision point DP7 on the purple route in

Fig. 1, where non-uniformitarian ways of enriching lithosphere by means other than plate subduction need to be considered. Here, as elsewhere in the Archean, there is no definitive answer as non-uniformitarian processes lack undisputed examples. However, given that the potential Archean inheritance examples in Fig. 5c are so similar to their Phanerozoic equivalents in Fig. 4f, and given that inherited subduction is extremely common in the Phanerozoic, the implication must be that subduction inheritance is the higher probability option for the examples just cited. That said, back-tracking through dating and isotope geochemistry to the sources of the proposed inherited magmas would provide important confirmatory information.

Indirect subduction signatures: Plume–SZLM interactions

Plume–SZLM interactions are difficult to recognise. They are found either where plume-derived magma interacts with SZLM or when plume-derived and SZLM-derived magmas undergo mixing. However, these processes can be difficult to distinguish from crustal contamination. One potential example (Fig. 5d) is the low-Ti and boninitic compositions from the Frotet–Evans greenstone belt (Boily and Dion 2002; Mole *et al.* 2021). The Frotet–Evans BADR series, shown in Fig. 5b, is a simple trend from the OcB array to Archean felsic crust and does not provide evidence for subduction. However, the associated low-Ti suite is different. It defines a near-vertical trend that could indicate interaction between an intraplate magma and metasomatized mantle lithosphere, either in the mantle or by magma mixing in the crust. If correct, it could indicate that the lithosphere beneath the Frotet–Evans greenstones experienced (otherwise hidden) subduction at some time in its history.

High probability active subduction signatures

A number of c. 2.7 Ga greenstones within the the Superior craton have been listed by Polat and Kerrich (2006) as examples of Archean active arc volcanism. Two of these, from the Wawa Domain (Polat and Kerrich 2000) and the Birch–Uchi Confederation (Hollings and Kerrich 2000), are plotted in Fig. 5e. They form BADR trends entirely within the VAB array, thereby following the high Th/Nb route in Fig. 1 consistent with the volcanic arc intrerpretations.

The third example in Fig. 5e is from the 3.12 Ga Whundo Group (West Pilbara Terrane) (Smithies *et al.* 2005a; Smithies *et al.* 2018). The Whundo section is described as comprising boninites and a calc-alkaline BADR sequence interspersed in places with tholeiitic basalts, all of greenschist facies metamorphic grade (Smithies *et al.* 2005a). In Fig. 5e, the 'calc-alkaline and boninite series' lavas form a trend fully within the VAB array (the tholeiites are transitional and not discussed here).

In terms of the flow chart in Fig. 1, DP5 is the key decision point between active and inherited arc magmatism. In all three examples in Fig. 5e, limited outcrops and metamorphism and deformation make it difficult to apply the DP5 criteria listed in Table 1, although the terrane-scale volcanic stratigraphy may be particularly significant. The Wawa and Uchi-Confederation examples are each part of a sequence of continental rifts and volcanic plateaux followed by an inferred volcanic arc and finally by collision (orogenic and post-orogenic) magmatism. This is a similar sequence to that in the Palaeoproterozoic Trans-Hudson Belt, even though the proposed arc events in the former may have been shorter-lived. Given that the late-stage collision volcanism has abundant examples of subduction inheritance, the c. 2.67 Ga diamond-bearing lamprophyres (Wyman and Kerrich 1989) being the best of many examples, it is logical that a preceding active arc was the source of the inherited metasomatizing melts and fluids. The c. 3.1 Ga Whundo sequence similarly lies between a long, older period of regional LIP volcanism (including the c. 3.45 Ga Apex/Panorama volcanics in Fig. 5b) and a younger period of inherited subduction magmatism (including the c. 3 Ga Mallina Basin in Fig 5d).

The decision to assign these volcanic rocks to the active arc group is not totally unambiguous. At decision point DP7a, non-uniformitarian translation of crustal materials into the mantle, for example of the type proposed for the Abitibi terrain by Bédard (2006), remains a topic in need of further investigation. A further point of note is that all three potential examples of active arc volcanism have been interpreted by the authors cited above as 'oceanic arcs'. While not conclusive, comparison of Fig. 5e with the active arc comparator diagram in Fig. 4e shows that their compositions resemble more closely continental arcs. The increase in Th/Nb and Nb/Yb from mafic to felsic and the resulting convergence on crustal compositions is particularly diagnostic, with all three Archean examples best matching the continental, hot-subduction Shasta comparator.

Eoarchean high Th/Nb signatures: true subduction or non-uniformitarian plume tectonics?

Two key localities for lavas with clear subduction-like signatures but insufficient data to confirm as active or inherited subduction subduction, are the 'low-Ti basalts' and 'boninites' of Isua and the Upper lavas of Nuvvuagittuq, both of likely 3.8–3.7 Ga age. In both cases, intense deformation, high metamorphic grade, limited outcrop size and unclear geological context make decision points DP5 and DP7 hard to apply and it is unsurprising that interpretations are controversial. Despite this, the crustal proxy diagram (Fig. 5f) does provide some constraints. The Isua supracrustal belt is one of the most controversial locations for tectonic fingerprinting. Polat *et al.* (2002) and Jenner *et al.* (2009) highlighted the presence of boninites and depleted tholeiites which they interpreted in terms of subduction initiation and oceanic arc settings. As investigated in the previous section, Th mobility during metamorphism is a major issue in data interpretation (Fig. 2f) as is data quality at such low abundances of Th and Nb. However, by carefully selecting the least metasomatized samples from the study of Polat *et al.* (2002) and by carrying out high precision analysis, Hoffmann *et al.* (2010) do appear to have circumvented these problems. Their 'filtered' data set, plotted on their Fig. 6G crustal proxy projection (and reproduced in our Fig. 5e), plots at the lower edge of the island arc tholeiite segment of the VAB array (cf. Fig. 4a). They are the only Archean basalts we have so far found to do so. It may also be significant that analyses by Hoffmann *et al.* (2011) of samples from the 'sheeted dyke' outcrop identified by Furnes *et al.* (2007) have a similar composition. If the outcrop is made up of sheeted dykes, which is by no means certain (Nutman and Friend 2007), the protoliths may indeed have been boninites from SSZ ophiolites associated with subduction initiation, as they and others have inferred.

Webb *et al.* (2020) and Rollinson (2022) present the main alternative view, that Isua's apparent plate tectonic indicators based on Th/Nb are unrelated to subduction and, instead, are the product of ultra-deep melting involving residual perovskite residues in a heat-pipe Earth. For that model to work, it also requires the magma source to comprise primitive mantle (silicate mantle prior to any crustal extraction), or magma ocean cumulates derived from primitive mantle, to provide sufficiently high Th/Nb mantle sources. In detail, the best estimate to date for the Th/Nb ratio of primitive mantle may be 0.136 by Lyubetskaya and Korenaga (2007), which is slightly higher than (though within error of) the commonly used 0.119 by Sun and McDonough

(1989). However, both are significantly higher than the estimate of 0.053 for present-day depleted MORB mantle (DMM) (Workman and Hart 2005) and, as a result, they plot close to the upper edge of the present day OcB array where Th/Nb = 0.15. Further, the mantle source must have been depleted much deeper than any mantle wedge to explain the HREE depletions, and Th/Nb must be increased still further than the primordial mantle ratio: the proponents argue that both features are potentially achievable in a heat pipe Earth. Moreover, the closer the age to the Hadean, the more likely it is that materials with primitive mantle compositions were available to provide a magma source.

The Nuvvuagittuq Upper Lavas have been assigned a low-Ti (enriched) classification which distinguishes them from the underlying high-Ti and low-Ti (depleted) lavas investigated in Fig. 3e (O'Neil *et al.* 2007; Turner *et al.* 2014). Unlike the underlying lavas, where the interpretation is masked by Th mobility (Fig. 3e), the Upper Lavas do not follow a low-high Th/Nb contamination trend. Instead, despite similarly pervasive metasomatism, the trend is of a more constant high Th/Nb indicative of potential subduction. From this, it is evident that the pre-metasomatic Th values must have been sufficiently high that Th addition during metamorphism had only a limited effect. Thus, despite metasomatism, the interpretation by Turner *et al.* (2014) that these rocks had arc-like geochemistry is supported by the crustal proxy projection where the data plot in the centre of the VAB array (Fig. 5f). As a result, the Nuvvuagittuq trend does resemble the other potential examples of Archean arc-like rocks in Figs. 5e and 5f and is very different from Isua, looking, for example, much more like a continental, as opposed to oceanic, arc.

On the flow chart (Fig. 1), lavas from both Isua and Nuvvuagittuq follow the high Th/Nb (red) route to potential subduction, but there are insufficient data to decide (at decision point DP5) whether that is active rather than inherited subduction and whether (at DP7) non-uniformitarian processes were involved. Consequently, there are still important decisions to be made if Eoarchean plate tectonics is to be confirmed. Clearly, these relatively small outcrops of amphibolite carry key information about early Earth tectonics that future work will hopefully help to unravel.

The metamorphic perspective

Metamorphic rocks record evidence of change in pressure (P) and temperature (T) with time (t), commonly expressed as a P–T–t path, which represents the record of heating and cooling during burial and exhumation derived from mineral assemblages and compositions combined with geochronology (Brown 1993; Brown 2001). The peak pressure may be achieved before the maximum temperature (clockwise P–T–t path), the maximum temperature may be achieved before the peak pressure (counter-clockwise P–T–t path) or the path may reach a coincident peak in pressure and temperature. The P–T–t path records the changing spectrum of transient geotherms characteristic of a particular tectonic setting (England and Richardson 1977; Richardson and England 1979; Thompson and England 1984), and the thermobaric ratio (T/P) at the metamorphic peak is characteristic of different plate tectonic settings (Brown and Johnson 2018, 2019a, b; Brown and Johnson 2019c). Insofar as metamorphic pressure can be translated to depth, the thermobaric ratio ($T/P \sim T/z$) can be viewed as a proxy for the transient geothermal gradient recorded by a metamorphic rock at the metamorphic peak.

The occurrence of metamorphic belts characterized by the juxtaposition of different sequences of mineral assemblages in orogens led Miyashiro (1961) to the concept of paired metamorphism, although we now know that the individual belts need not be contemporaneous, and one may be far-traveled relative to the other (Brown 2010). Paired metamorphism has been related to convergent plate boundaries, where the asymmetric (one-sided) subduction of ocean lithosphere depresses isotherms creating a cool (low T/P) metamorphic environment characterized by low heat flow. The breakdown of hydrous minerals in the descending slab generates fluids and/or melts at subcrustal depths that promote magma generation in the overlying mantle wedge, creating a warm (high T/P) metamorphic environment characterized by high heat flow in the orogenic backarc or hinterland (Oxburgh and Turcotte 1971; Hyndman *et al.* 2005). Blueschists and eclogites, which are characterized by low T/P ratios, are generally related to subduction, as confirmed by the transport of Paleogene blueschist fragments to the surface in a serpentine-mud volcano located above the subducting Pacific plate at the southern end of the Mariana trench (Maekawa *et al.* 1993; Tamblyn *et al.* 2019; Miladinova *et al.* 2024). Ultrahigh pressure metamorphic rocks of continental affinity are also related to subduction, as exemplified beneath the Pamir (Schneider *et al.* 2013). By contrast, lower crustal granulite xenoliths brought to the surface in the Kilbourne Hole maar in the Rio Grande Rift record high T/P ratios. They demonstrate that the contemporary lower crust is at granulite facies conditions,

in this case because crustal thickening was succeeded by lithospheric thinning and heating of the lower crust to granulite-facies conditions during orogenic collapse (Cipar *et al.* 2020).

Data collected during the last 50 years have been used to show that regional metamorphism is characterized globally by an increasingly divergent bimodal distribution of *T/P* ratios since the early Proterozoic (Holder *et al.* 2019). This bimodality reflects the different thermal gradients generated by tectonic coupling between the cold lithosphere returning to the mantle via subduction and the enhanced heat flow beneath the thinned lithosphere of the overlying orogenic hinterland (Brown and Johnson 2018; Holder *et al.* 2019; Holder and Viete 2023). To assess overall changes in the trend of crustal metamorphism through time, Brown *et al.* (2020b) applied locally weighted scatterplot smoothing (LOWESS) to the time series data of Brown and Johnson (2019c) to create a polynomial regression through the *T/P* ratios and applied sequential analysis (by cumulative sum) to quantify changes. *T/P* was generally high during the Neoarchean–Mesoproterozoic with a drop in *T/P* in the Orosirian, related to the formation of Nuna/Columbia, and a second, more dramatic two-stage drop in *T/P* in the Ediacaran–Cambrian, associated with the widespread appearance of blueschists and ultrahigh-pressure metamorphic rocks. These interpretations from the metamorphic record have been combined with other geological data to conclude that plate tectonics has been operating on Earth since at least the early Paleoproterozoic (Brown *et al.* 2020b).

Metamorphic dataset

The metamorphic dataset used in this study (Table S1) is based on the February 28, 2018 dataset of Brown and Johnson (2019c), which has been updated after an extensive review of the literature up to November 3, 2023. The dataset comprises localities with robust quantitative estimates of pressure (*P*), temperature (*T*) and age, and assumes equilibration at the *P* and *T* of interest. This is justified because prograde dehydration and melt loss generally produce mineral assemblages that are difficult to retrogress or overprint without fluid influx, and when evidence of post-peak reaction is present its effects generally can be accounted for, as detailed by Brown and Johnson (2018). The dataset has not been filtered based on presumed inferior quality or by removing data deemed to be outliers. As in previous versions, the dataset is restricted to crustal

protoliths, so orogenic peridotites and occurrences of ultrahigh-pressure minerals in chromitites associated with ophiolitic complexes, and mantle xenoliths are excluded.

One change from the previous iteration is the deletion of two low *T/P* (UHP) localities from the Nordre Strømfjord shear zone in the Paleoproterozoic Nagssugtoqidian Orogen of western Greenland (Glassley *et al.* 2014). Data from these localities have recently been called into question by Schönig *et al.* (2023), who found no evidence of low *T/P* (especially UHP) metamorphism in heavy minerals separated from modern sands representing eight catchments that drain the area. Another exclusion is the location at the northwestern end of the Isua supracrustal belt where rare lenses of mantle dunite occur in schistose ultramafic rocks (Nutman *et al.* 2020). Olivine in these rocks has intergrowths of titano-clinohumite replacing titano-chondrodite and is in equilibrium with antigorite, features that apparently record decompression through *P–T* conditions of 2.6–3.0 GPa and 500–700°C. However, how these rocks were emplaced into the crust is unknown, and without additional evidence of UHP metamorphism in the Isua supracrustal belt and a precise age the tectonic significance of these dunite lenses is ambiguous.

The current dataset includes 197 new localities, some of which replace a previous locality in the same geographic area, and incorporates updates to existing localities where new data have been published; overall the dataset is about 30% larger than its predecessor. However, in comparison with datasets used in other studies of secular change, the metamorphic dataset used here remains small with only 728 localities. These localities are globally distributed (Brown and Johnson 2019a) and include 75 localities that record Archean metamorphism, although most are Neoarchean in age, with only 10 of Mesoarchean, 12 of Paleoarchean and 2 of Eoarchean age.

Metamorphism: Results

The new metamorphic dataset has a similar *P–T* distribution to the previous dataset (Fig. 6a). Of 728 localities (Fig. 6b), 293 (~40%) record high T/P metamorphism ($T/P > 775$°C GPa^{-1}), 198 (~27%) record intermediate T/P metamorphism ($T/P = 375–775$°C GPa^{-1}), and 237 (~33%) record low T/P metamorphism ($T/P < 375$°C GPa^{-1}). The record of ocean basin evolution since the Triassic allows metamorphic belts younger than 195 Ma to be related directly to a plate tectonic setting. For orogens older than 195 Ma in age, we interpret low T/P metamorphism to be

related to subduction-related sutures, intermediate T/P metamorphism to record the thickened lithosphere of former mountain belts and high T/P metamorphism to be mostly related to late-orogenic extension (Hyndman *et al.* 2005; Brown and Johnson 2018; Hyndman 2019; Agard *et al.* 2023). Blueschists, all <850 Ma in age, and orogenic eclogites, mostly <850 Ma in age, are commonly interpreted as related to subduction (Stern 2005; Brown 2006; Tamblyn 2021) and are dominantly of low *T/P* type (Fig. 6c). Notably, older eclogites tend to record higher *T/P* ratios on average than younger eclogites (Fig. 6c). Furthermore, for data <850 Ma where there is consensus that plate tectonics has been operating, the metamorphic record is characterized by a bimodal distribution of *T/P* values that has been related to asymmetric subduction (Fig. 6d; cf. (Brown 2006; Holder *et al.* 2019).

A plot of number of localities versus age (Fig. 7) shows the data are not uniformly distributed but cluster coincident with the supercontinent cycle since the early Paleoproterozoic or the formation of supercratons during the Neoarchean (Brown and Johnson 2018; Liu *et al.* 2021). The peaks in the distribution of the metamorphic data correspond to peaks in the global distribution of igneous and detrital zircon U–Pb ages that likely reflect the cyclicity of crustal aggregation and breakup (Puetz *et al.* 2018). Furthermore, similarity in the age distribution of pre-Neoarchean metamorphic rocks and contemporaneous gneisses of broadly tonalite–trondhjemite–granodiorite (TTG) composition (Johnson *et al.* 2019) suggests similarly low rates of preservation before the crustal recycling rate decreased in the Neoarchean as the cratons stabilized (Dhuime *et al.* 2012; Aulbach and Smart 2023).

The temporal distribution of blueschists and eclogites, which are generally accepted as related to subduction (Brown and Johnson 2019b; Holder and Viete 2023), shows that the former are almost exclusively Phanerozoic in age while the latter are dominantly Phanerozoic in age (Brown 2023). The evolving style of plate tectonics through the Proterozoic into the Phanerozoic, which involved a change from warmer to colder subduction, may explain the sporadic distribution of eclogites in the Proterozoic and the appearance of blueschists since the Cryogenian (Sizova *et al.* 2014; Brown and Johnson 2019b; Holder *et al.* 2019; Chowdhury *et al.* 2021; Holder and Viete 2023). Alternatively, the widespread occurrence of eclogites and the first appearance of blueschists in the rock record could identify the emergence of modern plate tectonics on Earth (Stern 2008).

To evaluate secular change in *T*, *P* and *T/P* we consider the dataset as a single entity rather than by metamorphic type and use locally weighted scatterplot smoothing (LOWESS) to calculate continual smoothed curves and residuals (Fig. 8). Confidence intervals for the LOWESS curve were calculated using a *t*-distribution. We also calculate 95th and 5th percentiles of the data using rolling windows of the nearest 5% data. For the *T*, *P* and *T/P* data, next we performed bootstrap sampling 500 times on a random selection of 1000 data points using a CUSUM model. The changepoints were combined and fit with a kernel density estimation (KDE) to identify the most significant changepoints (Supplementary Fig. S1). Although the precise position of the KDE peaks differs due to the inherent randomness of the bootstrapping approach, the *T*, *P* and *T/P* data all show prominent KDE peaks (changepoints) at around 2.5 Ga, 1.9–1.8 Ga, 1.1–1.0 Ga, 0.4 Ga and 0.08 Ga.

The average *T* increases from the mid-Paleoarchean to the Proterozoic, and remains high through the Paleoproterozoic and Mesoproterozoic, before decreasing until the late Cretaceous (Fig. 8a). Average *P* increases slightly through the Archean, associated with the stabilization of the cratons, to the Orosirian, associated with the formation of the Nuna megacontinent (as emphasized by the 95th percentile curve), then drops to its lowest value during the Mesoproterozoic (Fig. 8b). From the Tonian to the Permian average *P* rises to a high of ~2.2 GPa prior to a decrease during the Mesozoic and Cenozoic (Fig. 8b). The average *T/P*, which reflects these changes in *T* and *P*, increases slightly through the Archean before decreasing slightly in the early Paleoproterozoic during the formation of the Nuna megacontinent (Fig. 8c). Average *T/P* reaches its peak in the early Mesoproterozoic before a stepwise decrease to the end of the Paleozoic (Fig. 8c).

To characterize secular change in the distributions of metamorphic *T/P*, we binned the data using natural breaks in the time series (vertical orange bars in Fig. II) as follows: >2.85 Ga, 2.85–2.25 Ga, 2.25–1.35 Ga, 1.35–0.85 Ga, 0.85–0.195 Ga and <0.195 Ga (cf. Holder *et al.* (2019). Histograms and probability distribution functions (PDFs) for *T/P* (°C GPa^{-1}) plotted logarithmically to emphasize variations in the distribution are shown in Fig. 9. Rather than fitting a Gaussian mixing model to each distribution (Holder *et al.* 2019), we used the *FindDistribution* function in Mathematica (https://reference.wolfram.com/mathematica) to identify a simple functional form to fit each distribution of $\log_{10}$ *T/P*. The data >2.85 Ga in age and for the period 2.85 to 2.25 Ga define single (unimodal) normal distributions (Fig. 9a,b), the data for the period

2.25 to 1.35 Ga exhibit a broad unimodal left-skewed distribution whereas the data for the period 1.35 to 0.85 Ga have a uniform distribution with the development of a distinct low *T/P* mode (Fig. 9c,d), and the data for the period 0.85 to 0.195 Ga define a broad trimodal distribution with the most prominent mode at lowest *T/P* whereas the data <0.195 Ga in age show a broad bimodal normal distribution, with distinct lower and higher *T/P* peaks (Fig. 9e,f). In essence, the data show a gradual transition from a narrower unimodal normal distribution of metamorphic *T/P* in the Archean eon to a broader bimodal normal distribution since the Triassic. The histogram distributions are qualitatively comparable to those in Holder *et al.* (2019) using the Brown and Johnson (2019a) dataset. In both cases, the low *T/P* peak becomes prominent only after the Mesoproterozoic, consistent with the first appearance of blueschists and UHP metamorphic rocks.

Metamorphism >2.25 Ga compared with results from numerical models

For metamorphic *T/P* data older than 2.25 Ga, when the prevailing tectonic mode is debated (Brown *et al.* 2020a), the $\log_{10}$ *T/P* data define single (unimodal) normal distributions that include both intermediate *T/P* and high *T/P* types of metamorphism (Fig. 10a). Here we compare the natural data with *P–T* information retrieved from markers (as analogues for rocks) in 2D thermomechanical models of geodynamics for which plate tectonic behaviour is not predicted.

First, we consider *P–T* information for 545 markers taken from different settings in an experiment performed using a model of a stagnant-deformable lid tectonic mode with initial conditions appropriate to the Archean (T_P = 250°C higher than the present day), no lateral lithological variation in the initial set-up but with a small temperature perturbation, and a model run time equivalent to c. 200 Myr (Sizova *et al.* 2015). The plots show clearly that the natural data are comparable to *T/P* values for markers from small-scale crustal overturns and downwelling of inter-domal crust (sagduction) and local thickening of the crust in the experiment (Fig. 10). Downwelling or dripping of crust into the mantle generates a range of *T/P* values at low *T* that overlap the low *T* part of the range defined by small-scale crustal overturns. Whether any of the natural data correspond to this tectonic setting is unclear.

More recent experiments have used a model that assumes subduction and continent–continent collision as the starting point to investigate what happens during ongoing

convergence after initial collision for a range of ambient mantle T_P (Chowdhury *et al.* 2017). In these experiments, the prescribed velocity field leading to the initial collision is removed towards the end of subduction and the subsequent convergence evolves spontaneously. Experiments at ambient mantle T_P appropriate to the Neoarchean (T_P = 200°C higher than the present day) predict a 'peel-back' style of behaviour that is transitional between stagnant-lid and plate tectonic modes. Markers in these experiments also reproduce the *P–T* conditions of natural data >2.25 Ga in age well, as shown by Chowdhury *et al.* (2020) in their Figs 3 and 5.

Modeling has also been used to investigate the role of an initial thinning perturbation of an otherwise uniformly thick lithosphere on the style of mantle convection and crustal thermal regimes (Capitanio *et al.* 2019a). At an ambient mantle T_P argued to be appropriate to the Archean (T_P = 260°C higher than the present day), a mobile-lid mode that differs from plate tectonics is predicted. However, in this experiment markers record predominantly intermediate *T/P* metamorphism and the model did not generate high *T/P* metamorphism (Capitanio *et al.* 2019a), their fig. 3B).

Importantly, the range of *T/P* values derived from these experiments using thermomechanical models is generally comparable to the range of *T/P* values retrieved from the early crustal archive. This similarity demonstrates that the single (unimodal) normal distributions of $\log_{10}$ *T/P* data >2.25 Ga old could have been generated in any of a variety of non-plate tectonic modes.

Discussion

If Earth has had plate tectonics essentially since crystallization of the last magma ocean, features that are considered diagnostic of plate tectonics since the Triassic should be recognizable (much) further back in time. We first assess whether the temporal distribution of diagnostic igneous and metamorphic rocks is broadly representative or, rather, is biased to the point of being unreliable. Then we discuss secular changes in the igneous and metamorphic records and consider the implications for the emergence of plate tectonics on Earth.

Bias and the petrological record

Given that geographic areas are not equally accessible and samples are generally selected non-randomly in both space and time, sometimes with preferences for some locations and/or rock types (and constituent minerals) over others, spatial and temporal bias in the petrological record is inevitable. In addition, the fidelity of the petrological record could be affected by differential recycling of crust back into the mantle, which could have biased the surviving crustal archive.

Hawkesworth *et al.* (2009) argued that the correlation between peaks in the distribution of zircon crystallization ages for continental crust and the supercontinent cycle or the formation of supercratons was a function of preservation, although this interpretation has been disputed, most recently by Puetz and Condie (2021). Similarly, the crustal record of metamorphism is related to the supercontinent cycle and the formation of supercratons (Brown 2007a), consistent with the expectation that most regional-scale metamorphic belts are related to convergent plate margins and collisional orogenesis (Liu *et al.* 2022). Prior to the formation of supercratons in the Neoarchean, preservation of crustal rocks was likely related to craton stabilization (Jaupart *et al.* 2014; Beall *et al.* 2018; Wang *et al.* 2018; Tang *et al.* 2020).

For oceanic crust, even Phanerozoic MORB are poorly preserved because they have the thinnest lithosphere and are typically subducted. Those that are preserved commonly occur in subduction–accretion complexes (e.g., the Franciscan; (Wakabayashi 2015). Oceanic plateau basalts are better preserved as oceanic plateaux are more difficult to subduct; remnants of accreted oceanic plateaux are found, for example, all around the Pacific Ocean (Safonova and Santosh 2014). In the Archean, subduction of oceanic crust could have been more difficult, but accretion more likely (Davies 1992).

Although metamorphic rocks with a wide range of *T/P* ratios have survived since the Mesoarchean (Fig. 8c), orogenic eclogites are conspicuously absent from the Archean record and occur only sporadically in the Proterozoic until the Cryogenian, after which their occurrence, together with the appearance of blueschists, becomes widespread (Fig. 7). One reason why the preservation of orogenic eclogites should not be a first order problem is that buoyant felsic continental crust, within which they commonly occur as boudinaged relics, resists recycling into the mantle (Sizova *et al.* 2012, 2014; Wang *et al.* 2021). Subduction of this buoyant crust requires it to be strong enough to remain coupled to the downgoing slab until the metamorphic peak, when sufficient weakening must occur that it can decouple from the slab but not be lost to the mantle (Warren *et al.* 2008). The temporal distribution of eclogites and blueschists suggests

these conditions were met sporadically during the Paleoproterozoic and widely since the late Tonian, consistent with secular change in ambient mantle T_P (Brown 2014; Brown 2023). The gap in orogenic eclogites from the Statherian to the Ectasian was likely due to a plate slowdown (O'Neill *et al.* 2022), leading to warmer subduction.

It is commonly argued that information is increasingly lost going back through time due to erosion of the older rock record (Möller *et al.* 1995; Willigers *et al.* 2002), or more specifically as a result of emplacement of low *T/P* rocks (blueschists and eclogites) at high structural levels in orogens (Copley and Weller 2024). However, the depth of erosion in Proterozoic and Phanerozoic orogens is variable, and low *T/P* rocks are common in some deeply-eroded Phanerozoic orogens while older orogens do not necessarily expose deeper crust (Weller *et al.* 2021). Thus, if formed, some relicts of Archean orogenic eclogite should have survived. This conclusion is supported by the results of experiments using a 2D thermomechanical model that simulate oceanic subduction then continental collision at ambient mantle T_P >100 ºC warmer than the present day, which predict large-scale trench rollback and slab breakoff at depths that generally preclude formation of low *T/P* metamorphic rocks (Sizova *et al.* 2014; Perchuk *et al.* 2019). Thus, the absence of orogenic eclogites from the Archean rock record likely indicates that an appropriate tectonic setting was not available (Sizova *et al.* 2014; Chowdhury *et al.* 2020; Tamblyn *et al.* 2021).

By contrast, cratonic eclogites preserved in the lithospheric mantle record *T/P* of 180–220 ºC GPa^{-1}, comparable to Phanerozoic blueschists and orogenic eclogites (Aulbach and Smart 2023). However, although the mechanisms by which the cratonic lithospheric mantle formed and cratonic eclogites were preserved are uncertain, the peak *P–T* conditions locate them at depths above the lithosphere–asthenosphere boundary (Aulbach and Smart 2023). Thus, the low *T/P* values recorded by cratonic eclogites likely represent conditions during craton formation.

It is possible that warmer ambient mantle T_P (Herzberg *et al.* 2010; Herzberg 2022) combined with slower average metamorphic cooling rates (Willigers *et al.* 2002; Chowdhury and Chakraborty 2019; Brown *et al.* 2022; Zou *et al.* 2023) and a different tectonic style (Sizova *et al.* 2014; Chowdhury and Chakraborty 2019) earlier in Earth history could have led to more widespread overprinting of eclogites during exhumation, whereas cooler ambient mantle T_P and faster average cooling rates since the Mesoproterozoic (Zou *et al.* 2023) could have limited retrogression of such rocks. However, as was pointed out a long time ago by Coleman *et al.*

(1965), there are "eclogites and eclogites". Overprinting is common in eclogites characterized by higher *T/P* values, which are generally associated with high-pressure granulites and migmatites; these are the "Group B" eclogites of Coleman *et al.* (1965) that occur throughout the Proterozoic and Phanerozoic rock record (Wang *et al.* 2021). The overprinting, which is generally partial rather than complete, may be related to a combination of slower cooling rates and longer exhumation times for these eclogites (Wang *et al.* 2021). By contrast, overprinting is both less common and less pervasive in eclogites characterized by lower *T/P* values ("Group C" eclogites of (Coleman *et al.* 1965), which are characterized by faster cooling rates and shorter exhumation times (Wang *et al.* 2021). That eclogites with low *T/P* values are largely absent from the record during the mid-Proterozoic, a time when mountain belts tended to be hotter and thinner due to a warmer mantle (Spencer *et al.* 2021; Zou *et al.* 2023), should not be a surprise. Notwithstanding, overprinting should not generate bias through time.

The appearance of blueschists in the rock record has been interpreted to register a change to colder subduction and the beginning of the modern plate tectonic regime (Brown 2006, 2007a; Brown 2007b; Sizova *et al.* 2014). Alternatively, it has been proposed that blueschists have become more prevalent since the late Precambrian due to secular change in the composition of oceanic crust (Palin and White 2016), which became less magnesian because of secular cooling and decreased mantle melting (Johnson *et al.* 2014). This hypothesis is based on the calculated *P–T* stability of glaucophane, which is modelled to be stable in rocks with MgO contents ≤11.2 wt%, but is not predicted to form in rocks with higher MgO contents at low *T/P* (Palin and White 2016). However, more than half of basalt compositions in ancient greenstone belts have MgO-poor (≤11.2 wt%) compositions (dataset of Condie *et al.* (2016); $n = 3414$). Furthermore, such MgO-poor basalts occur as blocks in ophiolitic melanges along an inferred arc–passive continental margin suture formed at ca. 2.5 Ga in the North China Craton (Wang *et al.* 2019; Jiang *et al.* 2020). Thus, if tectonic settings that could have generated low thermal gradients were widespread during the Precambrian, blueschists would be expected to have formed, although whether they could have all been lost (recycled) is an open question. The absence of blueschists prior to the late Tonian was not due to an absence of suitable rock compositions but to the prevailing tectonic mode (Foley 2020).

Ultrahigh-pressure (UHP) metamorphic rocks are variably distributed but occur throughout the geological record since the Tonian with no protracted gaps (Brown and Johnson

2018, 2019a, b). By contrast, except for a single eclogite xenolith in a Paleoproterozoic carbonatite in the North China craton (Xu *et al.* 2018), UHP metamorphic rocks are absent from the rock record before the Cryogenian. Subduction of continental lithosphere to mantle depths requires that slab breakoff occurred after the leading edge of the continent had reached UHP conditions and below the subducting continent, otherwise the continental lithosphere could have been recycled back into the mantle (Sizova *et al.* 2014). This condition has only been met since the Cryogenian (Brown and Johnson 2019b). Consistent with this interpretation, there is no evidence from the mantle isotope record of recycled upper continental crust before the Phanerozoic (Doucet *et al.* 2020; Jackson and Macdonald 2022), which suggests that shallow slab breakoff or a change in subduction dynamics may have been the limiting factor in the secular distribution of UHP eclogites (Sizova *et al.* 2014; Foley 2020; Chowdhury *et al.* 2021; Gunawardana *et al.* 2024).

Archean oceanic crust

Our search for oceanic crust in the geological record found the oldest examples of non-subduction ophiolites that satisfy both geochemical and geological criteria for plate tectonic behaviour are the well-studied Palaeoproterozoic (c. 2 Ga) examples from Northern Scandinavia and Canada. The great majority of Archaean greenstones identified as potential ophiolites do not fall within the low Th/Nb oceanic basalt (OcB) array. Instead, they form trends towards continental crust indicative of continental intraplate settings (Fig. 3b-c). Part of the problem may be the informal expansion of the definition of ophiolite to allow submarine volcanism and associated subvolcanic intrusive rocks in continental rift zones to be included as ophiolites.

Moreover, even the rare 'ophiolites' that do satisfy geochemical criteria for oceanic crust commonly have geological criteria (e.g., matching 'ophiolitic dykes' with dykes intruding continental basement; presence of xenocryst older crustal zircons; presence of clastic, detrital sediments) that favour highly attenuated continental rift settings ahead of ocean ridges or plateaux. From a geochemical perspective, the most promising examples of oceanic crust are from the Baltic Shield, although these await full evaluation of geological criteria. Because of insufficient geochemical data, we did not consider a small number of terranes where the geological criteria point to an oceanic setting, for example the Aberdeen Lake Supracrustal Belt

in the Central Rae terrane, Canada (Hunter *et al.* 2018). Nor did we consider several examples of proposed oceanic crust that have experienced upper amphibolite facies metamorphism leading to Th mobility during high-temperature deformation, metamorphism and anatexis (Fig. 3 d, e). These amphibolites include Neoarchean examples from the North China Craton and Eoarchean examples from Northern Canada and Greenland, any of which could be found to have oceanic affinities following more detailed assessment. However, at the time of writing, we are not aware of any Archean greenstones that pass all our geochemical and geological tests for an oceanic crust origin.

The lava- and dyke-based study presented here is also consistent with studies of the deeper parts of ophiolite complexes that, although beyond the scope of this study, are typically less diagnostic and can even give misleading results. For example, although mantle tectonites in ophiolites are good plate tectonic indicators, they can be difficult to distinguish from metamorphosed and deformed ultramafic cumulates from plume-derived large igneous provinces. The fact that several of these proposed Archean oceanic mantle outcrops have since been shown to have a cumulate origin (Szilas *et al.* 2015; Waterton *et al.* 2022; Zhang and Szilas 2024) emphasises the likely dearth of oceanic lithosphere in the Archean. In our view, the only clear example of an Archean mantle tectonite lies within the chromites and peridotites of the c. 2.5 Ga Dongwanzi ophiolite (Kusky *et al.* 2004), although that is not of MOR-type.

It is difficult to escape the conclusion that almost all proposed examples of Archean oceanic crust were the product of plumes, resulting in mantle melting beneath variably extended continental lithosphere. With increased extension, the magmas had less and less crust to assimilate and the volcanic rocks thus appear increasingly oceanic in their geology and geochemistry. Eventually, in a subset of cases, the beta value approached infinity and oceanic crust, in the likely form of a volcanic plateau, was the result. The key question is whether that plateau developed into a stable and long-lived spreading axis, the crust from which has since been lost during subduction,or whether extension and oceanic crust generation stopped before any sizeable ocean formed. In the latter case, the volcanic plateau might subsequently have become accreted and preserved when the local tectonic regime reverted to convergence, but this would not be a plate tectonic indicator.

To understand better this Archean transition between rifting and potential spreading, an important consideration from an igneous perspective is the relative role of active (plume/uplift-

driven) versus passive (horizontal, tensional stress-driven) rifting (Merle 2011). The present understanding is that most of the Archean was dominated by active rifting, although the later stages of such rifting (i.e. at the continent–ocean transition) might still have developed a passive rifting component. Putirka (2016), using direct determinations of T_P from ultramafic and mafic Archean igneous rocks, obtained a bimodal T_P distribution made up of a larger (plume T_P) and a smaller (ambient T_P) peak which could be interpreted, in part at least, as reflecting contributions from both active and passive rifting. Combining T_P measurements with geochemical proxies of the type used in this study might provide useful new information on the transition from rifting to possible sea-floor spreading in the Archean.

Archean 'arc' magmatism

As with the search for oceanic crust, our search for arc magmatism in the Precambrian geological record finds the oldest clear example of a volcanic arc in the Paleoproterozoic (c. 2 Ga) Trans-Hudson Belt of Northern Canada. Here, volcanic arc magmas erupted during a long period of ocean closure as part of a tectonic (Wilson) cycle that included earlier sea floor spreading and subsequent terminal collision leading to the formation of the Nuna/Columbia supercontinent. However, in our geochemical evaluation of the Archean volcanic units purported to be subduction-related, we find most to be the products of interaction between intraplate magmas and crust. Of the remainder, Archean volcanic rocks related to active subduction are rare, but include the 3.12 Ga Whundo Terrane in the Pilbara craton and various units of c. 2.7 Ga age within the Superior Province. Although described as 'island arcs', these more closely resemble continental arcs on the projection used.

Further, there is good evidence for active arc magmatism in the Eoarchean, with parts of both the Isua and Nuvvuagittuq terranes having arc-like characteristics, although alternative, non-uniformitarian options that may explain the data still need to be fully addressed. An additional, but important, plate tectonic indicator is the inherited subduction signature found in lavas sourced from metasomatised mantle lithosphere and erupted in intraplate, post-subduction settings. Some of these can be traced to an earlier period of active subduction, whereas others cannot, the latter suggesting that subduction was more widespread than the relatively few convincing examples of active arc magmatism might imply.

There is insufficient space to cover the role of plutonic rocks in the search for plate tectonics, although much of the relevant Archean granitoid literature has been summarized recently, including by Halla *et al.* (2017), Moyen and Laurent (2018), Moyen (2020) and Laurent *et al.* (2024). However, the links between these granitoids and the different types of mafic–felsic volcanic series (non-arc, active arc and inherited arc) identified in Fig. 5 are less well understood, but considered briefly on the Th/Yb–Nb/Yb projection shown in Fig. 11. The starting point is the base diagram in Fig. 11a, which shows density contours based on the 566 granitoids with all three Th, Nb and Yb analyses from the Moyen and Laurent (2018) Archean granitoid database. Average values for the main granitoid types (from Table 2 of Moyen and Martin (2012)) all lie within the 80% contour and are closely spaced on this scale. Figs 9b–d then compares three examples of granitic rocks that are coeval with each of the three main types of Archean volcanic series:

(1) The intraplate trend (Fig. 11b) focuses on the East Pilbara greenstones in Fig. 5b, expanded to all suites in the c. 3.47–3.45 Ga age range, together with granodiorites from the coeval (c. 3.46 Ga) part of the Shaw batholith (Bickle *et al.* 1983). The BADR volcanic trend ends with overlap between rhyolitic volcanics and granodiorites, which can be inferred to represent the crustal end-members of a plume–crust interaction trend.

(2) The inherited subduction trend (Fig. 11c) focuses on the Mallina Basin (Bookingarra group) volcanic rocks in Fig. 5c (Smithies *et al.* 2004), together with data from the high-Mg diorite (sanukitoid) intrusives of similar age (c. 3 Ga) from the same tectonic setting (Smithies and Champion 2000). This SHMB–HMA volcanic trend extends towards the sanukitoids, which Smithies and Champion (2000) showed to have a mantle origin, formed by fractionation of the mantle derived SHMB series (coupled with variations in composition and melting of the SZLM source) with limited crustal input.

(3) The active arc trend (Fig. 11d) focuses on the 2.74 Ga Uchi–Confederation volcanic sequence in the Birch–Uchi greenstone belt plotted in Fig. 5f (Hollings and Kerrich 2000) together with the coeval hornblende tonalite-granodiorite component of the adjacent Berens River intrusive sub-province (Stone 1998; Stevenson *et al.* 2009). This volcanic BADR trend

ends with overlap with the tonalites and granodiorites, which would be expected, by analogy with present-day arcs, to be the product of interactions between mantle wedge-derived magma and continental crust in deep crustal hot zones and discrete magma chambers.

On the projection shown in Fig. 11b–d, the principal Archean plate tectonic indicator is the distinction made here (and, in part, by Smithies *et al.* (2018) between the mafic lavas of the subduction-related series with constantly high Th/Nb and the mafic intraplate lavas with low-high Th/Nb. However, as compositions become more felsic, the trends merge and their effectiveness as plate tectonic indicators becomes less. For these examples, the distinction between inherited subduction and active subduction is negligible, in which case the distinctive mineralogical and geochemical characteristics of sanukitoids described in detail by Smithies *et al.* (2019) provide an effective identifier of inherited subduction at decision point DP5 in Fig. 1. In terms of the granite classification of Moyen (2020), the granitoid end-members of the intraplate series are C (crustal) type, mainly low- and medium-pressure TTGs, which have little obvious tectonic significance, the granitoid endmembers of the inherited series are of the M (mantle) type, which have the tectonic significance noted above, and the active arc granitoid end-members of hybrid type, the significance of which will likely depend on whether or not the crustal input has masked the mantle-wedge-derived magma contributions.

Overall, the igneous data evaluated here indicate that crustal materials were almost certainly subducted into the Archean mantle, both into mantle wedges to produce active arc magmas and into sub-continental mantle lithosphere producing subduction signatures that were inherited by subsequent continental intraplate magmas. There is some periodicity to this process in areas studied to date, but a more complete picture awaits a broader geographic coverage and a more thorough tracing of inherited subduction signals back to their sources. Nevertheless, the rarity and ephemeral nature of subduction-related magmatic events in the Archean best supports the concept of short-lived episodes of convergence (Van Hunen and Moyen 2012), perhaps lasting just a few million years as modelled by Foley (2020), that only became of global extent in the Paleoproterozoic.

Metamorphism and plate tectonics

Metamorphism from the Neogene back to the mid-Tonian is characterized by two prominent features, a bimodal (or trimodal) normal distribution of *T/P* values with a prominent low-*T/P* peak (Fig. 9a,b), all known blueschists and most orogenic eclogites (Fig. 7). This period corresponds to the modern plate tectonic regime of Brown (2006). From the mid-Tonian back to the early Paleoproterozoic, the lower *T* peak is first diminished and then eliminated (Fig. 9c,d), corresponding to the Proterozoic plate tectonic regime of (Brown 2006), leaving an Archean era in which metamorphism is characterized by a single (unimodal) normal distribution of high *T/P* values (Fig. 9e,f) and uncertain tectonic mode. However, these data can also be explained by the variety of tectonic processes that operate in a stagnant-deformable (squishy) lid tectonic mode at higher ambient mantle T_P than today (Fig. 10; (Sizova *et al.* 2015). Overall, the distribution of metamorphic *T/P* has gradually became broader and more distinctly bimodal since the early Paleoproterozoic; orogenic eclogites are not known from the Archean rock record. The change from a unimodal distribution of metamorphic *T/P* values in the Archean to a distinctly bimodal distribution since the Mesoproterozoic has been interpreted as recording the emergence and evolution of plate tectonics during the Paleoproterozoic and Mesoproterozoic into its modern style due to secular cooling of the mantle (Holder *et al.* 2019; Brown *et al.* 2022).

We argue that the appearance of blueschists in the late Neoproterozoic and eclogites in the early Paleoproterozoic eras is not the result of bias introduced through recycling. However, the absence from the Archean rock record of these rock types, which are regarded by many as diagnostic of subduction, may be insufficient to falsify the hypothesis that plate tectonics has operated throughout geological history, given auxiliary assumptions (Cleland 2013) and secular changes in, for example, ambient mantle T_P and mantle degassing and regassing (Herzberg *et al.* 2010; Parai and Mukhopadhyay 2018). Notwithstanding, if we accept the metamorphic record at face value, an alternative hypothesis holds that the first appearance of eclogite then blueschist record fundamental shifts in global tectonics with secular cooling (Brown 2006; Stern 2008), consistent with other geological evidence in the Paleoproterozoic, including the occurrence of contemporary-style continent–continent collision in the 2 Ga Limpopo belt (Yin *et al.* 2020). Whether this was a change in the style of plate tectonics or a transition from sluggish lid to plate tectonics is uncertain (Höink *et al.* 2013; Fuentes *et al.* 2019).

An integrated perspective

An interesting outcome arising from these studies is the extent to which the igneous and metamorphic perspectives reach the same conclusions about the advent of widespread subduction and the emergence of global plate tectonics. Both perspectives recognise the breakup of several supercratons and their dispersion in the early Paleoproterozoic, followed by convergence and accretion leading to the creation of the Nuna/Columbia supercontinent in the late Palaeoproterozoic, as providing the first clear evidence of global plate tectonics. Based on a near-absence of thick volcanic arc sequences and extensive calc-alkaline intrusive systems (the igneous perspective) and of low *T/P* metamorphic rocks (the metamorphic perspective), neither approach finds support for anything other than short-lived and local plate-like behaviour in the Archean.

The igneous perspective highlights the possibility that much of Archean tectonics is based on crustal extension (divergence) and subsequent shortening (convergence), where crustal terranes may sometimes be extended sufficiently to form oceanic crust. Where this may have been the case, as in the Baltic Shield (Puchtel *et al.* 1998; Puchtel *et al.* 1999), the oceanic crust in question most resembles present-day oceanic plateaux and, while these may be accreted, there is no evidence for bona fide volcanic arcs. Overall, Archean arc volcanic sequences are rare and, although the presence of subduction-modified lithosphere supports the concept of Archean subduction, these likely reflect short-lived ('failed') subduction incapable of producing much arc volcanism (Smithies *et al.* 2018). This concept of local divergence and convergence driven by mantle flow is similar in several respects to the model of Bedard *et al.* (2013) for the Abitibi Belt in the southern Superior craton. Although it is conceivable that there were larger oceans than envisaged here and that Archean subduction dynamics resulted in a series of short-lived subduction events, we find no evidence for this interpretation.

From the metamorphic perspective, the principal consequence of these short-lived subduction episodes in the Archean is that the processes were essentially 'frozen' at the subduction initiation stage. Furthermore, if subduction was sluggish and drip-like, as modelled by Foley (2020), then the slab had more time to heat at shallow depths, inhibiting formation of low *T/P* metamorphic rocks. Thus, Archean subduction was likely of the 'hot subduction type', as proposed by Polat and Kerrich (2006) and others. Notably, hot subduction results in amphibolite facies metamorphism, not the blueschist or eclogite facies conditions that have been

the focus of the search for subduction-related metamorphism prior to the Proterozoic. Amphibolite facies oceanic basalts supporting this assertion may be found throughout the Pacific margins (Sorensen and Grossman 1989; Sorensen and Grossman 1993) (Fig. 2f) and in the metamorphic soles of many SSZ ophiolite complexes (Cowan *et al.* 2014).

In the Western Pacific forearcs, the type examples of modern subduction initiation, although blueschists record oceanic crust accretion during mature subduction (Maekawa *et al.* 1993; Tamblyn *et al.* 2019), amphibolites were accreted during the initial stages of subduction (Shiraki *et al.* 1978). Similarly, boninitic rocks with geochemical signatures of shallow slab melting in the amphibolite facies (e.g., high Hf/Sm) form the earliest Western Pacific protoarcs, whereas the more recent volcanic arcs carry signatures of deeper, garnet-facies slab melting and/or dehydration (low Hf/Sm and Hf/Yb) (Li *et al.* 2022). This may reflect the temporal change in the thermal gradient at the top of the subducting slab from higher *T/P* at subduction initiation to lower *T/P* as the mantle wedge cools. Thus, in the Archean, an absence of long-lived subduction could help explain the lack of low *T/P* metamorphic rocks.

The temporal evolution of tectonic style is presented schematically in Fig. 12, which shows a plot of divergence versus convergence over time. Depending on the extent of divergence, subsequent convergence yields different outcomes. At one end of the spectrum (Path 1), extension does not continue beyond the continental rift stage, in which case convergence creates a moderate *T/P* metamorphic fold and thrust belt with no (or limited) magmatism. With further extension, to an oceanic crust transition zone (Path 2), some of the resulting terrane may be accreted and partly underplated before terminal collision. Further divergence creates an oceanic plateau with no continental basement, but which does not develop into an ocean of significant size (Path 3). This may allow sufficient subduction to form a short-lived volcanic arc (protoarc) before collision, but under intermediate *T/P* (high-P amphibolite or granulite facies) conditions and without sufficient mantle flow or slab pull to drag the colliding margin to eclogite-facies depths. Paths 4 and 5 then represent closure of major ocean basins via long-lived subduction of oceanic lithosphere that likely created volcanic arcs. These two paths are interpreted to represent a global plate tectonic system, with the difference being the colder thermal gradients of Path 5 as recorded by the appearance of blueschists and ultrahigh pressure (UHP) metamorphic rocks in the late Neoproterozoic. The longer subduction continues, the lower the *T/P* and the greater the likelihood of blueschist or UHP metamorphism. We argue that

paths 1–3 are characteristic of most of the Archean, Path 4 is characteristic of at least parts of the Paleoproterozoic and Path 5 is characteristic of present-day long-lived subduction.

A possible late Archean to early Proterozoic tectonic transition

A plethora of geological, geochemical and geophysical data has been used to argue for a change in tectonic mode sometime during the Mesoarchean to Neoarchean (3.2–2.5 Ga), as reviewed recently by Cawood *et al.* (2022). Although a comprehensive review of the literature on this topic is beyond the scope of this article, we briefly consider the results and implications of a few recent studies.

The isotope systematics and trace-element geochemistry of Archean komatiites strongly indicate that the contemporary mantle comprised chemically diverse domains as relics of accretion and magma ocean crystallization. The disappearance of these mantle heterogeneities by the end of the Archean indicates they had largely been eliminated by up to 2 Gyr of convective mixing (Puchtel *et al.* 2022). Secular change in the isotopic composition of the mantle from the Archean to the Proterozoic includes a decrease in δ^{49}Ti in mantle-derived rocks from +0.053‰ around 3.8–3.5 Ga to +0.001‰ by c. 2.7 Ga, which corresponds to the modern depleted MORB mantle composition (Deng *et al.* 2023). This secular decrease in δ^{49}Ti through the Archean requires progressive recycling of both TTG and their residues, with mixing in the upper mantle sufficient to ensure isotopic homogeneity in subsequent mantle melting events (Deng *et al.* 2023). Furthermore, resolvable ^{142}Nd and ^{182}W anomalies present through the Archean were sufficiently diluted by the Proterozoic that they are unrecognisable (Carlson *et al.* 2019; Nakanishi *et al.* 2023). In each case, among several possible explanations, a transition from a precursor tectonic mode to plate tectonics is plausible. Additional support for such a transition comes from noble gas studies (particularly Xe) that show recycling was unlikely to have been effective before 2.8 Ga, and by 2.5 Ga the convecting mantle had shifted from net degassing to net regassing consistent with subduction of hydrated oceanic crust (Parai and Mukhopadhyay 2018; Péron and Moreira 2018; Zhang *et al.* 2024b).

Paleomagnetic data have been used to argue for differential motion between supercratons and/or cratons for short periods between the mid-Neoarchean and mid-Paleoproterozoic (Mitchell *et al.* 2014; Liu *et al.* 2021; Salminen *et al.* 2021), and for cratonic drift rates that were

comparable to or exceeded current plate velocities as far back as the Mesoarchean (Brenner *et al.* 2023; Kasbohm *et al.* 2023). Liu *et al.* (2021) propose that the data provide evidence for a fundamentally different style of geodynamics in the Neoarchean compared to the Proterozoic–Phanerozoic, whereas Salminen *et al.* (2021) interpret these data as evidence of plate tectonics. These contrasting interpretations may reflect datasets that are not global in extent, and both could be consistent with a transition to plate tectonics, which was likely completed as the Nuna megacontinent began to assemble (Wan *et al.* 2020). Consistent with this conclusion and the first widespread appearance of orogenic eclogites in the Paleoproterozoic crustal record, the first direct evidence of cold deep subduction into the lower mantle has recently been reported from mineral inclusions in sublithospheric diamonds retrieved from a kimberlite in the Slave craton (Zhang *et al.* 2024a).

Lastly, we consider how early subduction zones could have formed and propagated into a network of plate boundaries. On modern Earth, subduction initiation may be spontaneous and due to large lateral density contrasts across lithospheric weaknesses, occurring for example at transform plate boundaries or along a plume head margin, or induced by plate convergence, including polarity reversals (Stern and Gerya 2018). By contrast, initiation of the first subduction zones in the Hadean or Archean is poorly understood, with both endogenic (mantle plume) and exogenic (impact-driven) processes as plausible triggers (Gerya *et al.* 2015; Davaille *et al.* 2017; O'Neill *et al.* 2017; O'Neill *et al.* 2020).

In numerical models of contemporary Earth, subduction initiates where a density instability develops and where the local stress exceeds the yield stress (Rolf and Tackley 2011; Coltice 2023). Stronger lithosphere increases the probability of subduction initiation in the vicinity of continental margins (Ulvrova *et al.* 2019) or along microcontinental edges (Zhu *et al.* 2023). Although the collapse of passive margins is poorly understood, weakening by grain damage (reduction in grain size) is the likely mechanism of subduction initiation at such sites (Mulyukova and Bercovici 2018; Bercovici and Mulyukova 2021). The formation and stabilization of cratons may have been a prerequisite for propagating a plate boundary network. As Earth's mantle began to cool and cratonic lithosphere strengthened (Rey and Coltice 2008) and stabilized (Laurent *et al.* 2014; Aulbach and Smart 2023), new subduction could have initiated along their margins (Rey *et al.* 2024). Other factors including continental emergence (Flament *et al.* 2008), increased rates of sedimentation (Sobolev and Brown 2019) or the

deposition of dense banded iron formation (Zhang *et al.* 2023) could have facilitated the transition to global plate tectonics. As subduction zones lengthened and spread from one or more centers, a connected plate boundary network was arguably completed by the early Paleoproterozoic, although whether plate tectonics has been continuous since is contentious (Brown *et al.* 2020a; Stern 2020; Spencer *et al.* 2021; O'Neill *et al.* 2022; Roberts *et al.* 2022; Stern 2023).

The most likely interpretation of the changes discussed above is that they record different traces of a common cause (Cleland 2013)—the emergence of plate tectonics by the Proterozoic. Whether they do should be tested quantitatively using numerical models (e.g., Seales *et al.* 2022).

Concluding remarks

The distinctive petrological features of recent ocean crust, subduction-related magmatism and regional metamorphism generally cannot be unambiguously identified in the Archean geological record. Based on the petrological record, a global plate tectonic mode can plausibly be extended back to the Paleoproterozoic but not clearly into the Neoarchean. Whatever the mode, Archean mafic magmatism was dominantly related to plumes rather than divergent or convergent plate margins. Metamorphic rocks commonly considered diagnostic of subduction—blueschists and orogenic eclogites—are absent from the Archean. Overall, the Archean metamorphic record is consistent with a stagnant-deformable (or squishy) lid (Sizova *et al.* 2015; Lourenço *et al.* 2020). However, the formation of Neoarchean supercratons requires mobility, supporting a sluggish lid (Fuentes *et al.* 2019) or multi-mode regime, such as lid and plate (Capitanio *et al.* 2019a).

Other types of geochemical and geophysical data record secular changes, but these occur at different times, from before the Mesoarchean into the early Paleoproterozoic, suggesting a long transition to global plate tectonics. Thus, from a petrological perspective, global plate tectonics is probably a Paleoproterozic and younger phenomenon, contrary to results of recent thermal modeling (Seales and Lenardic 2020; Seales *et al.* 2022). That interpretations based on the Archean petrological record and the modelling seemingly contradict provides motivation for future research.

Acknowledgements We thank Richard Arculus, Keith Putirka and Hugh Rollinson for review comments; any remaining errors or misconceptions are ours.

Author contributions MB: conceptualization (lead – equal), data curation (lead), formal analysis (lead – equal), investigation (lead – equal), methodology (equal), writing – original draft (lead – equal), writing – review & editing (equal); JAP: conceptualization (lead – equal), formal analysis (lead – equal), investigation (lead – equal), methodology (equal), writing – original draft (lead – equal), review & editing (equal); TEJ: conceptualization (supporting), formal analysis (supporting), investigation (supporting), methodology (equal), writing – review & editing (equal).

Funding M.B. and T.E.J. acknowledge funding from Australian Research Council Discovery Project DP200101104 and support from the State Key Laboratory for Geological Processes and Mineral Resources, China University of Geosciences, Wuhan (Open Fund GPMR201903).

Competing interests The authors declare that they have no known competing financial interests or personal relationships that could have appeared to influence the work reported in this paper.

Data availability The dataset of November 3, 2023, is provided in the Supplementary material as Table S1. The Python script used to calculate the LOWESS curves, the 95th and 5th percentiles of the data, and the change points is provided as Supplementary material Text file S1. The KDE plots that identify the most significant change points derived from bootstrap sampling using a CUSUM model are shown in Fig. S1.

Scientific editing by

Figure captions

Fig. 1. Flow diagram summarizing how Archean volcanic rocks can be assigned to process and hence to tectonic setting using Th/Nb in conjunction with geological and other criteria. According to this methodology, there are three routes to potential plate tectonic indicators: (1)

the green route recognises oceanic crust and oceanic supracrustal magmatism such as oceanic islands and oceanic plateaux as a necessary requirement for plate tectonics; (2) the red route recognises volcanic arc magmas that are the expected products of active subduction; and (3) the purple route recognises volcanic arc signatures in non-subduction settings that are the result of post-subduction inheritance via storage in sub-continental lithospheric mantle. The blue route identifies magmas from large igneous provinces and other intraplate settings that are independent of plate tectonic processes. Non-uniformitarian, non-plate tectonic alternatives to subduction, for which there is theoretical evidence but no clear examples, are represented by dashed blue lines. Routes diverge at decision points, with each decision marked by a number (See Table 1 for details). Note that, for proper use, the basic principles of geochemical fingerprinting need to be applied. In particular: (1) sample selection should be as representative as possible, ideally (for volcanic rocks) following the construction of a lava stratigraphy or (for dykes and sills) following mapping and recording the orientations of the intrusive rocks; (2) the least altered samples should be selected from each lava unit or dyke swarm and preparation should include removal of weathered edges and veins; (3) analysis using ICP-MS or similar quality techniques should be undertaken with appropriate care, using international standards (e.g., low abundance basalt such as BIR-1 for low-abundance unknowns) and blanks to quantify accuracy and detection limits, respectively; (4) a quality check should be used to filter out bad analyses, including those with undissolved minor minerals such as zircon; (5) the data should be assigned a rock-type name using TAS or its immobile equivalent and mafic rocks (basaltic and basaltic andesite) selected for the initial plot (BADR series can also be plotted, as in some parts of this study, but note that the defined fields and probabilities apply only to mafic rocks); (6) a check for Th, Nb and Yb mobility should be carried out and used (if necessary) in conjunction with decision point 3b; and (7) plate tectonic assignments should be made by combining geochemistry with geology and other parameters as laid out in this diagram and Table 1. Although the decision point criteria can be expanded as new methodologies are developed, we recommend keeping Th/Nb as the primary criterion as it the most insensitive LILE/HFSE ratio to melting, source enrichment and depletion, and alteration.

Fig. 2. Use of the crustal proxy diagram, Th/Yb v Nb/Yb (Pearce 2008; Pearce *et al.* 2021), for identifying oceanic crust in the geologic record. (a) Combined data for mid-ocean ridge

(MORB), oceanic plateau (OPB) and ocean island basalts (OIB) are used to define the MORB–OPB–OIB array (here termed the Oceanic Basalt, OcB, array). Correctly assigned past oceanic crust should plot fully in that array. The parallel and higher Th/Nb array, which is based on volcanic arc basalts (VAB), also contains almost all continental crust, including felsic continental crust (FCC). (b) Data field for Phanerozoic Large Igneous Provinces (LIP) basalts with estimated 95% and 99.7% contours (equivalent to 2σ and 3σ normal distribution boundaries), highlighting the overlap between these non-plate tectonic indicators and the OcB field containing the ocean crust plate tectonic indicators. (c) Examples of Phanerozoic oceanic plateaux as Archean oceanic crust comparators. (d) A typical example (from the c. 60–55 Ma North Atlantic Igneous Province) of the transition from pre-rift through rift to oceanic plateau showing how the compositions become more 'oceanic' with increasing attenuation. (e) Models for assimilation and fractional crystallization (AFC), partial melting and mantle depletion explaining some of the observed variations. (f). The array co-ordinates and data in (a) and (b) are from Pearce *et al.* (2021), and modelling in (d) is from Supplement B in the same paper. For data sources, see the references in the text.

Fig. 3. Application of the Th/Yb v Nb/Yb projection to the search for Archean oceanic crust. (a) Data from the oldest (Paleoproterozoic), best-defined ophiolites for comparison with Archean examples, demonstrating that these lie fully within and along the MORB–OPB–OIB array, the principal geochemical oceanic crust characteristic. (b) Shows proposed Archaean oceanic crust that plots on plume-crust interaction trends rather than within the oceanic crust array. (c) Plots Archean 'MORB-OIB' complexes that have other origins according to their Th/Nb characteristics. (d and e) Highlight amphibolites that could have an oceanic crust origin but their true character is masked by high temperature metasomatism. (f) Shows the most probable examples of Archean oceanic crust, but which still require further checks to distinguish them from highly attenuated continental rift settings. For data sources, see the text.

Fig. 4. The basis of the methodology for using the crustal proxy diagram, Th/Yb v Nb/Yb, for identifying subduction in the Archean geologic record. (a) Gives further detail on the volcanic arc basalt (VAB) array, including averages and fields for oceanic (Oc) arc basalts and continental (Cont) arc basalts. (b) Includes the field for Phanerozoic Large Igneous Provinces (LIPs) as in

Fig. 2b, here highlighting the LIP–VAB overlap. (c) Provides examples of low-high Th/Nb resulting from plume–crust interactions. (d) Provides examples of low-high Th/Nb resulting from interaction resulting from plume–SZLM (subduction-modified continental lithosphere) interactions. (e) Shows examples of active arc volcanism highlighting the range of compositions forming the VAB array and emphasising their common high Th/Nb character. (f) Shows examples of volcanism in intraplate settings with high Th/Nb as evidence of subduction inheritance due to SZLM melting. Where possible, the full BADR (basalt–basaltic andesite, andesite, dacite–rhyolite) sequence has been shown, rather than just the basic rocks. For data sources, see the text.

Fig. 5. Application of the Th/Yb v Nb/Yb projection in the search for Archean subduction showing: (a) the oldest, best-defined Paleoproterozoic arc volcanic province for comparison with Archean examples; (b) Archean examples of low-high Th/Nb indicative of plume–crust interaction; (c) examples of high Th/Nb subduction inheritance from Archean SZLM sources; (d) a possible example of Archean plume–lithosphere interaction; (e) the best examples of potential active Archean volcanic arcs with diagnostic high Th/Nb; and (f) Eoarchean examples of potential arc volcanism, but subject to the possibility of explanation by non-uniformitarian processes. For BADR symbols, see Fig. 4a. For data sources, see the text.

Fig. 6. (a) *P–T* data used in this study. The dataset comprises 728 localities of which 197 are new (dark grey) and the remainder (light grey) are data carried over from the previous dataset (Brown and Johnson 2019a). Both types of data have similar distributions suggesting that the dataset is likely representative of the preserved metamorphic rock record. (b) Conditions of peak metamorphism for 728 localities with robust pressure (*P*), temperature (*T*), and age grouped by type, with representative thermal gradients (purple dashed lines). Three types of metamorphism are distinguished based on thermobaric ratios (*T/P*): high *T/P* metamorphism (*T/P* > 775°C GPa^{-1}, 293 localities shown in red), intermediate *T/P* metamorphism (*T/P* = 375−775°C GPa^{-1}, 198 localities shown in orange), and low *T/P* metamorphism (*T/P* < 375°C GPa^{-1}, 237 localities shown in blue). (c) A *P–T* plot of data for blueschists and orogenic eclogites shows that these rocks are mostly <850 Ma in age and dominantly of low *T/P* type. (d) A *P–T* plot of data <850 Ma in age—the period for which there is consensus that plate tectonics has been the tectonic

mode operating on Earth—contoured for density (contours are smooth kernel density estimates for which the bandwidth was computed automatically using the DensityPlot function in Wolfram Mathematica) to emphasize the characteristic bimodality of crustal metamorphism related to plate tectonics.

Fig. 7. Histogram of ages and probability density function for metamorphism at 728 localities. The vertical orange bars represent natural breaks in the time series that separate the four supercontinent cycles (the current post-Pangean cycle is unlabelled) and the supercraton cycle of the late Archean and early Paleoproterozoic.

Fig. 8. (a) Metamorphic temperature (*T*), (b) metamorphic pressure (*P*), and (c) metamorphic thermobaric ratio (*T/P*) for 728 localities plotted against age. Locally weighted scatterplot smoothing (LOWESS) curves are shown in solid blue and the 95th and 5th percentiles of the data are shown in dashed blue. Significant changepoints for each of *T*, *P* and *T/P* are shown in magenta; all three variables show changepoints at around 2.5 Ga, 1.9–1.8 Ga, 1.1–1.0 Ga, 0.4 Ga and 0.08 Ga. Abbreviations in the top row are: C, Cenozoic; M, Mesozoic; P, Paleozoic; NP, Neoproterozoic; MP, Mesoproterozoic; PP, Paleoproterozoic; NA, Neoarchean; MA, Mesoarchean; PA, Paleoarchean; and, EA, Eoarchean. Abbreviations in the second row are: E, Ediacaran; C, Cryogenian; To, Tonian; Ste, Stenian; Ec, Ectasian; Ca, Calymmian; Sta, Statherian; Or, Orosirian; Rh, Rhyacian; and, Si, Siderian.

Fig. 9. Histograms and probability distribution functions (PDFs) for *T/P* (°C GPa^{-1}) plotted logarithmically. (a) Data >2.85 Ga in age define a relatively narrow single (unimodal) normal distribution (mean $\log_{10} T/P = 2.93 \pm 0.25$ (2 s.d.)); (b) data for the period 2.85 to 2.25 Ga represent a broad single (unimodal) normal distribution (mean $\log_{10} T/P = 2.97 \pm 0.31$ (2 s.d.)); (c) data for the period 2.25 to 1.35 Ga exhibit a broad unimodal left-skewed distribution extending towards lower *T/P* than the Archean data; (d) data for the period 1.35 to 0.85 Ga have a uniform distribution but show the development of a distinct low *T/P* mode that is not apparent before 1.35 Ga in age; (e) data for the period 0.85 to 0.195 Ga define a broad trimodal distribution (i.e. a mixture of three normal distributions with mean $\log_{10} T/P$ values of 2.99 ± 0.26, 2.67 ± 0.36, and 2.35 ± 0.20 (2 s.d.)), with the most prominent mode at lowest *T/P*; and (f)

data <0.195 Ga in age show a broad bimodal normal distribution, with distinct lower and higher *T/P* peaks (i.e. a mixture of two normal distributions with mean $\log_{10}$ *T/P* values of 2.94 ± 0.27 and 2.45 ± 0.28 (2 s.d.)).

Fig. 10. (a) Natural *P–T* data older than 2.25 Ga in age—a period for which there is no consensus that plate tectonics was the tectonic mode operating on Earth. (b) A *P–T* plot for 545 markers taken from different settings in an experiment performed using a 2D coupled petrological-thermomechanical tectono-magmatic numerical model of a stagnant-deformable lid tectonic mode with initial conditions appropriate to the Archean (Sizova *et al.* 2015).

Fig. 11. Examples of relationships between Archean granitoid intrusions and the volcanic routes to plate tectonics used in Figs 1-5. Abbreviations for mafic magma types are from Figs 2 and 4; A-FCC is the Archaean Felsic Continental Crust estimate used in Figs 3 and 5. Fig. 11a repeats the crustal proxy diagram used in Figs 2-5 but with added granitoid information, namely the distribution of granitoid data used by Moyen and Laurent (2018) and some specific granitoid averages from Moyen and Martin (2012): L-, M- and U-TTG refer to 'low, medium and high pressure' tonalite–trondhjemite–granodiorite bodies. Fig. 11b gives a type example of intraplate (plume-related) magma evolution (the blue route in Fig. 1) with no plate tectonic connotations and– typically crustal (C-type) granitoid end members. Fig 11c gives a type example of inherited SZLM-sourced magma evolution (the purple route in Fig. 1) with indirect plate tectonic connotations; note that the role of crust in the 'SZLM-crust interaction' trend is actually very limited with mantle (M-type) granitoids the norm for this group. Fig 11d gives a type example of active arc magma evolution (the red route in Fig. 1) with direct plate tectonic connotations and (C-M) hybrid granitoid end members. See the text for references to the sources and interpretations of granitoid data.

Fig. 12. A plot of divergence v convergence over time showing how increasing timescales of divergence, and hence convergence, can influence both the magmatic and metamorphic indicators of plate tectonics discussed in this publication. The shorter cycles (1-2) give negative plate tectonic signals; intermediate cycles (3) can give positive plate tectonic signals but via local divergence–convergence events; while the longest cycles (4-5) both give positive plate tectonic

signals and require divergence–convergence events on a global scale (i.e. plate tectonics). See text for discussion).

Table 1. Detail on decision points (DP) for identification of plate tectonic signatures as represented in the flow chart in Fig. 1.

References

1981. Archean Life. *Developments in Precambrian Geology*, 261-273.
Agard, P., Soret, M., Bonnet, G., Ninkabou, D., Plunder, A., Prigent, C. and Yamato, P. 2023. Subduction and Obduction Processes: The Fate of Oceanic Lithosphere Revealed by Blueschists, Eclogites, and Ophiolites. *Compressional Tectonics: Plate Convergence to Mountain Building*, **1**, 21-45.
Anonymous 1972. Penrose field conference on ophiolites. *Geotimes*, **17**, 24-25.
Arculus, R.J. 2003. Use and abuse of the terms calcalkaline and calcalkalic. *Journal of Petrology*, **44**, 929–935.
Aulbach, S. and Arndt, N.T. 2019. Eclogites as palaeodynamic archives: evidence for warm (not hot) and depleted (but heterogeneous) Archaean ambient mantle. *Earth and Planetary Science Letters*, **505**, 162-172.
Aulbach, S. and Smart, K.A. 2023. Petrogenesis and Geodynamic Significance of Xenolithic Eclogites. *Annual Review of Earth and Planetary Sciences*, **51**, 521-549.
Ayer, J., Amelin, Y., Corfu, F., Kamo, S., Ketchum, J., Kwok, K. and Trowell, N. 2002. Evolution of the southern Abitibi greenstone belt based on U–Pb geochronology: autochthonous volcanic construction followed by plutonism, regional deformation and sedimentation. *Precambrian Research*, **115**, 63-95.
Babechuk, M.G. and Kamber, B.S. 2011. An estimate of 1.9 Ga mantle depletion using the high-field-strength elements and Nd–Pb isotopes of ocean floor basalts, Flin Flon Belt, Canada. *Precambrian Research*, **189**, 114-139.
Baragar, W.R. 1966. Geochemistry of the Yellowknife volcanic rocks. *Canadian Journal of Earth Sciences*, **3**, 9-30.
Barnes, S.J., van Kranendonk, M.J. and Sonntag, I. 2012. Geochemistry and tectonic setting of basalts from the Eastern Goldfields Superterrane. *Australian Journal of Earth Sciences*, **59**, 707-735, https://doi.org/10.1080/08120099.2012.687398.
Beall, A.P., Moresi, L. and Cooper, C.M. 2018. Formation of cratonic lithosphere during the initiation of plate tectonics. *Geology*, **46**, 487-490, https://doi.org/10.1130/G39943.1.
Bedard, J.H., Harris, L.B. and Thurston, P.C. 2013. The hunting of the snArc. *Precambrian Research*, **229**, 20-48.
Bédard, J.H. 2006. A catalytic delamination-driven model for coupled genesis of Archaean crust and sub-continental lithospheric mantle. *Geochimica et Cosmochimica Acta*, **70**, 1188-1214.

Bédard, J.H. 2024. A gradual Proterozoic transition from an Unstable Stagnant Lid to the modern Plate Tectonic system. The Geological Society of London, jgs2024-2023.
Bédard, J.H. and Harris, L.B. 2014. Neoarchean disaggregation and reassembly of the Superior craton. *Geology*, **42**, 951-954.
Bercovici, D. and Ricard, Y. 2014. Plate tectonics, damage and inheritance. *Nature*, **508**, 513-516.
Bercovici, D. and Mulyukova, E. 2021. Evolution and demise of passive margins through grain mixing and damage. *Proceedings of the National Academy of Sciences*, **118**, e2011247118.
Bickle, M., Nisbet, E. and Martin, A. 1994. Archean greenstone belts are not oceanic crust. *The Journal of Geology*, **102**, 121-137.
Bickle, M., Bettenay, L., Barley, M., Chapman, H., Groves, D., Campbell, I. and De Laeter, J. 1983. A 3500 Ma plutonic and volcanic calc-alkaline province in the Archaean East Pilbara Block. *Contributions to Mineralogy and Petrology*, **84**, 25-35.
Bjorkman, K.E., Lu, Y., McCuaig, T.C., Kemp, A.I. and Hollings, P. 2024. Linked evolution and in situ growth of the Wabigoon superterrane, Superior Craton: evidence from zircon U-Pb isotopes and whole-rock geochemistry. *Precambrian Research*, **404**, 107341.
Boehnke, P., Bell, E.A. *et al.* 2018. Potassic, high-silica Hadean crust. *Proceedings of the National Academy of Sciences of the United States of America*, **115**, 6353-6356, https://doi.org/10.1073/pnas.1720880115.
Boily, M. and Dion, C. 2002. Geochemistry of boninite-type volcanic rocks in the Frotet-Evans greenstone belt, Opatica subprovince, Quebec: implications for the evolution of Archaean greenstone belts. *Precambrian Research*, **115**, 349-371.
Bowring, S.A. and Williams, I.S. 1999. Priscoan (4.00–4.03 Ga) orthogneisses from northwestern Canada. *Contributions to Mineralogy and Petrology*, **134**, 3-16.
Brenner, A.R., Fu, R.R., Kylander-Clark, A.R., Hudak, G.J. and Foley, B.J. 2023. Reply to Mitchell and Jing: True polar wander alone is insufficient to drive measured Paleoarchean lithospheric motions. *Proceedings of the National Academy of Sciences*, **120**, e2219560120.
Brown, M. 1993. P–T–t evolution of orogenic belts and the causes of regional metamorphism. *Journal of the Geological Society*, **150**, 227-241.
Brown, M. 2001. From microscope to mountain belt: 150 years of petrology and its contribution to understanding geodynamics, particularly the tectonics of orogens. *Journal of Geodynamics*, **32**, 115-164.
Brown, M. 2006. Duality of thermal regimes is the distinctive characteristic of plate tectonics since the Neoarchean. *Geology*, **34**, 961-964.
Brown, M. 2007a. Metamorphism, plate tectonics, and the supercontinent cycle. *Earth Science Frontiers*, **14**, 1-18.
Brown, M. 2007b. Metamorphic conditions in orogenic belts: a record of secular change. *International Geology Review*, **49**, 193-234.
Brown, M. 2010. Paired metamorphic belts revisited. *Gondwana Research*, **18**, 46-59.
Brown, M. 2014. The contribution of metamorphic petrology to understanding lithosphere evolution and geodynamics. *Geoscience Frontiers*, **5**, 553-569, https://doi.org/10.1016/j.gsf.2014.02.005.
Brown, M. 2023. Some thoughts about eclogites and related rocks. *European Journal of Mineralogy*, **35**, 523-547.

Brown, M. and Johnson, T. 2018. Secular change in metamorphism and the onset of global plate tectonics. *American Mineralogist*, **103**, 181-196.
Brown, M. and Johnson, T. 2019a. Time's arrow, time's cycle: Granulite metamorphism and geodynamics. *Mineralogical Magazine*, **83**, 323-338.
Brown, M. and Johnson, T. 2019b. Metamorphism and the evolution of subduction on Earth. *American Mineralogist*, **104**, 1065-1082.
Brown, M. and Johnson, T. 2019c. Global age, temperature and pressure data for secular change in metamorphism. *EarthChem Library, DOI*, **10**.
Brown, M., Johnson, T. and Gardiner, N.J. 2020a. Plate Tectonics and the Archean Earth. *Annual Review of Earth and Planetary Sciences*, 291-320.
Brown, M., Kirkland, C.L. and Johnson, T.E. 2020b. Evolution of geodynamics since the Archean: Significant change at the dawn of the Phanerozoic. *Geology*, **48**, 488-492, https://doi.org/10.1130/G47417.1.
Brown, M., Johnson, T. and Spencer, C.J. 2022. Secular changes in metamorphism and metamorphic cooling rates track the evolving plate-tectonic regime on Earth. *Journal of the Geological Society*, **179**, jgs2022-2050.
Buchanan, P.C., Koeberl, C. and Reimold, W.U. 1999. Petrogenesis of the Dullstroom formation, Bushveld magmatic province, South Africa. *Contributions to Mineralogy and Petrology*, **137**, 133-146.
Cannat, M., Sauter, D. *et al.* 2006. Modes of seafloor generation at a melt-poor ultraslow-spreading ridge. *Geology*, **34**, 605-608.
Capitanio, F.A., Nebel, O., Cawood, P.A., Weinberg, R.F. and Chowdhury, P. 2019a. Reconciling thermal regimes and tectonics of the early Earth. *Geology*, **47**, 923-927, https://doi.org/10.1130/G46239.1.
Capitanio, F.A., Nebel, O., Cawood, P.A., Weinberg, R.F. and Clos, F. 2019b. Lithosphere differentiation in the early Earth controls Archean tectonics. *Earth and Planetary Science Letters*, **525**, https://doi.org/10.1016/j.epsl.2019.115755.
Carlson, R.W., Garçon, M., O'neil, J., Reimink, J. and Rizo, H. 2019. The nature of Earth's first crust. *Chemical Geology*, **530**, 119321.
Castillo, P.R. 2012. Adakite petrogenesis. *LITHOS*, **134**, 304-316.
Cawood, P.A., Chowdhury, P., Mulder, J.A., Hawkesworth, C.J., Capitanio, F.A., Gunawardana, P.M. and Nebel, O. 2022. Secular evolution of continents and the Earth system.
Chauvel, C., Arndt, N., Kielinzcuk, S. and Thom, A. 1987. Formation of Canadian 1.9 Ga old continental crust. I: Nd isotopic data. *Canadian Journal of Earth Sciences*, **24**, 396-406.
Choi, S.H., Mukasa, S.B., Ravizza, G., Fleming, T.H., Marsh, B.D. and Bédard, J.H. 2019. Fossil subduction zone origin for magmas in the Ferrar Large Igneous Province, Antarctica: Evidence from PGE and Os isotope systematics in the Basement Sill of the McMurdo Dry Valleys. *Earth and Planetary Science Letters*, **506**, 507-519.
Chowdhury, P. and Chakraborty, S. 2019. Slow Cooling at Higher Temperatures Recorded within High- P Mafic Granulites from the Southern Granulite Terrain, India: Implications for the Presence and Style of Plate Tectonics near the Archean-Proterozoic Boundary. *Journal of Petrology*, **60**, 441-485, https://doi.org/10.1093/petrology/egz001.

Chowdhury, P., Gerya, T. and Chakraborty, S. 2017. Emergence of silicic continents as the lower crust peels off on a hot plate-tectonic Earth. *Nature Geoscience*, **10**, 698-703, https://doi.org/10.1038/ngeo3010.
Chowdhury, P., Chakraborty, S. and Gerya, T.V. 2021. Time will tell: secular change in metamorphic timescales and the tectonic implications. *Gondwana Research*, **93**, 291-310.
Chowdhury, P., Chakraborty, S., Gerya, T.V., Cawood, P.A. and Capitanio, F.A. 2020. Peel-back controlled lithospheric convergence explains the secular transitions in Archean metamorphism and magmatism. *Earth and Planetary Science Letters*, **538**, 116224.
Cipar, J.H., Garber, J.M., Kylander-Clark, A.R. and Smye, A.J. 2020. Active crustal differentiation beneath the Rio Grande Rift. *Nature Geoscience*, **13**, 758-763.
Cleland, C.E. 2013. Common cause explanation and the search for a smoking gun. *Geological Society of America Special Papers*, **502**, 1-9.
Coleman, R., Lee, D.E., Beatty, L. and Brannock, W.W. 1965. Eclogites and eclogites: their differences and similarities. *Geological Society of America Bulletin*, **76**, 483-508.
Coltice, N. 2023. Tectonics is a Hologram *Dynamics of Plate Tectonics and Mantle Convection*. Elsevier, 105-125.
Coltice, N., Husson, L., Faccenna, C. and Arnould, M. 2019. What drives tectonic plates? *Science Advances*, **5**, eaax4295.
Condie, K.C. and Stern, R.J. 2023. Ophiolites: Identification and tectonic significance in space and time. *Geoscience Frontiers*, **14**, 101680.
Condie, K.C., Aster, R.C. and Van Hunen, J. 2016. A great thermal divergence in the mantle beginning 2.5 Ga: Geochemical constraints from greenstone basalts and komatiites. *Geoscience Frontiers*, **7**, 543-553.
Copley, A. and Weller, O.M. 2024. Modern-style continental tectonics since the early Archean. *Precambrian Research*, **403**, 107324.
Corcoran, P., Mueller, W. and Kusky, T. 2004. Inferred ophiolites in the Archean Slave craton. *Developments in Precambrian Geology*, **13**, 363-404.
Corcoran, P.L. 2001. Physical volcanology, geochemistry, and tectonic evolution of three selected areas in the Point Lake and Beaulieu River volcanic belts, Slave Province, Northwest Territories, Canada.
Corrigan, D., Pehrsson, S., Wodicka, N. and De Kemp, E. 2009. The Palaeoproterozoic Trans-Hudson Orogen: a prototype of modern accretionary processes. *Geological Society, London, Special Publications*, **327**, 457-479.
Cousens, B.L. 2000. Geochemistry of the archean Kam group, Yellowknife greenstone belt, slave province, Canada. *The Journal of Geology*, **108**, 181-197.
Cowan, R., Searle, M. and Waters, D. 2014. Structure of the metamorphic sole to the Oman Ophiolite, Sumeini Window and Wadi Tayyin: implications for ophiolite obduction processes. *Geological Society, London, Special Publications*, **392**, 155-175.
Crameri, F., Conrad, C.P., Montési, L. and Lithgow-Bertelloni, C.R. 2019. The dynamic life of an oceanic plate. *Tectonophysics*, **760**, 107-135.
Dalton, C.A., Langmuir, C.H. and Gale, A. 2014. Geophysical and geochemical evidence for deep temperature variations beneath mid-ocean ridges. *Science*, **344**, 80-83.
Davaille, A., Smrekar, S. and Tomlinson, S. 2017. Experimental and observational evidence for plume-induced subduction on Venus. *Nature Geoscience*, **10**, 349-355.

Davies, G.F. 1992. On the emergence of plate tectonics. *Geology*, **20**, 963-966.
Davis, J. and Hawkesworth, C. 1994. Early calc-alkaline magmatism in the Mogollon-Data Volcanic Field, New Mexico, USA. *Journal of the Geological Society*, **151**, 825-843.
de Wit, M.J. 2004. Archean greenstone belts do contain fragments of ophiolites. *Developments in Precambrian Geology*, **13**, 599-614.
Defant, M.J. and Drummond, M.S. 1990. Derivation of some modern arc magmas by melting of young subducted lithosphere. *Nature*, **347**, 662-665.
Deng, Z., Schiller, M. *et al.* 2023. Earth's evolving geodynamic regime recorded by titanium isotopes. *Nature*, **621**, 100-104.
DePaolo, D.J. 1981. Neodymium isotopes in the Colorado Front Range and crust–mantle evolution in the Proterozoic. *Nature*, **291**, 193-196.
Dewey, J., Kiseeva, E.S., Pearce, J. and Robb, L. 2021. Precambrian tectonic evolution of Earth: an outline. *South African Journal of Geology 2021*, **124**, 141-162.
Dhuime, B., Hawkesworth, C.J., Cawood, P.A. and Storey, C.D. 2012. A change in the geodynamics of continental growth 3 billion years ago. *Science*, **335**, 1334-1336, https://doi.org/10.1126/science.1216066.
Dilek, Y. and Furnes, H. 2011. Ophiolite genesis and global tectonics: Geochemical and tectonic fingerprinting of ancient oceanic lithosphere. *Bulletin*, **123**, 387-411.
Dilek, Y. and Furnes, H. 2014. Ophiolites and their origins. *Elements*, **10**, 93-100.
Doucet, L.S., Laurent, O., Ionov, D.A., Mattielli, N., Debaille, V. and Debouge, W. 2020. Archean lithospheric differentiation: Insights from Fe and Zn isotopes. *Geology*, **48**, 1028-1032, https://doi.org/10.1130/G47647.1.
England, P.C. and Richardson, S. 1977. The influence of erosion upon the mineral fades of rocks from different metamorphic environments. *Journal of the Geological Society*, **134**, 201-213.
Ernst, R. and Bleeker, W. 2010. Large igneous provinces (LIPs), giant dyke swarms, and mantle plumes: significance for breakup events within Canada and adjacent regions from 2.5 Ga to the Present. *Canadian Journal of Earth Sciences*, **47**, 695-739.
Ernst, R.E. 2014. *Large igneous provinces*. Cambridge University Press.
Fan, J. and Kerrich, R. 1997. Geochemical characteristics of aluminum depleted and undepleted komatiites and HREE-enriched low-Ti tholeiites, western Abitibi greenstone belt: A heterogeneous mantle plume-convergent margin environment. *Geochimica et Cosmochimica Acta*, **61**, 4723-4744.
Finlayson, V.A., Haller, M. *et al.* 2023. Oceanic and Continental Lithospheric Mantle in the 1.95-Ga Jormua Ophiolite Complex, Finland: Implications for Mantle and Crustal Evolution. *Journal of Petrology*, **64**, egad080.
Fischer, R. and Gerya, T. 2016. Early Earth plume-lid tectonics: A high-resolution 3D numerical modelling approach. *Journal of Geodynamics*, **100**, 198-214, https://doi.org/10.1016/j.jog.2016.03.004.
Fitton, J., Larsen, L., Saunders, A., Hardarson, B. and Kempton, P. 2000. Palaeogene continental to oceanic magmatism on the SE Greenland continental margin at 63 N: a review of the results of Ocean Drilling Program Legs 152 and 163. *Journal of Petrology*, **41**, 951-966.
Flament, N., Coltice, N. and Rey, P.F. 2008. A case for late-Archaean continental emergence from thermal evolution models and hypsometry. *Earth and Planetary Science Letters*, **275**, 326-336, https://doi.org/10.1016/j.epsl.2008.08.029.

Foley, B.J. 2018. The dependence of planetary tectonics on mantle thermal state: Applications to early Earth evolution. *Philosophical Transactions of the Royal Society A: Mathematical, Physical and Engineering Sciences*, **376**, https://doi.org/10.1098/rsta.2017.0409.
Foley, B.J. 2020. Timescale of Short-Term Subduction Episodicity in Convection Models With Grain Damage: Applications to Archean Tectonics. *Journal of Geophysical Research: Solid Earth*, **125**, e2020JB020478.
Francalanci, L., Avanzinelli, R., Tommasini, S. and Heuman, A. 2007. A west-east geochemical and isotopic traverse along the volcanism of the Aeolian Island arc, southern Tyrrhenian Sea, Italy: Inferences on mantle source processes.
Frei, R., Rosing, M.T., Waight, T.E. and Ulfbeck, D.G. 2002. Hydrothermal-metasomatic and tectono-metamorphic processes in the Isua supracrustal belt (West Greenland): A multi-isotopic investigation of their effects on the Earth's oldest oceanic crustal sequence. *Geochimica et Cosmochimica Acta*, **66**, 467-486.
Fuentes, J.J., Crowley, J.W., Dasgupta, R. and Mitrovica, J.X. 2019. The influence of plate tectonic style on melt production and CO 2 outgassing flux at mid-ocean ridges. *Earth and Planetary Science Letters*, **511**, 154-163, https://doi.org/10.1016/j.epsl.2019.01.020.
Furnes, H. and Dilek, Y. 2022. Archean versus Phanerozoic oceanic crust formation and tectonics: ophiolites through time. *Geosystems and Geoenvironment*, **1**, 100004.
Furnes, H., De Wit, M. and Dilek, Y. 2014. Four billion years of ophiolites reveal secular trends in oceanic crust formation. *Geoscience Frontiers*, **5**, 571-603.
Furnes, H., Banerjee, N.R., Staudigel, H., Muehlenbachs, K., McLoughlin, N., de Wit, M. and Van Kranendonk, M. 2007. Comparing petrographic signatures of bioalteration in recent to Mesoarchean pillow lavas: Tracing subsurface life in oceanic igneous rocks. *Precambrian Research*, **158**, 156-176, https://doi.org/10.1016/j.precamres.2007.04.012.
Garcia, M.O. 1978. Criteria for the identification of ancient volcanic arcs. *Earth-Science Reviews*, **14**, 147-165.
Geldmacher, J., Haase, K.M., Devey, C.W. and Garbe-Schönberg, C.D. 1998. The petrogenesis of Tertiary cone-sheets in Ardnamurchan, NW Scotland: petrological and geochemical constraints on crustal contamination and partial melting. *Contributions to Mineralogy and Petrology*, **131**, 196-209.
Gerya, T. 2014. Precambrian geodynamics: Concepts and models. *Gondwana Research*, **25**, 442-463, https://doi.org/10.1016/j.gr.2012.11.008.
Gerya, T.V., Bercovici, D. and Becker, T.W. 2021. Dynamic slab segmentation due to brittle–ductile damage in the outer rise. *Nature*, **599**, 245-250.
Gerya, T.V., Stern, R.J., Baes, M., Sobolev, S.V. and Whattam, S.A. 2015. Plate tectonics on the Earth triggered by plume-induced subduction initiation. *Nature*, **527**, 221-225, https://doi.org/10.1038/nature15752.
Gill, J.B. 2012. *Orogenic andesites and plate tectonics*. Springer Science & Business Media.
Glassley, W.E., Korstgård, J.A., Sørensen, K. and Platou, S.W. 2014. A new UHP metamorphic complex in the~ 1.8 Ga Nagssugtoqidian Orogen of West Greenland. *American Mineralogist*, **99**, 1315-1334.
Golowin, R., Portnyagin, M., Hoernle, K., Hauff, F., Werner, R. and Garbe-Schönberg, D. 2018. Geochemistry of deep Manihiki Plateau crust: Implications for compositional diversity of large igneous provinces in the Western Pacific and their genetic link. *Chemical Geology*, **493**, 553-566.

Golowin, R., Portnyagin, M. *et al.* 2017. Boninite-like intraplate magmas from Manihiki Plateau require ultra-depleted and enriched source components. *Nature Communications*, **8**, 14322.
Grosch, E.G. and Slama, J. 2017. Evidence for 3.3-billion-year-old oceanic crust in the Barberton greenstone belt, South Africa. *Geology*, **45**, 695-698, https://doi.org/10.1130/G39035.1.
Grossman, J., Gottfried, D. and Froelich, A.J. 1991. *Geochemical data for Jurassic diabase associated with Early Mesozoic basins in the eastern United States* Report **2331-1258**.
Grove, T., Parman, S., Bowring, S., Price, R. and Baker, M. 2002. The role of an H 2 O-rich fluid component in the generation of primitive basaltic andesites and andesites from the Mt. Shasta region, N California. *Contributions to Mineralogy and Petrology*, **142**, 375-396.
Grove, T.L., Baker, M.B., Price, R.C., Parman, S.W., Elkins-Tanton, L.T., Chatterjee, N. and Müntener, O. 2005. Magnesian andesite and dacite lavas from Mt. Shasta, northern California: products of fractional crystallization of H 2 O-rich mantle melts. *Contributions to Mineralogy and Petrology*, **148**, 542-565.
Gunawardana, P.M., Chowdhury, P., Morra, G. and Cawood, P.A. 2024. Correlating mantle cooling with tectonic transitions on early Earth. *Geology*.
Halla, J., Whitehouse, M.J., Ahmad, T. and Bagai, Z. 2017. Archaean granitoids: An overview and significance from a tectonic perspective. *Geological Society Special Publication*, 1-18.
Hamilton, W.B. 2007. Earth's first two billion years—the era of internally mobile crust.
Hanghøj, K., Storey, M. and Stecher, O. 2003. An isotope and trace element study of the East Greenland Tertiary dyke swarm: constraints on temporal and spatial evolution during continental rifting. *Journal of Petrology*, **44**, 2081-2112.
Harrison, T.M. 2020. *Hadean Earth*. Springer.
Harrison, T.M. 2024. We don't know when plate tectonics began. The Geological Society of London, jgs2023-2212.
Hawkesworth, C., Cawood, P.A., Dhuime, B. and Kemp, T. 2024. Tectonic processes and the evolution of the continental crust. The Geological Society of London, jgs2024-2027.
Hawkesworth, C., Cawood, P., Kemp, T., Storey, C. and Dhuime, B. 2009. A matter of preservation. *Science*, **323**, 49-50.
Helmstaedt, H., Padgham, W. and Brophy, J.A. 1986. Multiple dikes in Lower Kam Group, Yellowknife greenstone belt: evidence for Archean sea-floor spreading? *Geology*, **14**, 562-566.
Hergt, J., Peate, D. and Hawkesworth, C. 1991. The petrogenesis of Mesozoic Gondwana low-Ti flood basalts. *Earth and Planetary Science Letters*, **105**, 134-148.
Herzberg, C. 2022. Understanding the Paleoproterozoic Circum-Superior Large Igneous Province constrains the thermal properties of Earth's mantle through time. *Precambrian Research*, **375**, 106671.
Herzberg, C., Condie, K. and Korenaga, J. 2010. Thermal history of the Earth and its petrological expression. *Earth and Planetary Science Letters*, **292**, 79-88, https://doi.org/10.1016/j.epsl.2010.01.022.
Hickey-Vargas, R., Ishizuka, O. and Bizimis, M. 2013. Age and geochemistry of volcanic clasts from DSDP Site 445, Daito Ridge and relationship to Minami-Daito Basin and early Izu-Bonin arc magmatism. *Journal of Asian Earth Sciences*, **70**, 193-208.
Hickman, A.H. 2016. *Northwest Pilbara craton: a record of 450 million years in the growth of Archean continental crust*.

Hildreth, W., Halliday, A.N. and Christiansen, R.L. 1991. Isotopic and chemical evidence concerning the genesis and contamination of basaltic and rhyolitic magma beneath the Yellowstone Plateau volcanic field. *Journal of Petrology*, **32**, 63-138.
Hoffman, P.F. 1988. United plates of America, the birth of a craton: Early Proterozoic assembly and growth of Laurentia. *Annual Review of Earth and Planetary Sciences*, **16**, 543-603.
Hoffmann, J.E., Münker, C., Polat, A., Rosing, M.T. and Schulz, T. 2011. The origin of decoupled Hf-Nd isotope compositions in Eoarchean rocks from southern West Greenland. *Geochimica et Cosmochimica Acta*, **75**, 6610-6628, https://doi.org/10.1016/j.gca.2011.08.018.
Hoffmann, J.E., Münker, C., Polat, A., König, S., Mezger, K. and Rosing, M.T. 2010. Highly depleted Hadean mantle reservoirs in the sources of early Archean arc-like rocks, Isua supracrustal belt, southern West Greenland. *Geochimica et Cosmochimica Acta*, **74**, 7236-7260, https://doi.org/10.1016/j.gca.2010.09.027.
Höink, T., Lenardic, A. and Jellinek, A.M. 2013. Earth's thermal evolution with multiple convection modes: A Monte-Carlo approach. *Physics of the Earth and Planetary Interiors*, **221**, 22-26.
Holder, R.M. and Viete, D.R. 2023. The metamorphic rock record through Earth's history.
Holder, R.M., Viete, D.R., Brown, M. and Johnson, T.E. 2019. Metamorphism and the evolution of plate tectonics. *Nature*, **572**, 378-381.
Hollings, P. and Kerrich, R. 2000. An Archean arc basalt–Nb-enriched basalt–adakite association: the 2.7 Ga Confederation assemblage of the Birch–Uchi greenstone belt, Superior Province. *Contributions to Mineralogy and Petrology*, **139**, 208-226.
Hunter, R., Lafrance, B., Heaman, L., Zaluski, G. and Thomas, D. 2018. Geology, lithogeochemistry and U-Pb geochronology of the Aberdeen Lake Area, Nunavut: new insights into the Neoarchean tectonic evolution of the central Rae domain. *Precambrian Research*, **310**, 114-132.
Hyndman, R. 2019. Mountain building orogeny in precollision hot backarcs: North American Cordillera, India-Tibet, and Grenville Province. *Journal of Geophysical Research: Solid Earth*, **124**, 2057-2079.
Hyndman, R.D., Currie, C.A. and Mazzotti, S.P. 2005. Subduction zone backarcs, mobile belts, and orogenic heat. *GSA Today*, **15**, 4-10.
Jackson, M.G. and Macdonald, F. 2022. Hemispheric geochemical dichotomy of the mantle is a legacy of austral supercontinent assembly and onset of deep continental crust subduction. *AGU Advances*, **3**, e2022AV000664.
Jaupart, C., Mareschal, J.C., Bouquerel, H. and Phaneuf, C. 2014. The building and stabilization of an Archean Craton in the Superior Province, Canada, from a heat flow perspective. *Journal of Geophysical Research: Solid Earth*, **119**, 9130-9155.
Jenner, F.E., Bennett, V.C., Nutman, A.P., Friend, C.R.L., Norman, M.D. and Yaxley, G. 2009. Evidence for subduction at 3.8 Ga: Geochemistry of arc-like metabasalts from the southern edge of the Isua Supracrustal Belt. *Chemical Geology*, **261**, 83-98, https://doi.org/10.1016/j.chemgeo.2008.09.016.
Jiang, K., Wang, J., Kusky, T., Polat, A., Deng, H. and Wang, L. 2020. Neoarchean seafloor hydrothermal metamorphism of basalts in the Zanhuang ophiolitic mélange, North China Craton. *Precambrian Research*, **347**, https://doi.org/10.1016/j.precamres.2020.105832.

Johnson, T., Kirkland, C., Gardiner, N., Brown, M., Smithies, R. and Santosh, M. 2019. Secular change in TTG compositions: Implications for the evolution of Archaean geodynamics. *Earth and Planetary Science Letters*, **505**, 65-75.
Johnson, T.E., Brown, M., Kaus, B.J. and VanTongeren, J.A. 2014. Delamination and recycling of Archaean crust caused by gravitational instabilities. *Nature Geoscience*, **7**, 47-52.
Kankanamge, D.G. and Moore, W.B. 2016. Heat transport in the Hadean mantle: From heat pipes to plates. *Geophysical Research Letters*, **43**, 3208-3214.
Kasbohm, J., Schoene, B., Maclennan, S.A., Evans, D.A. and Weiss, B.P. 2023. Paleogeography and high-precision geochronology of the Neoarchean Fortescue Group, Pilbara, Western Australia. *Precambrian Research*, **394**, 107114.
Kerr, A.C., White, R.V. and Saunders, A.D. 2000. LIP reading: recognizing oceanic plateaux in the geological record. *Journal of Petrology*, **41**, 1041-1056.
Kerr, A.C., Tarney, J., Marriner, G.F., Nivia, A. and Saunders, A.D. 1997. The Caribbean-Colombian Cretaceous igneous province: The internal anatomy of an oceanic plateau. *Geophysical monograph-American Geophysical Union*, **100**, 123-144.
Kerrich, R., Polat, A., Wyman, D. and Hollings, P. 1999. Trace element systematics of Mg-, to Fe-tholeiitic basalt suites of the Superior Province: Implications for Archean mantle reservoirs and greenstone belt genesis. *LITHOS*, **46**, 163-187, https://doi.org/10.1016/s0024-4937(98)00059-0.
Kiyokawa, S., Aihara, Y., Takehara, M. and Horie, K. 2019. Timing and development of sedimentation of the Cleaverville Formation and a post-accretion pull-apart system in the Cleaverville area, coastal Pilbara Terrane, Pilbara, Western Australia. *Island Arc*, **28**, e12324.
Kokfelt, T.F., Hoernle, K., Hauff, F., Fiebig, J., Werner, R. and Garbe-Schoenberg, D. 2006. Combined trace element and Pb-Nd–Sr-O isotope evidence for recycled oceanic crust (upper and lower) in the Iceland mantle plume. *Journal of Petrology*, **47**, 1705-1749.
Komiya, T. 1995. Geochemistry of the oldest MORB and OIB of the World, Isua (3.8 Ga), Greenland. *EOS Transaction*, **76**, 700.
Komiya, T., Maruyama, S., Hirata, T. and Yurimoto, H. 2002. Petrology and geochemistry of MORB and OIB in the mid-Archean North Pole region, Pilbara craton, Western Australia: implications for the composition and temperature of the upper mantle at 3.5 Ga. *International Geology Review*, **44**, 988-1016.
Komiya, T., Maruyama, S., Hirata, T., Yurimoto, H. and Nohda, S. 2004. Geochemistry of the oldest MORB and OIB in the Isua Supracrustal Belt, southern West Greenland: implications for the composition and temperature of early Archean upper mantle. *Island Arc*, **13**, 47-72.
Komiya, T., Maruyama, S., Masuda, T., Nohda, S., Hayashi, M. and Okamoto, K. 1999. Plate tectonics at 3.8–3.7 Ga: Field evidence from the Isua accretionary complex, southern West Greenland. *The Journal of Geology*, **107**, 515-554.
König, S., Schuth, S., Münker, C. and Qopoto, C. 2007. The role of slab melting in the petrogenesis of high-Mg andesites: evidence from Simbo Volcano, Solomon Islands. *Contributions to Mineralogy and Petrology*, **153**, 85-103.
Korenaga, J. 2013. Archean Geodynamics and the Thermal Evolution of Earth *Archean Geodynamics and Environments*. 7-32, https://doi.org/10.1029/164GM03.
Kusky, T., Wang, J. *et al.* 2020. Mélanges through time: Life cycle of the world's largest Archean mélange compared with Mesozoic and Paleozoic subduction-accretion-collision mélanges. *Earth-Science Reviews*, **209**, 103303.

Kusky, T.M. 2004. *Precambrian ophiolites and related rocks*. Elsevier.
Kusky, T.M., Li, J., Glass, A. and Huang, X. 2004. Origin and emplacement of Archean ophiolites of the Central Orogenic belt, North China Craton. *Developments in Precambrian Geology*, **13**, 223-274.
Labrosse, S. and Jaupart, C. 2007. Thermal evolution of the Earth: secular changes and fluctuations of plate characteristics. *Earth and Planetary Science Letters*, **260**, 465-481.
Laurent, O., Martin, H., Moyen, J.-F. and Doucelance, R. 2014. The diversity and evolution of late-Archean granitoids: Evidence for the onset of "modern-style" plate tectonics between 3.0 and 2.5 Ga. *LITHOS*, **205**, 208-235.
Laurent, O., Guitreau, M., Bruand, E. and Moyen, J.-F. 2024. At the dawn of continents: Archean tonalite-trondhjemite-granodiorite suites. *Elements*, **20**, 174-179.
Lenardic, A. 2018. The diversity of tectonic modes and thoughts about transitions between them. *Philosophical Transactions of the Royal Society A: Mathematical, Physical and Engineering Sciences*, **376**, 20170416.
Leybourne, M., Van Wagoner, N. and Ayres, L. 1997. Chemical stratigraphy and petrogenesis of the early Proterozoic Amisk Lake volcanic sequence, Flin Flon–Snow Lake greenstone belt, Canada. *Journal of Petrology*, **38**, 1541-1564.
Li, H., Hermann, J. and Zhang, L. 2022. Melting of subducted slab dictates trace element recycling in global arcs. *Science Advances*, **8**, eabh2166.
Lightfoot, P.C., Naldrett, A., Gorbachev, N., Doherty, W. and Fedorenko, V.A. 1990. Geochemistry of the Siberian Trap of the Noril'sk area, USSR, with implications for the relative contributions of crust and mantle to flood basalt magmatism. *Contributions to Mineralogy and Petrology*, **104**, 631-644.
Liu, L., Zhu, D.C. *et al.* 2022. Leucogranite records multiple collisional orogenies. *Geophysical Research Letters*, **49**, e2021GL096817.
Liu, Y., Mitchell, R.N., Li, Z.-X., Kirscher, U., Pisarevsky, S.A. and Wang, C. 2021. Archean geodynamics: Ephemeral supercontinents or long-lived supercratons. *Geology*, **49**, 794-798.
Lourenço, D.L., Rozel, A.B., Ballmer, M.D. and Tackley, P.J. 2020. Plutonic-Squishy Lid: A New Global Tectonic Regime Generated by Intrusive Magmatism on Earth-Like Planets. *Geochemistry, Geophysics, Geosystems*, **21**, https://doi.org/10.1029/2019GC008756.
Lyubetskaya, T. and Korenaga, J. 2007. Chemical composition of Earth's primitive mantle and its variance: 1. Method and results. *Journal of Geophysical Research: Solid Earth*, **112**.
Maekawa, H., Shozui, M., Fryer, P. and Pearce, J.A. 1993. Blueschist metamorphism in an active subduction zone. *Nature*, **364**, 520-523.
Maier, W.D., Barnes, S.-J. and Karykowski, B. 2016. A chilled margin of komatiite and Mg-rich basaltic andesite in the western Bushveld Complex, South Africa. *Contributions to Mineralogy and Petrology*, **171**, 1-22.
Merle, O. 2011. A simple continental rift classification. *Tectonophysics*, **513**, 88-95.
Miladinova, I., Kurz, W. and Auer, G. 2024. Two-stage exhumation of high-pressure rocks by corner flow and mud volcanism within an active subduction zone–A case study from serpentinite mud volcanoes along the Mariana convergent margin. *Earth and Planetary Science Letters*, **636**, 118717.

Mitchell, R.N., Bleeker, W., Van Breemen, O., Lecheminant, T.N., Peng, P., Nilsson, M.K. and Evans, D.A. 2014. Plate tectonics before 2.0 Ga: Evidence from paleomagnetism of cratons within supercontinent Nuna. *American Journal of Science*, **314**, 878-894.
Miyashiro, A. 1961. Evolution of metamorphic belts. *Journal of Petrology*, **2**, 277-311.
Mole, D., Thurston, P., Marsh, J., Stern, R., Ayer, J., Martin, L. and Lu, Y. 2021. The formation of Neoarchean continental crust in the south-east Superior Craton by two distinct geodynamic processes. *Precambrian Research*, **356**, 106104.
Mole, D.R., Kirkland, C.L. *et al.* 2019. Time-space evolution of an Archean craton: A Hf-isotope window into continent formation. *Earth-Science Reviews*, **196**, https://doi.org/10.1016/j.earscirev.2019.04.003.
Möller, A., Appel, P., Mezger, K. and Schenk, V. 1995. Evidence for a 2 Ga subduction zone: eclogites in the Usagaran belt of Tanzania. *Geology*, **23**, 1067-1070.
Moores, E.M. 2002. Pre-1 Ga (pre-Rodinian) ophiolites: Their tectonic and environmental implications. *Bulletin of the Geological Society of America*, **114**, 80-95, https://doi.org/10.1130/0016-7606(2002)114<0080:PGPROT>2.0.CO;2.
Morrison, G.W. 1980. Characteristics and tectonic setting of the shoshonite rock association. *LITHOS*, **13**, 97-108.
Moyen, J.-F. 2020. Granites and crustal heat budget. *Geological Society, London, Special Publications*, **491**, 77-100.
Moyen, J.-F. and Martin, H. 2012. Forty years of TTG research. *LITHOS*, **148**, 312-336.
Moyen, J.F. and Laurent, O. 2018. Archaean tectonic systems: A view from igneous rocks. *LITHOS*, **302-303**, 99-125, https://doi.org/10.1016/j.lithos.2017.11.038.
Mulyukova, E. and Bercovici, D. 2018. Collapse of passive margins by lithospheric damage and plunging grain size. *Earth and Planetary Science Letters*, **484**, 341-352.
Nakamura, H., Sano, A., Kagami, S., Yokoyama, T., Ishikawa, A., Komiya, T. and Iwamori, H. 2020. Compositional heterogeneity of Archean mantle estimated from Sr and Nd isotopic systematics of basaltic rocks from North Pole, Australia, and the Isua supracrustal belt, Greenland. *Precambrian Research*, **347**, 105803.
Nakanishi, N., Puchtel, I.S., Walker, R.J. and Nabelek, P.I. 2023. Dissipation of Tungsten-182 Anomalies in the Archean Upper Mantle: Evidence from the Black Hills, South Dakota, USA. *Chemical Geology*, **617**, 121255.
Ning, W., Kusky, T., Wang, L. and Huang, B. 2022. Archean eclogite-facies oceanic crust indicates modern-style plate tectonics. *Proceedings of the National Academy of Sciences*, **119**, e2117529119.
Northrup, C., Isachsen, C. and Bowring, S. 1999. Field relations, U-Pb geochronology, and Sm-Nd isotope geochemistry of the Point Lake greenstone belt and adjacent gneisses, central Slave craton, NWT, Canada. *Canadian Journal of Earth Sciences*, **36**, 1043-1059.
Nutman, A.P. and Friend, C.R. 2007. Adjacent terranes with ca. 2715 and 2650 Ma high-pressure metamorphic assemblages in the Nuuk region of the North Atlantic Craton, southern West Greenland: Complexities of Neoarchaean collisional orogeny. *Precambrian Research*, **155**, 159-203.
Nutman, A.P., Bennett, V.C., Friend, C.R.L. and Yi, K. 2020. Eoarchean contrasting ultra-high-pressure to low-pressure metamorphisms (<250 to >1000 °C/GPa) explained by tectonic plate

convergence in deep time. *Precambrian Research*, **344**, https://doi.org/10.1016/j.precamres.2020.105770.
O'Neil, J., Francis, D. and Carlson, R.W. 2011. Implications of the Nuvvuagittuq greenstone belt for the formation of earth's early crust. *Journal of Petrology*, **52**, 985-1009, https://doi.org/10.1093/petrology/egr014.
O'Neil, J., Maurice, C., Stevenson, R.K., Larocque, J., Cloquet, C., David, J. and Francis, D. 2007. The geology of the 3.8 Ga Nuvvuagittuq (Porpoise Cove) greenstone belt, northeastern Superior province, Canada. *Developments in Precambrian Geology*, **15**, 219-250.
O'Neill, C., Turner, S. and Rushmer, T. 2018. The inception of plate tectonics: A record of failure. *Philosophical Transactions of the Royal Society A: Mathematical, Physical and Engineering Sciences*, **376**, https://doi.org/10.1098/rsta.2017.0414.
O'Neill, C., Lenardic, A., Weller, M., Moresi, L., Quenette, S. and Zhang, S. 2016. A window for plate tectonics in terrestrial planet evolution? *Physics of the Earth and Planetary Interiors*, **255**, 80-92, https://doi.org/10.1016/j.pepi.2016.04.002.
O'Neill, C., Marchi, S., Zhang, S. and Bottke, W. 2017. Impact-driven subduction on the Hadean Earth. *Nature Geoscience*, **10**, 793-797.
O'Neill, C., Marchi, S., Bottke, W. and Fu, R. 2020. The role of impacts on Archaean tectonics. *Geology*, **48**, 174-178.
O'Neill, C., Brown, M., Schaefer, B. and Gazi, J. 2022. Earth's anomalous middle-age magmatism driven by plate slowdown. *Scientific Reports*, **12**, 10460.
Ohta, H., Maruyama, S., Takahashi, E., Watanabe, Y. and Kato, Y. 1996. Field occurrence, geochemistry and petrogenesis of the Archean mid-oceanic ridge basalts (AMORBs) of the Cleaverville area, Pilbara craton, Western Australia. *LITHOS*, **37**, 199-221.
Olierook, H.K., Jourdan, F., Merle, R.E., Timms, N.E., Kusznir, N. and Muhling, J.R. 2016. Bunbury Basalt: Gondwana breakup products or earliest vestiges of the Kerguelen mantle plume? *Earth and Planetary Science Letters*, **440**, 20-32.
Oxburgh, E. and Turcotte, D. 1971. Origin of paired metamorphic belts and crustal dilation in island arc regions. *Journal of Geophysical Research*, **76**, 1315-1327.
Palin, R.M. and White, R.W. 2016. Emergence of blueschists on Earth linked to secular changes in oceanic crust composition. *Nature Geoscience*, **9**, 60-64, https://doi.org/10.1038/ngeo2605.
Parai, R. and Mukhopadhyay, S. 2018. Xenon isotopic constraints on the history of volatile recycling into the mantle. *Nature*, **560**, 223-227.
Pearce, J.A. 2008. Geochemical fingerprinting of oceanic basalts with applications to ophiolite classification and the search for Archean oceanic crust. *LITHOS*, **100**, 14-48.
Pearce, J.A. 2014. Immobile element fingerprinting of ophiolites. *Elements*, **10**, 101-108.
Pearce, J.A. and Reagan, M.K. 2019. Identification, classification, and interpretation of boninites from Anthropocene to Eoarchean using Si-Mg-Ti systematics. *Geosphere*, **15**, 1008-1037.
Pearce, J.A., Lippard, S. and Roberts, S. 1984. Characteristics and tectonic significance of supra-subduction zone ophiolites. *Geological Society, London, Special Publications*, **16**, 77-94.
Pearce, J.A., Baker, P.E., Harvey, P.K. and Luff, I.W. 1995. Geochemical evidence for subduction fluxes, mantle melting and fractional crystallization beneath the South Sandwich island arc. *Journal of Petrology*, **36**, 1073-1109.
Pearce, J.A., Ernst, R.E., Peate, D.W. and Rogers, C. 2021. LIP printing: Use of immobile element proxies to characterize Large Igneous Provinces in the geologic record. *LITHOS*, **392**, 106068.

Pearce, J.A., Bender, J. *et al.* 1990. Genesis of collision volcanism in Eastern Anatolia, Turkey. *Journal of Volcanology and Geothermal Research*, **44**, 189-229.
Peccerillo, A. and Taylor, S. 1976. Geochemistry of Eocene calc-alkaline volcanic rocks from the Kastamonu area, northern Turkey. *Contributions to Mineralogy and Petrology*, **58**, 63-81.
Peccerillo, A., De Astis, G., Faraone, D., Forni, F. and Frezzotti, M. 2013. Chapter 15 Compositional variations of magmas in the Aeolian arc: implications for petrogenesis and geodynamics. *Geological Society, London, Memoirs*, **37**, 491-510.
Peltonen, P., Kontinen, A. and Huhma, H. 1996. Petrology and geochemistry of metabasalts from the 1.95 Ga Jormua ophiolite, northeastern Finland. *Journal of Petrology*, **37**, 1359-1383.
Peltonen, P., Mänttäri, I., Huhma, H. and Kontinen, A. 2003. Archean zircons from the mantle: the Jormua ophiolite revisited. *Geology*, **31**, 645-648.
Perchuk, A.L., Zakharov, V.S., Gerya, T.V. and Brown, M. 2019. Hotter mantle but colder subduction in the Precambrian: What are the implications? *Precambrian Research*, **330**, 20-34, https://doi.org/10.1016/j.precamres.2019.04.023.
Péron, S. and Moreira, M. 2018. Onset of volatile recycling into the mantle determined by xenon anomalies. *Geochemical Perspectives Letters*, 21-25.
Polat, A. 2009. The geochemistry of Neoarchean (ca. 2700 Ma) tholeiitic basalts, transitional to alkaline basalts, and gabbros, Wawa Subprovince, Canada: Implications for petrogenetic and geodynamic processes. *Precambrian Research*, **168**, 83-105.
Polat, A. and Kerrich, R. 2000. Archean greenstone belt magmatism and the continental growth–mantle evolution connection: constraints from Th–U–Nb–LREE systematics of the 2.7 Ga Wawa subprovince, Superior Province, Canada. *Earth and Planetary Science Letters*, **175**, 41-54.
Polat, A. and Hofmann, A. 2003. Alteration and geochemical patterns in the 3.7–3.8 Ga Isua greenstone belt, West Greenland. *Precambrian Research*, **126**, 197-218.
Polat, A. and Kerrich, R. 2006. Reading the geochemical fingerprints of Archean hot subduction volcanic rocks: evidence for accretion and crustal recycling in a mobile tectonic regime. *Geophysical Monograph Series*, **164**, 189-213.
Polat, A., Hofmann, A. and Rosing, M.T. 2002. Boninite-like volcanic rocks in the 3.7–3.8 Ga Isua greenstone belt, West Greenland: geochemical evidence for intra-oceanic subduction zone processes in the early Earth. *Chemical Geology*, **184**, 231-254.
Puchtel, I., Hofmann, A., Mezger, K., Jochum, K., Shchipansky, A. and Samsonov, A. 1998. Oceanic plateau model for continental crustal growth in the Archaean: a case study from the Kostomuksha greenstone belt, NW Baltic Shield. *Earth and Planetary Science Letters*, **155**, 57-74.
Puchtel, I., Hofmann, A., Amelin, Y.V., Garbe-Schönberg, C.-D., Samsonov, A. and Shchipansky, A. 1999. Combined mantle plume-island arc model for the formation of the 2.9 Ga Sumozero-Kenozero greenstone belt, SE Baltic Shield: Isotope and trace element constraints. *Geochimica et Cosmochimica Acta*, **63**, 3579-3595.
Puchtel, I.S., Blichert-Toft, J., Horan, M.F., Touboul, M. and Walker, R.J. 2022. The komatiite testimony to ancient mantle heterogeneity. *Chemical Geology*, **594**, 120776.
Puetz, S.J. and Condie, K.C. 2021. Applying Popperian falsifiability to geodynamic hypotheses: empirical testing of the episodic crustal/zircon production hypothesis and selective preservation hypothesis. *International Geology Review*, **63**, 1920-1950.
Puetz, S.J., Ganade, C.E., Zimmermann, U. and Borchardt, G. 2018. Statistical analyses of global U-Pb database 2017. *Geoscience Frontiers*, **9**, 121-145.

Putirka, K. 2016. Special collection: Olivine: Rates and styles of planetary cooling on Earth, Moon, Mars, and Vesta, using new models for oxygen fugacity, ferric-ferrous ratios, olivine-liquid Fe-Mg exchange, and mantle potential temperature. *American Mineralogist*, **101**, 819-840, https://doi.org/10.2138/am-2016-5402.
Putirka, K. and Platt, B. 2012. Basin and Range volcanism as a passive response to extensional tectonics. *Geosphere*, **8**, 1274-1285.
Rapp, R.P., Shimizu, N., Norman, M.D. and Applegate, G.S. 1999. Reaction between slab-derived melts and peridotite in the mantle wedge: Experimental constraints at 3.8 GPa. *Chemical Geology*, **160**, 335-356, https://doi.org/10.1016/S0009-2541(99)00106-0.
Reimink, J.R., Chacko, T., Stern, R.A. and Heaman, L.M. 2016. The birth of a cratonic nucleus: Lithogeochemical evolution of the 4.02-2.94 Ga Acasta Gneiss Complex. *Precambrian Research*, **281**, 453-472, https://doi.org/10.1016/j.precamres.2016.06.007.
Rey, P.F. and Coltice, N. 2008. Neoarchean lithospheric strengthening and the coupling of Earth's geochemical reservoirs. *Geology*, **36**, 635-638.
Rey, P.F., Coltice, N. and Flament, N. 2024. Archean geodynamics underneath weak, flat, and flooded continents. *Elements*, **20**, 180-186.
Richardson, S. and England, P. 1979. Metamorphic consequences of crustal eclogite production in overthrust orogenic zones. *Earth and Planetary Science Letters*, **42**, 183-190.
Roberts, N.M., Salminen, J., Johansson, Å., Mitchell, R.N., Palin, R.M., Condie, K.C. and Spencer, C.J. 2022. On the enigmatic mid-Proterozoic: Single-lid versus plate tectonics. *Earth and Planetary Science Letters*, **594**, 117749.
Robin-Popieul, C.C., Arndt, N.T., Chauvel, C., Byerly, G.R., Sobolev, A.V. and Wilson, A. 2012. A new model for Barberton komatiites: deep critical melting with high melt retention. *Journal of Petrology*, **53**, 2191-2229.
Rolf, T. and Tackley, P. 2011. Focussing of stress by continents in 3D spherical mantle convection with self-consistent plate tectonics. *Geophysical Research Letters*, **38**.
Rollinson, H. 2022. No plate tectonics necessary to explain Eoarchean rocks at Isua (Greenland). *Geology*, **50**, 147-151.
Rudnick, R.L. and Fountain, D.M. 1995. Nature and composition of the continental crust: a lower crustal perspective. *Reviews of Geophysics*, **33**, 267-309.
Safonova, I.Y. and Santosh, M. 2014. Accretionary complexes in the Asia-Pacific region: tracing archives of ocean plate stratigraphy and tracking mantle plumes. *Gondwana Research*, **25**, 126-158.
Said, N. and Kerrich, R. 2009. Geochemistry of coexisting depleted and enriched Paringa Basalts, in the 2.7 Ga Kalgoorlie Terrane, Yilgarn Craton, Western Australia: evidence for a heterogeneous mantle plume event. *Precambrian Research*, **174**, 287-309.
Said, N., Kerrich, R. and Groves, D. 2010. Geochemical systematics of basalts of the Lower Basalt Unit, 2.7 Ga Kambalda Sequence, Yilgarn craton, Australia: plume impingement at a rifted craton margin. *LITHOS*, **115**, 82-100.
Said, N., Kerrich, R., Cassidy, K. and Champion, D. 2012. Characteristics and geodynamic setting of the 2.7 Ga Yilgarn heterogeneous plume and its interaction with continental lithosphere: evidence from komatiitic basalt and basalt geochemistry of the Eastern Goldfields Superterrane. *Australian Journal of Earth Sciences*, **59**, 737-763.

Salminen, J., Elming, S.-Å., Mertanen, S., Wang, C., Almqvist, B. and Moakhar, M.O. 2021. Paleomagnetic studies of rapakivi complexes in the Fennoscandian shield–Implications to the origin of Proterozoic massif-type anorthosite magmatism. *Precambrian Research*, **365**, 106406.
Schmidt, M.W. and Jagoutz, O. 2017. The global systematics of primitive arc melts. *Geochemistry, Geophysics, Geosystems*, **18**, 2817-2854.
Schneider, F., Yuan, X. *et al.* 2013. Seismic imaging of subducting continental lower crust beneath the Pamir. *Earth and Planetary Science Letters*, **375**, 101-112.
Schönig, J., Benner, C., Meinhold, G., von Eynatten, H. and Lünsdorf, N.K. 2023. Detrital garnet petrology challenges Paleoproterozoic ultrahigh-pressure metamorphism in western Greenland. *European Journal of Mineralogy*, **35**, 479-498.
Scott, D., Helmstaedt, H. and Bickle, M. 1992. Purtuniq ophiolite, Cape Smith belt, northern Quebec, Canada: A reconstructed section of Early Proterozoic oceanic crust. *Geology*, **20**, 173-176.
Scott, D.J., St-Onge, M., Lucas, S. and Helmstaedt, H. 1991. Geology and chemistry of the early Proterozoic Purtuniq ophiolite, Cape Smith belt, northern Quebec, Canada. *Ophiolite Genesis and Evolution of the Oceanic Lithosphere: Proceedings of the Ophiolite Conference, held in Muscat, Oman, 7–18 January 1990.* Springer, 817-849.
Scott, D.J., St-Onge, M.R., Lucas, S.B. and Helmstaedt, H. 1999. The 2.00 Ga Purtuniq ophiolite, Cape Smith Belt, Canada: MORB-like crust intruded by OIB-like magmatism. *Ofioliti*, **24**, 199-215.
Seales, J. and Lenardic, A. 2020. Deep Water Cycling and the Multi-Stage Cooling of the Earth. *Geochemistry, Geophysics, Geosystems*, **21**, e2020GC009106.
Seales, J., Lenardic, A. and Tomasini, J.G. 2022. Plate tectonics, mixed heating convection, and the divergence of mantle and plume temperatures. *Geology*, **50**, 1377-1381.
Şengör, A.C. 2001. *Is the present the key to the past or is the past the key to the present? James Hutton and Adam Smith versus Abraham Gottlob Werner and Karl Marx in interpreting history*. Geological Society of America.
Shervais, J.W. 1982. Ti-V plots and the petrogenesis of modern and ophiolitic lavas. *Earth and Planetary Science Letters*, **59**, 101-118.
Shimizu, K., Nakamura, E. and Maruyama, S. 2005. The geochemistry of ultramafic to mafic volcanics from the Belingwe greenstone belt, Zimbabwe: magmatism in an Archean continental large igneous province. *Journal of Petrology*, **46**, 2367-2394.
Shimizu, K., Nakamura, E., Kobayashi, K. and Maruyama, S. 2004. Discovery of Archean continental and mantle fragments inferred from xenocrysts in komatiites, the Belingwe greenstone belt, Zimbabwe. *Geology*, **32**, 285-288.
Shiraki, K., Kuroda, N., Maruyama, S. and Urano, H. 1978. Evolution of the Tertiary volcanic rocks in the Izu-Mariana arc. *Bulletin Volcanologique*, **41**, 548-562.
Sizova, E., Gerya, T. and Brown, M. 2012. Exhumation mechanisms of melt-bearing ultrahigh pressure crustal rocks during collision of spontaneously moving plates. *Journal of Metamorphic Geology*, **30**, 927-955, https://doi.org/10.1111/j.1525-1314.2012.01004.x.
Sizova, E., Gerya, T. and Brown, M. 2014. Contrasting styles of Phanerozoic and Precambrian continental collision. *Gondwana Research*, **25**, 522-545, https://doi.org/10.1016/j.gr.2012.12.011.

Sizova, E., Gerya, T., Brown, M. and Perchuk, L.L. 2010. Subduction styles in the Precambrian: Insight from numerical experiments. *LITHOS*, **116**, 209-229, https://doi.org/10.1016/j.lithos.2009.05.028.

Sizova, E., Gerya, T., Stüwe, K. and Brown, M. 2015. Generation of felsic crust in the Archean: A geodynamic modeling perspective. *Precambrian Research*, **271**, 198-224, https://doi.org/10.1016/j.precamres.2015.10.005.

Smithies, R. and Champion, D. 2000. The Archaean high-Mg diorite suite: links to tonalite–trondhjemite–granodiorite magmatism and implications for early Archaean crustal growth. *Journal of Petrology*, **41**, 1653-1671.

Smithies, R., Champion, D. and Sun, S.-S. 2004. Evidence for early LREE-enriched mantle source regions: diverse magmas from the c. 3· 0 Ga Mallina Basin, Pilbara Craton, NW Australia. *Journal of Petrology*, **45**, 1515-1537.

Smithies, R.H., Van Kranendonk, M.J. and Champion, D.C. 2005a. It started with a plume - Early Archaean basaltic proto-continental crust. *Earth and Planetary Science Letters*, **238**, 284-297, https://doi.org/10.1016/j.epsl.2005.07.023.

Smithies, R.H., Champion, D.C. and Van Kranendonk, M.J. 2007. Chapter 4.2 The Oldest Well-Preserved Felsic Volcanic Rocks on Earth: Geochemical Clues to the Early Evolution of the Pilbara Supergroup and Implications for the Growth of a Paleoarchean Protocontinent. *Developments in Precambrian Geology*, 339-367.

Smithies, R.H., Champion, D.C., Van Kranendonk, M.J., Howard, H.M. and Hickman, A.H. 2005b. Modern-style subduction processes in the Mesoarchaean: Geochemical evidence from the 3.12 Ga Whundo intra-oceanic arc. *Earth and Planetary Science Letters*, **231**, 221-237, https://doi.org/10.1016/j.epsl.2004.12.026.

Smithies, R.H., Ivanic, T.J., Lowrey, J.R., Morris, P.A., Barnes, S.J., Wyche, S. and Lu, Y.-J. 2018. Two distinct origins for Archean greenstone belts. *Earth and Planetary Science Letters*, **487**, 106-116.

Smithies, R.H., Lu, Y. *et al.* 2019. No evidence for high-pressure melting of Earth's crust in the Archean. *Nature Communications*, **10**, https://doi.org/10.1038/s41467-019-13547-x.

Sobolev, S.V. and Brown, M. 2019. Surface erosion events controlled the evolution of plate tectonics on Earth. *Nature*, **570**, 52-57.

Sorensen, S.S. and Grossman, J. 1989. Enrichment of trace elements in garnet amphibolites from a paleo-subduction zone: Catalina Schist, southern California. *Geochimica et Cosmochimica Acta*, **53**, 3155-3177.

Sorensen, S.S. and Grossman, J.N. 1993. Accessory minerals and subduction zone metasomatism: a geochemical comparison of two mélanges (Washington and California, USA). *Chemical Geology*, **110**, 269-297.

Sotiriou, P., Polat, A., Windley, B.F. and Kusky, T. 2022. Temporal variations in the incompatible trace element systematics of Archean volcanic rocks: Implications for tectonic processes in the early Earth. *Precambrian Research*, **368**, 106487.

Spencer, C.J., Mitchell, R.N. and Brown, M. 2021. Enigmatic Mid-Proterozoic orogens: Hot, thin, and low. *Geophysical Research Letters*, **48**, e2021GL093312.

Stern, R.A., Syme, E.C., Bailes, A.H. and Lucas, S.B. 1995. Paleoproterozoic (1.90–1.86 Ga) arc volcanism in the Flin Flon Belt, Trans-Hudson Orogen, Canada. *Contributions to Mineralogy and Petrology*, **119**, 117-141.

Stern, R.J. 2005. Evidence from ophiolites, blueschists, and ultrahigh-pressure metamorphic terranes that the modern episode of subduction tectonics began in Neoproterozoic time. *Geology*, **33**, 557-560.
Stern, R.J. 2008. Modern-style plate tectonics began in Neoproterozoic time: An alternative interpretation of Earth's tectonic history. *When did plate tectonics begin on planet Earth*, **440**, 265-280.
Stern, R.J. 2020. The Mesoproterozoic single-lid tectonic episode: Prelude to modern plate tectonics. *GSA Today*, **30**, 4-10.
Stern, R.J. 2023. The Orosirian (1800-2050 Ma) plate tectonic episode: Key for reconstructing the Proterozoic tectonic record. *Geoscience Frontiers*, 101553.
Stern, R.J. and Gerya, T. 2018. Subduction initiation in nature and models: A review. *Tectonophysics*, **746**, 173-198.
Stevenson, R.K., Henry, P. and Gariépy, C. 2009. Isotopic and geochemical evidence for differentiation and crustal contamination from granitoids of the Berens river subprovince, Superior province, Canada. *Precambrian Research*, **168**, 123-133.
Stone, D. 1998. *Precambrian geology of the Berens River area, northwest Ontario*. Ontario Geological Survey.
Streck, M.J., Leeman, W.P. and Chesley, J. 2007. High-magnesian andesite from Mount Shasta: a product of magma mixing and contamination, not a primitive mantle melt. *Geology*, **35**, 351-354.
Sun, S. and Hickman, A.H. 1999. Geochemical characteristics of ca 3.0-Ga Cleaverville greenstones and later mafic dykes, west Pilbara: implication for Archaean crustal accretion. *Australian Geological Survey Organisation, Research Newsletter*, 23-29.
Sun, S.-S. and McDonough, W.F. 1989. Chemical and isotopic systematics of oceanic basalts: implications for mantle composition and processes. *Geological Society, London, Special Publications*, **42**, 313-345.
Szilas, K., Kelemen, P.B. and Rosing, M.T. 2015. The petrogenesis of ultramafic rocks in the> 3.7 Ga Isua supracrustal belt, southern West Greenland: Geochemical evidence for two distinct magmatic cumulate trends. *Gondwana Research*, **28**, 565-580.
Tamblyn, R., Brown, D., Hand, M., Morrissey, L., Clark, C. and Anczkiewicz, R. 2021. The 2 Ga eclogites of Central Tanzania: directly linking age and metamorphism. *LITHOS*, **380**, 105890.
Tamblyn, R., Zack, T. *et al.* 2019. Blueschist from the Mariana forearc records long-lived residence of material in the subduction channel. *Earth and Planetary Science Letters*, **519**, 171-181.
Tamblyn, R.J. 2021. *Subduction zone metamorphism: Timescales and emergence in the geological record.*
Tang, M., Lee, C.-T.A., Rudnick, R.L. and Condie, K.C. 2020. Rapid mantle convection drove massive crustal thickening in the late Archean. *Geochimica et Cosmochimica Acta*, **278**, 6-15.
Tejada, M., Mahoney, J., Duncan, R. and Hawkins, M. 1996. Age and geochemistry of basement and alkalic rocks of Malaita and Santa Isabel, Solomon Islands, southern margin of Ontong Java Plateau. *Journal of Petrology*, **37**, 361-394.
Tejada, M., Suzuki, K. *et al.* 2013. Cryptic lower crustal signature in the source of the Ontong Java Plateau revealed by Os and Hf isotopes. *Earth and Planetary Science Letters*, **377**, 84-96.

Tetreault, J. and Buiter, S. 2014. Future accreted terranes: a compilation of island arcs, oceanic plateaus, submarine ridges, seamounts, and continental fragments. *Solid Earth*, **5**, 1243-1275.
Thom, A., Arndt, N., Chauvel, C. and Stauffer, M. 1990. Flin Flon and western La Ronge belts, Saskatchewan: products of Proterozoic subduction-related volcanism. *The Early Proterozoic Trans-Hudson Orogen of North America. Edited by JF Lewry and MR Stauffer. Geological Association of Canada, Special Paper*, **37**, 163-176.
Thompson, A.B. and England, P.C. 1984. Pressure—temperature—time paths of regional metamorphism II. Their inference and interpretation using mineral assemblages in metamorphic rocks. *Journal of Petrology*, **25**, 929-955.
Thompson, R., Riches, A. *et al.* 2007. Origin of CFB magmatism: multi-tiered intracrustal picrite–rhyolite magmatic plumbing at Spitzkoppe, western Namibia, during early Cretaceous Etendeka magmatism. *Journal of Petrology*, **48**, 1119-1154.
Thurston, P. 2002. Autochthonous development of Superior Province greenstone belts? *Precambrian Research*, **115**, 11-36.
Tomlinson, K.Y. and Condie, K.C. 2001. Archean mantle plumes: evidence from greenstone belt geochemistry. *Special Papers-Geological Society of America*, 341-358.
Trail, D., Tailby, N., Wang, Y., Mark Harrison, T. and Boehnke, P. 2017. Aluminum in zircon as evidence for peraluminous and metaluminous melts from the H adean to present. *Geochemistry, Geophysics, Geosystems*, **18**, 1580-1593.
Turner, S., Rushmer, T., Reagan, M. and Moyen, J.F. 2014. Heading down early on? Start of subduction on earth. *Geology*, **42**, 139-142, https://doi.org/10.1130/G34886.1.
Turner, S., Wilde, S., Wörner, G., Schaefer, B. and Lai, Y.J. 2020. An andesitic source for Jack Hills zircon supports onset of plate tectonics in the Hadean. *Nature Communications*, **11**, https://doi.org/10.1038/s41467-020-14857-1.
Ulvrova, M.M., Coltice, N., Williams, S. and Tackley, P.J. 2019. Where does subduction initiate and cease? A global scale perspective. *Earth and Planetary Science Letters*, **528**, 115836.
Valley, J.W., Peck, W.H., King, E.M. and Wilde, S.A. 2002. A cool early Earth. *Geology*, **30**, 351-354, https://doi.org/10.1130/0091-7613(2002)030<0351:ACEE>2.0.CO;2.
van Hunen, J. and van den Berg, A.P. 2008. Plate tectonics on the early Earth: limitations imposed by strength and buoyancy of subducted lithosphere. *LITHOS*, **103**, 217-235.
Van Hunen, J. and Moyen, J.F. 2012. Archean subduction: Fact or fiction? *Annual Review of Earth and Planetary Sciences*, 195-219.
Van Kranendonk, M.J., Hugh Smithies, R. *et al.* 2015. Making it thick: A volcanic plateau origin of Palaeoarchean continental lithosphere of the Pilbara and Kaapvaal cratons. *Geological Society Special Publication*, 83-111.
Wakabayashi, J. 2015. Anatomy of a subduction complex: Architecture of the Franciscan Complex, California, at multiple length and time scales. *International Geology Review*, **57**, 669-746.
Walker, R.J., Shirey, S.B., Hanson, G.N., Rajamani, V. and Horan, M.F. 1989. Re-Os, Rb-Sr, and O isotopic systematics of the Archean Kolar schist belt, Karnataka, India. *Geochimica et Cosmochimica Acta*, **53**, 3005-3013, https://doi.org/10.1016/0016-7037(89)90176-2.
Wan, B., Yang, X., Tian, X., Yuan, H., Kirscher, U. and Mitchell, R.N. 2020. Seismological evidence for the earliest global subduction network at 2 Ga ago. *Science Advances*, **6**, https://doi.org/10.1126/sciadv.abc5491.

Wang, J., Li, X., Ning, W., Kusky, T., Wang, L., Polat, A. and Deng, H. 2019. Geology of a Neoarchean suture: evidence from the Zunhua ophiolitic mélange of the Eastern Hebei Province, North China Craton. *GSA Bulletin*, **131**, 1943-1964.

Wang, J.-M., Lanari, P., Wu, F.-Y., Zhang, J.-J., Khanal, G.P. and Yang, L. 2021. First evidence of eclogites overprinted by ultrahigh temperature metamorphism in Everest East, Himalaya: Implications for collisional tectonics on early Earth. *Earth and Planetary Science Letters*, **558**, 116760.

Wang, Y., Zhou, L., Liu, S., Li, J. and Yang, T. 2018. Post-cratonization deformation processes and tectonic evolution of the North China Craton. *Earth-Science Reviews*, **177**, 320-365.

Wang, Z., Wilde, S.A., Wang, K. and Yu, L. 2004. A MORB-arc basalt–adakite association in the 2.5 Ga Wutai greenstone belt: late Archean magmatism and crustal growth in the North China Craton. *Precambrian Research*, **131**, 323-343.

Warren, C., Beaumont, C. and Jamieson, R.A. 2008. Modelling tectonic styles and ultra-high pressure (UHP) rock exhumation during the transition from oceanic subduction to continental collision. *Earth and Planetary Science Letters*, **267**, 129-145.

Waterton, P., Guotana, J. *et al.* 2022. No mantle residues in the Isua Supracrustal Belt. *Earth and Planetary Science Letters*, **579**, 117348.

Watson, E.B. and Harrison, T.M. 2005. Zircon thermometer reveals minimum melting conditions on earliest earth. *Science*, **308**, 841-844, https://doi.org/10.1126/science.1110873.

Watters, B. and Pearce, J.A. 1987. Metavolcanic rocks of the La Ronge Domain in the Churchill Province, Saskatchewan: geochemical evidence for a volcanic arc origin. *Geological Society, London, Special Publications*, **33**, 167-182.

Webb, A.A.G., Müller, T., Zuo, J., Haproff, P.J. and Ramírez-Salazar, A. 2020. A non-plate tectonic model for the Eoarchean Isua supracrustal belt. *Lithosphere*, **12**, 166-179, https://doi.org/10.1130/L1130.1.

Weller, O.M., Mottram, C.M., St-Onge, M.R., Möller, C., Strachan, R., Rivers, T. and Copley, A. 2021. The metamorphic and magmatic record of collisional orogens. *Nature Reviews Earth & Environment*, **2**, 781-799.

Wilde, S.A., Valley, J.W., Peck, W.H. and Graham, C.M. 2001. Evidence from detrital zircons for the existence of continental crust and oceans on the Earth 4.4 Gyr ago. *Nature*, **409**, 175-178.

Willigers, B., Van Gool, J., Wijbrans, J., Krogstad, E. and Mezger, K. 2002. Posttectonic cooling of the Nagssugtoqidian orogen and a comparison of contrasting cooling histories in Precambrian and Phanerozoic orogens. *The Journal of Geology*, **110**, 503-517.

Windley, B.F., Kusky, T. and Polat, A. 2021. Onset of plate tectonics by the Eoarchean. *Precambrian Research*, **352**, 105980.

Wood, D.A. 1980. The application of a ThHfTa diagram to problems of tectonomagmatic classification and to establishing the nature of crustal contamination of basaltic lavas of the British Tertiary Volcanic Province. *Earth and Planetary Science Letters*, **50**, 11-30.

Workman, R.K. and Hart, S.R. 2005. Major and trace element composition of the depleted MORB mantle (DMM). *Earth and Planetary Science Letters*, **231**, 53-72.

Wyman, D. and Kerrich, R. 1989. Archean lamprophyre dikes of the Superior Province, Canada: distribution, petrology, and geochemical characteristics. *Journal of Geophysical Research: Solid Earth*, **94**, 4667-4696.

Xiao, Y., Hoefs, J., Hou, Z., Simon, K. and Zhang, Z. 2011. Fluid/rock interaction and mass transfer in continental subduction zones: constraints from trace elements and isotopes (Li, B, O, Sr, Nd, Pb) in UHP rocks from the Chinese Continental Scientific Drilling Program, Sulu, East China. *Contributions to Mineralogy and Petrology*, **162**, 797-819.

Xu, W.C., Luo, B.J., Xu, Y.J., Wang, L. and Chen, Q. 2018. Geochronology, geochemistry, and petrogenesis of late Permian to early Triassic mafic rocks from Darongshan, South China: Implications for ultrahigh-temperature metamorphism and S-type granite generation. *LITHOS*, **308-309**, 168-180, https://doi.org/10.1016/j.lithos.2018.03.004.

Yeh, Y.-C., Lin, J.-Y., Hsu, S.-K., Tsai, C.-H. and Chang, C.-M. 2021. Separation of Gagua Rise from Great Benham Rise in the West Philippine Basin during the Middle Eocene. *Scientific Reports*, **11**, 21775.

Yin, A., Brandl, G. and Kröner, A. 2020. Plate-tectonic processes at ca. 2.0 Ga: Evidence from> 600 km of plate convergence. *Geology*, **48**, 103-107.

Zellmer, G., Hawkesworth, C., Sparks, R., Thomas, L., Harford, C., Brewer, T. and Loughlin, S. 2003. Geochemical evolution of the Soufriere Hills volcano, Montserrat, Lesser Antilles volcanic arc. *Journal of Petrology*, **44**, 1349-1374.

Zhang, L. and Szilas, K. 2024. Eoarchean ultramafic rocks represent crustal cumulates: A case study of the Narssaq ultramafic body, southern West Greenland. *Earth and Planetary Science Letters*, **625**, 118508.

Zhang, Q., Timmerman, S. *et al.* 2024a. Sublithospheric diamonds extend Paleoproterozoic record of cold deep subduction into the lower mantle. *Earth and Planetary Science Letters*, **634**, 118675.

Zhang, S., Li, Y., Leng, W. and Gurnis, M. 2023. Photoferrotrophic bacteria initiated plate tectonics in the Neoarchean. *Geophysical Research Letters*, **50**, e2023GL103553.

Zhang, X.J., Parai, R. and Lassiter, J.C. 2024b. Primordial and recycled noble gases in the Cook-Austral HIMU mantle: Insights into the onset of volatile subduction. *Earth and Planetary Science Letters*, **629**, 118591.

Zhu, M., Yan, Z. *et al.* 2023. Do microcontinents nucleate subduction initiation? *Geology*.

Zou, Y., Mitchell, R.N. *et al.* 2023. Surface evolution during the mid-proterozoic stalled by mantle warming under Columbia–Rodinia. *Earth and Planetary Science Letters*, **607**, 118055.

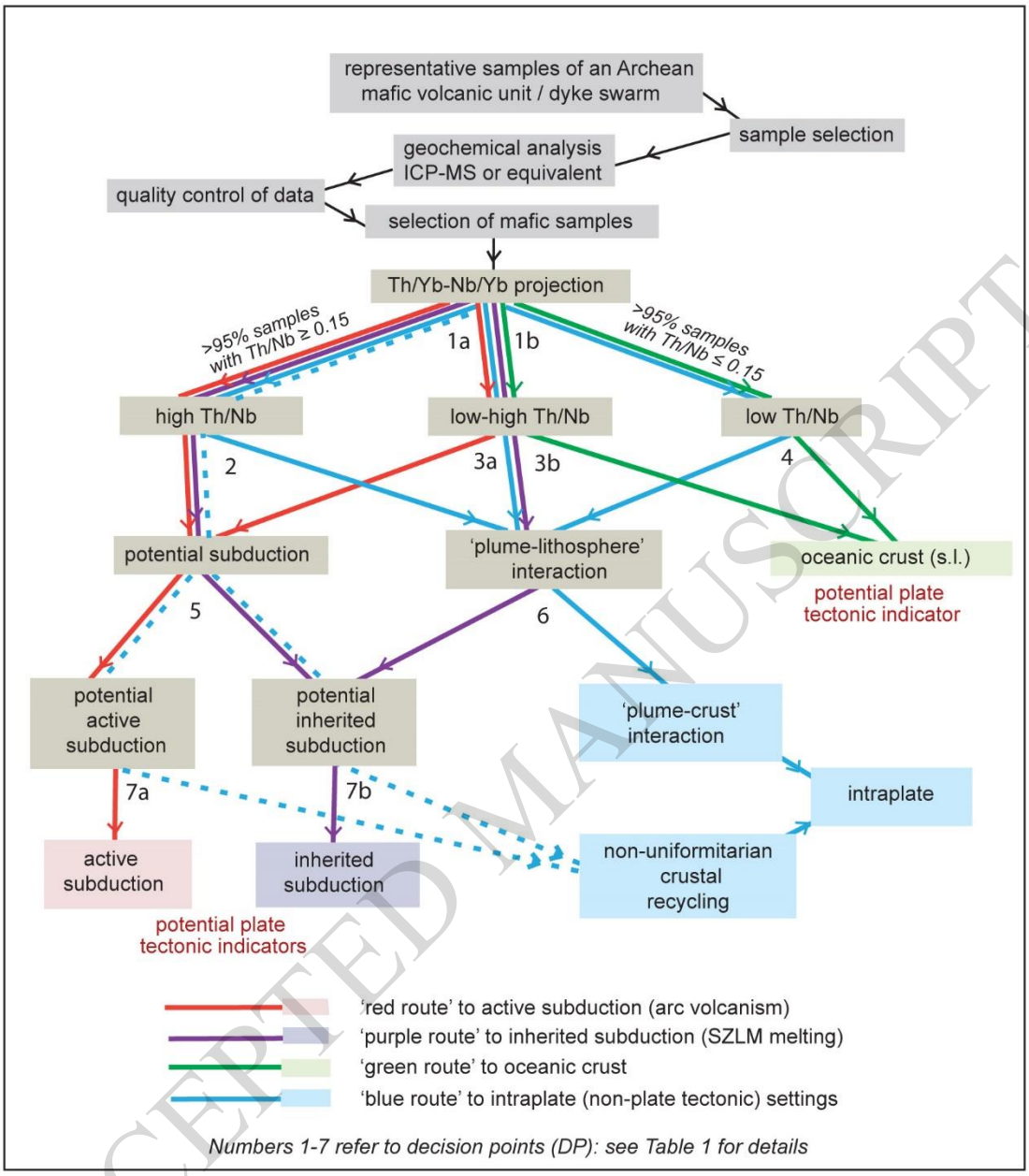

Figure 1

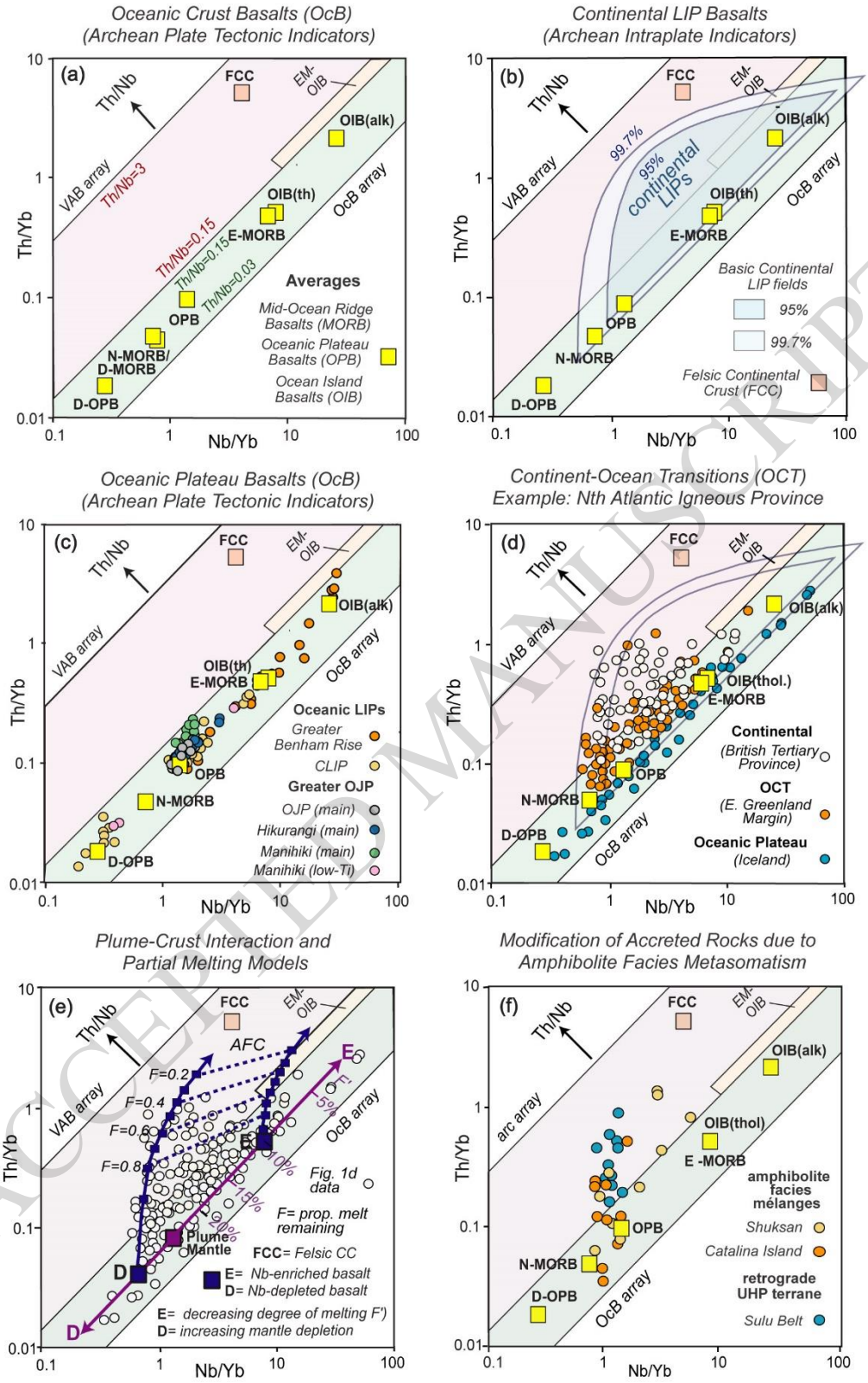

Figure 2

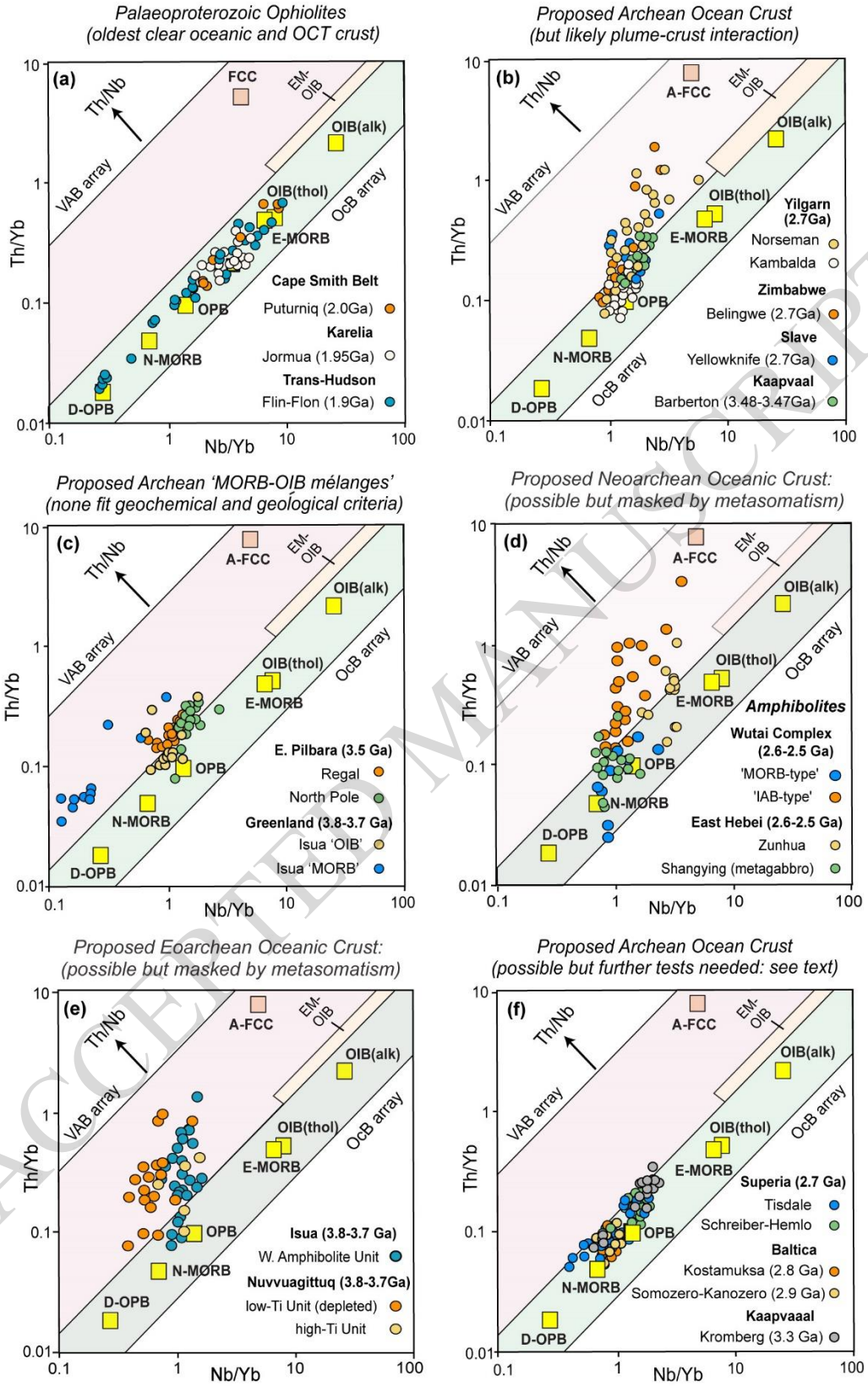

Figure 3

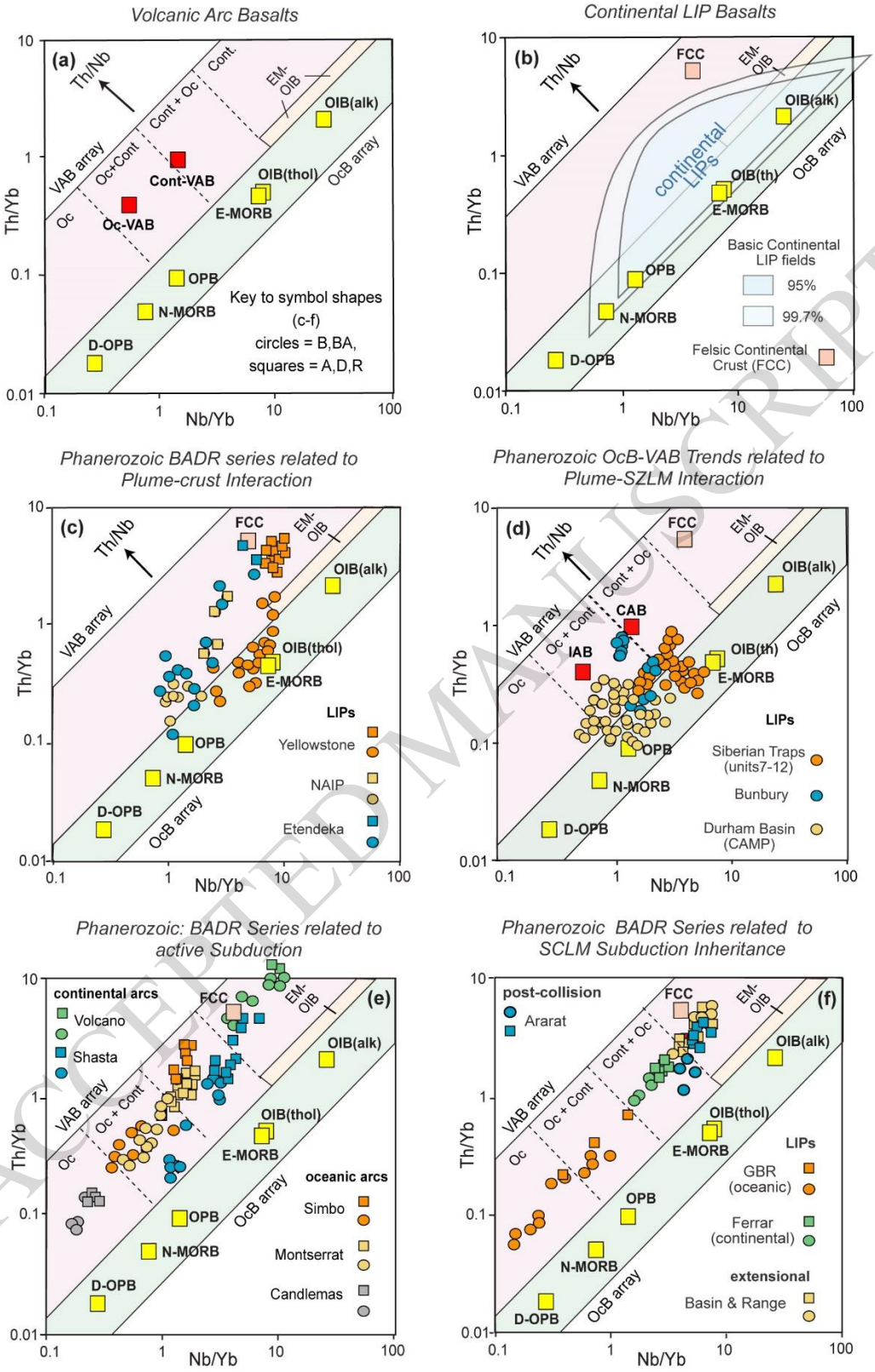

Figure 4

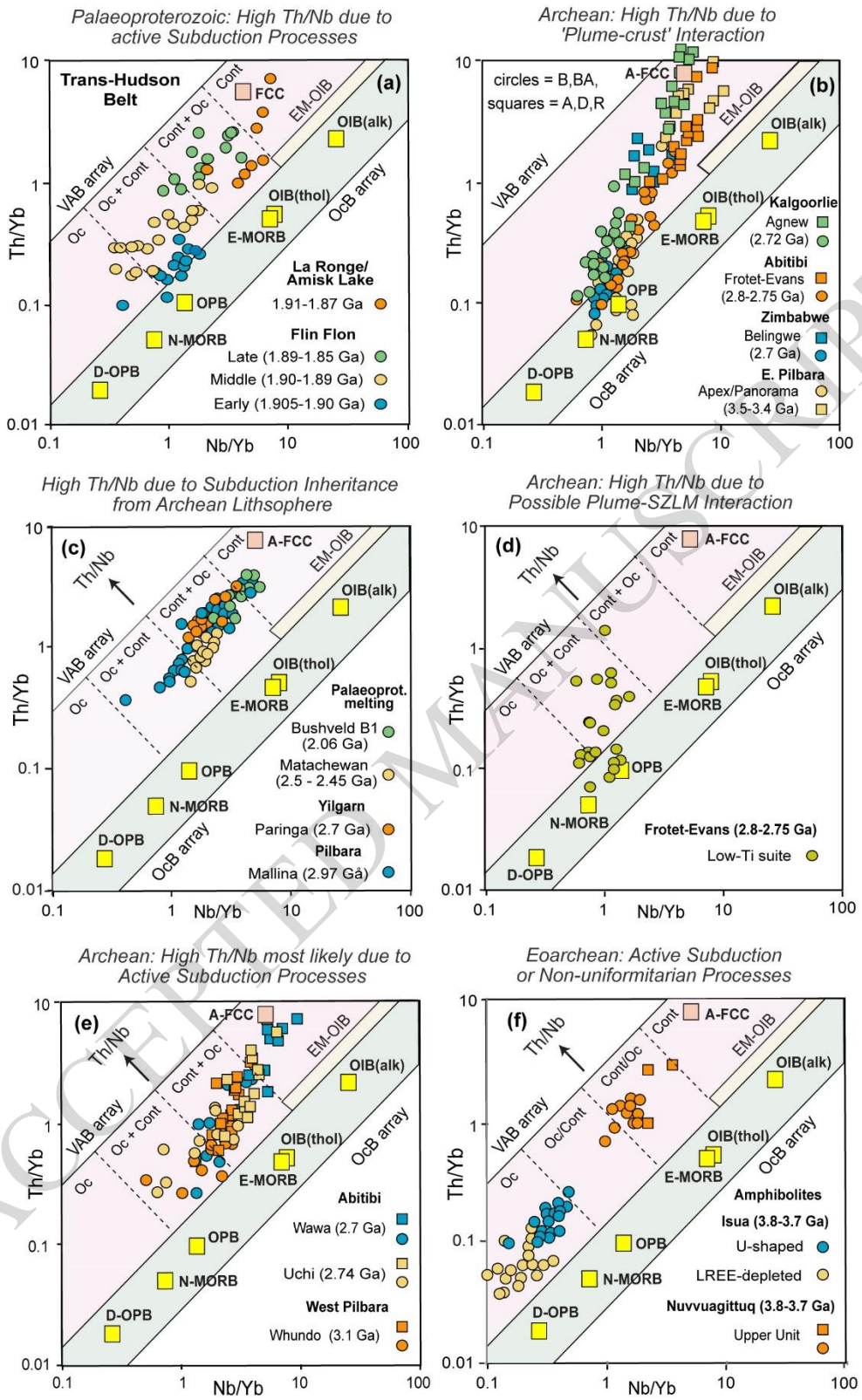

Figure 5

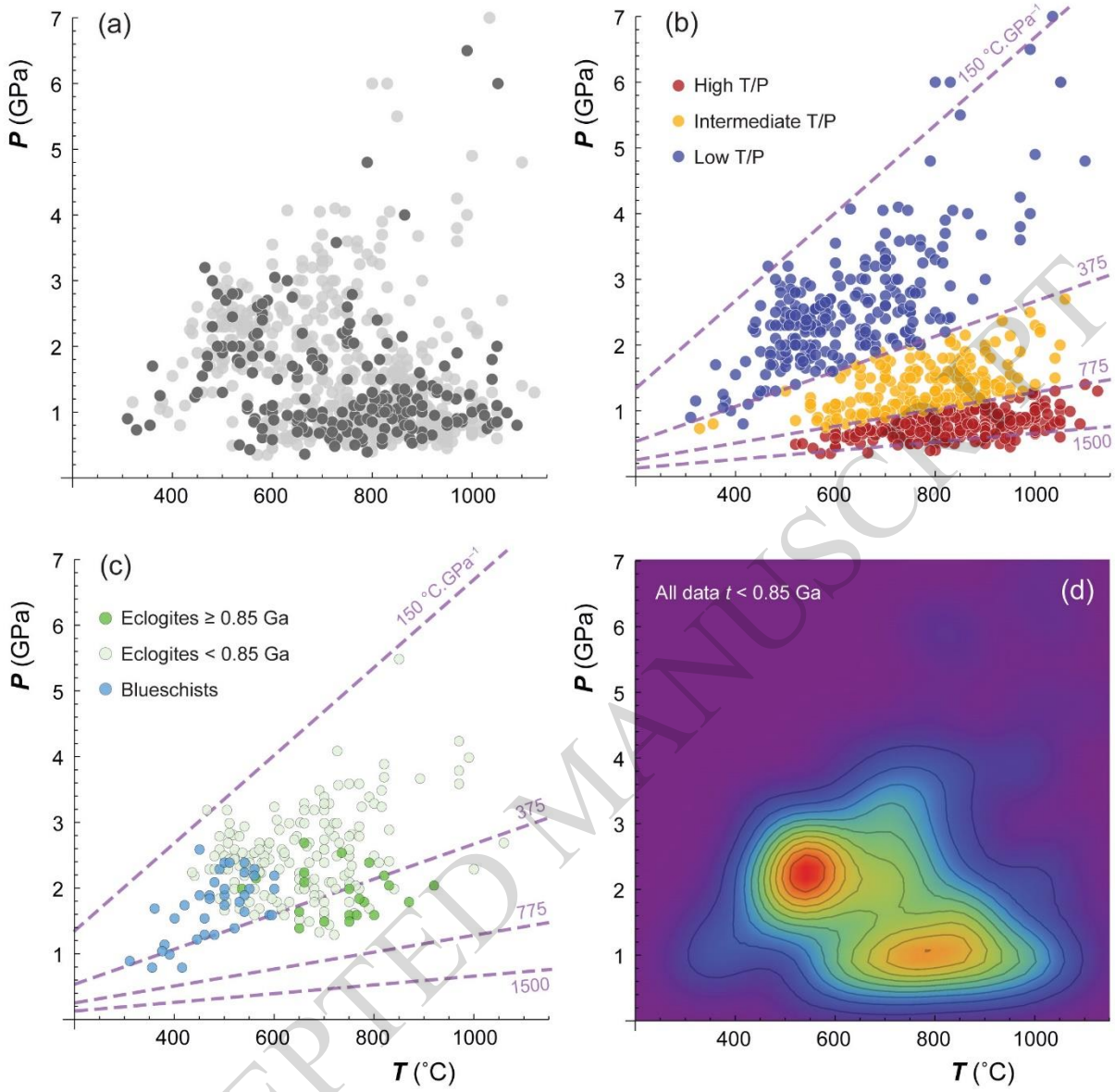

Figure 6

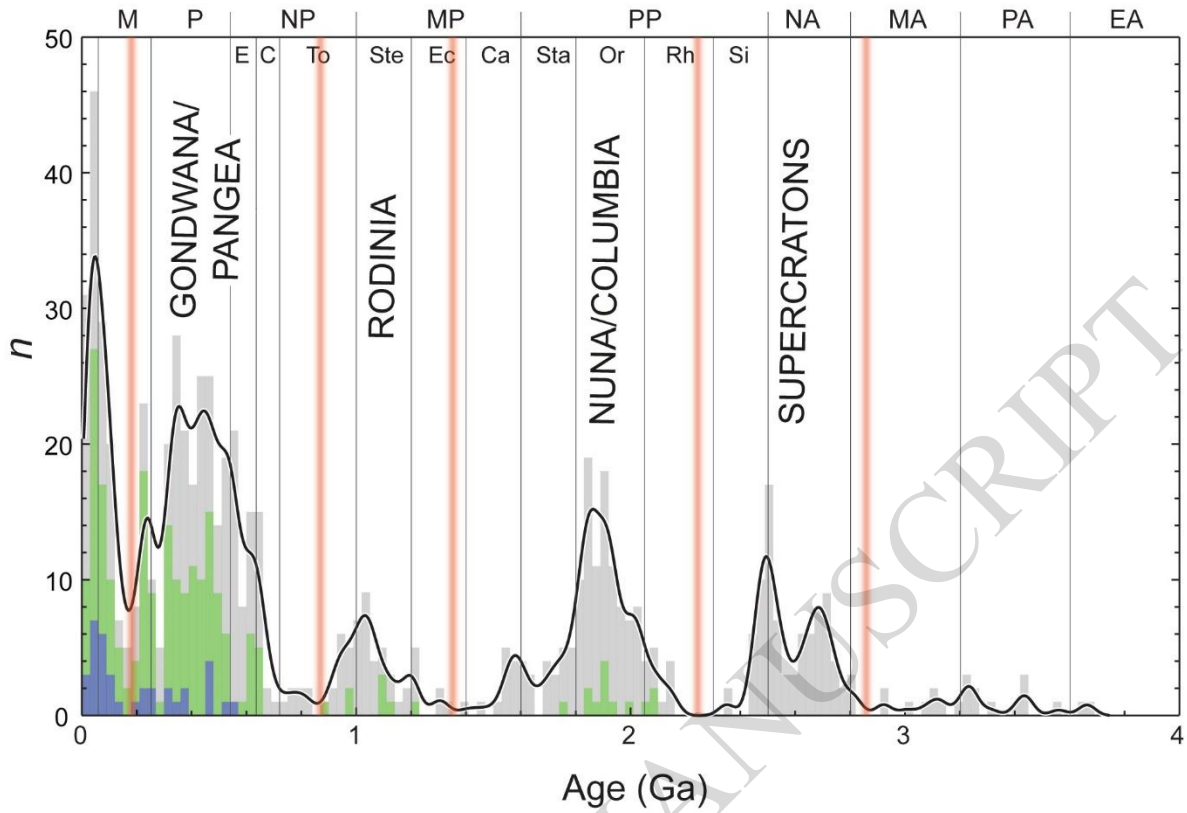

Figure 7

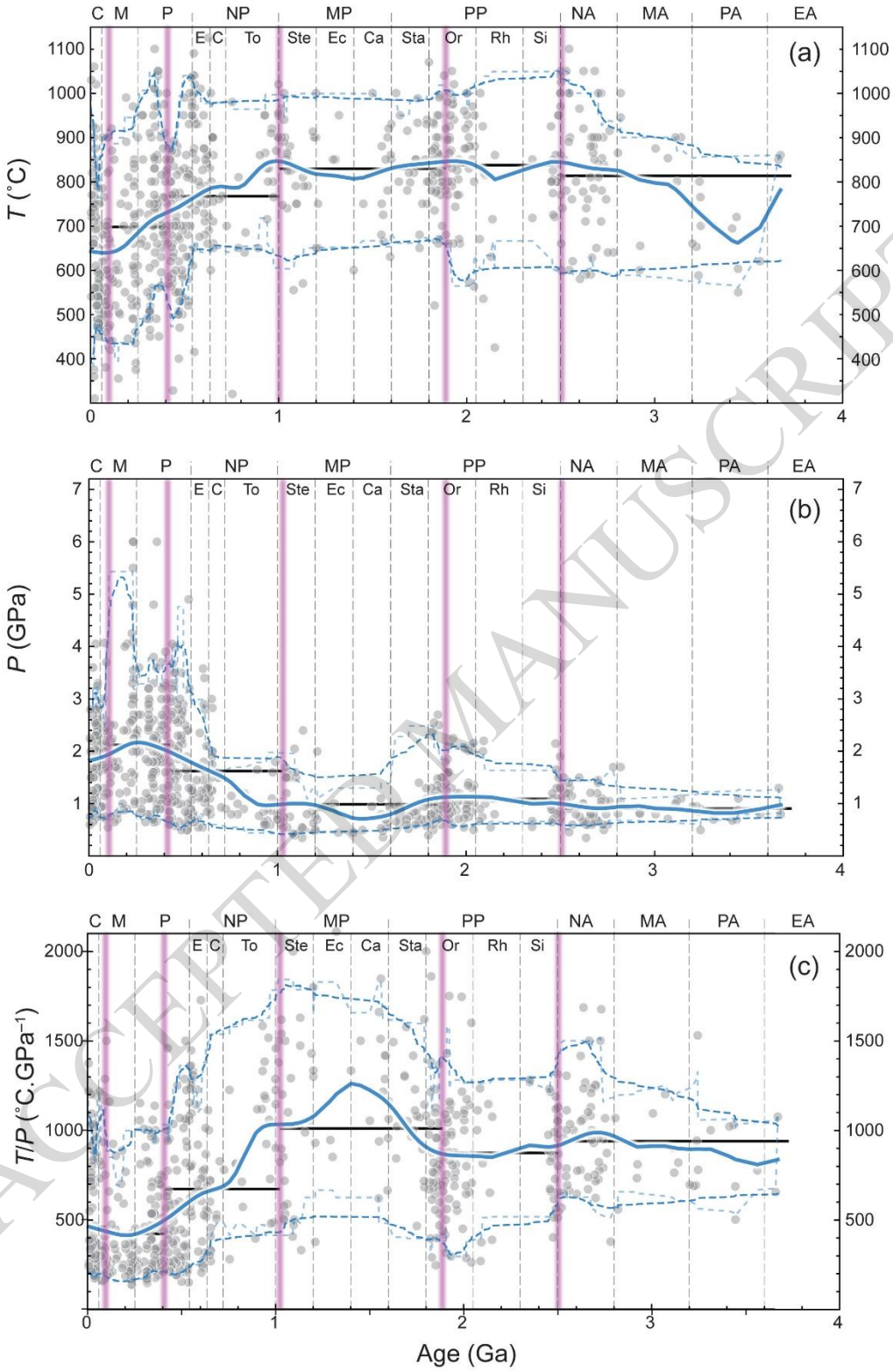

Figure 8

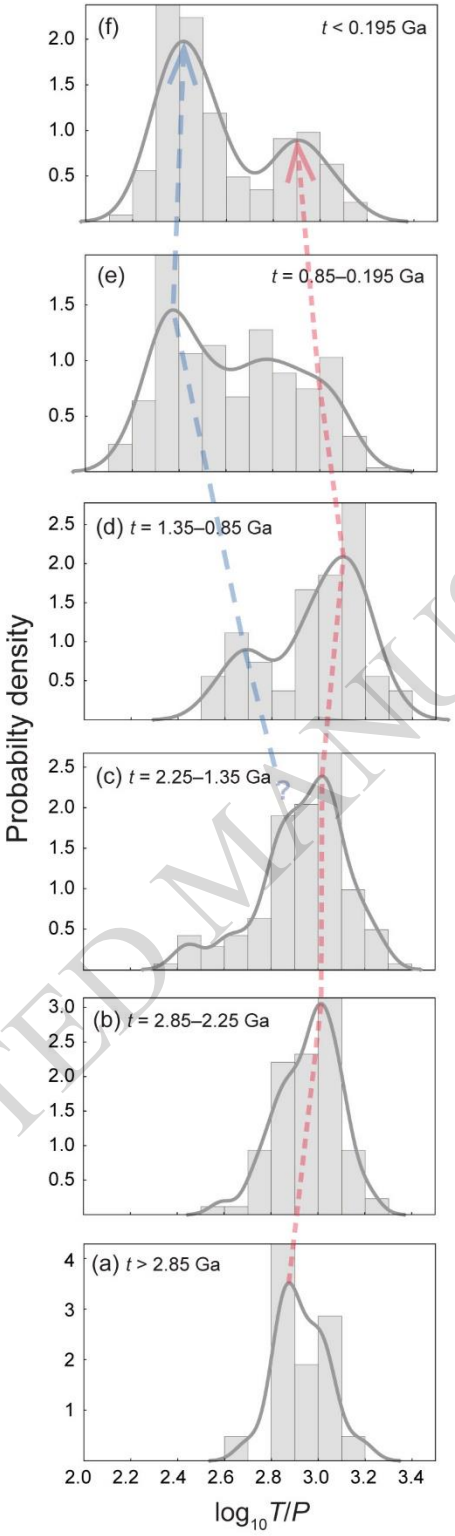

Figure 9

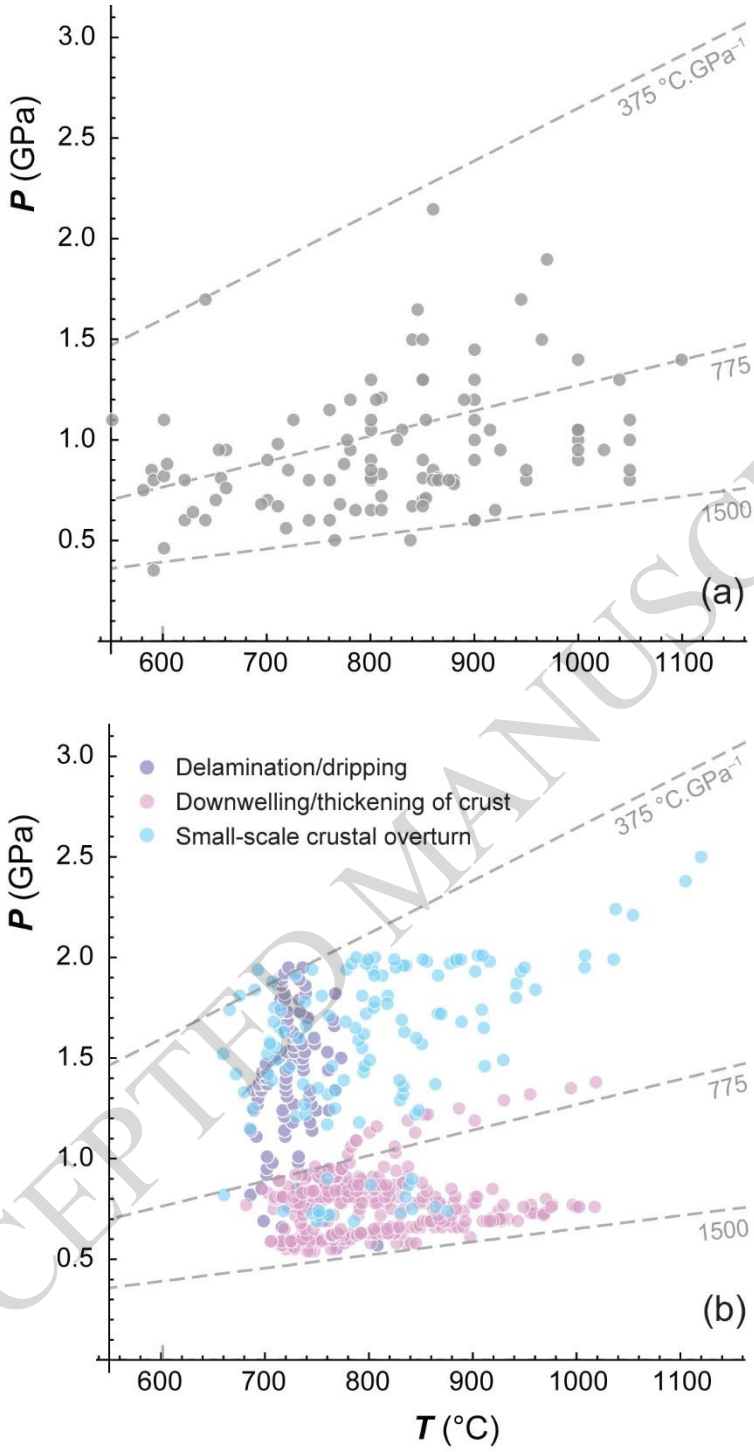

Figure 10

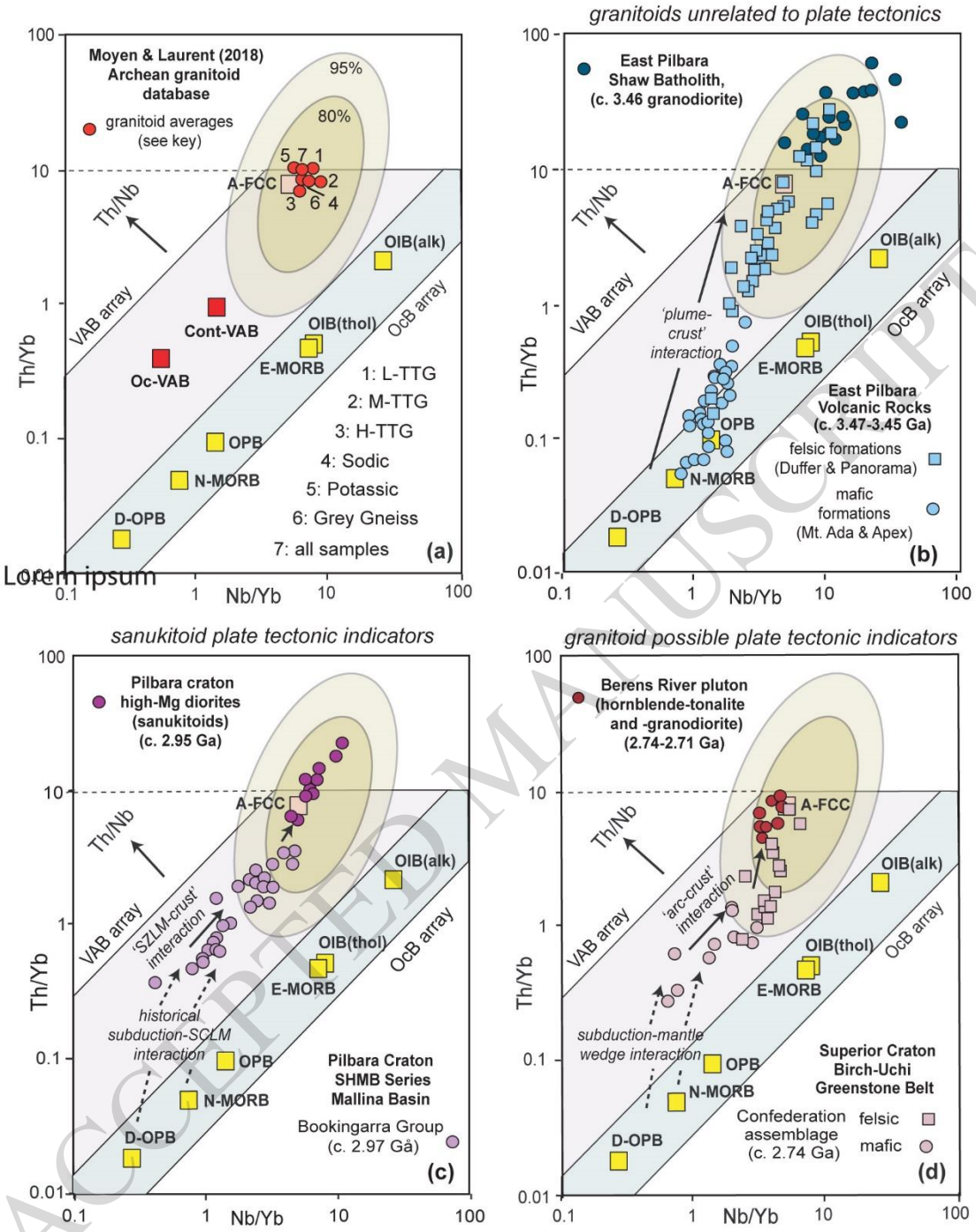

Lorem ipsum

Figure 11

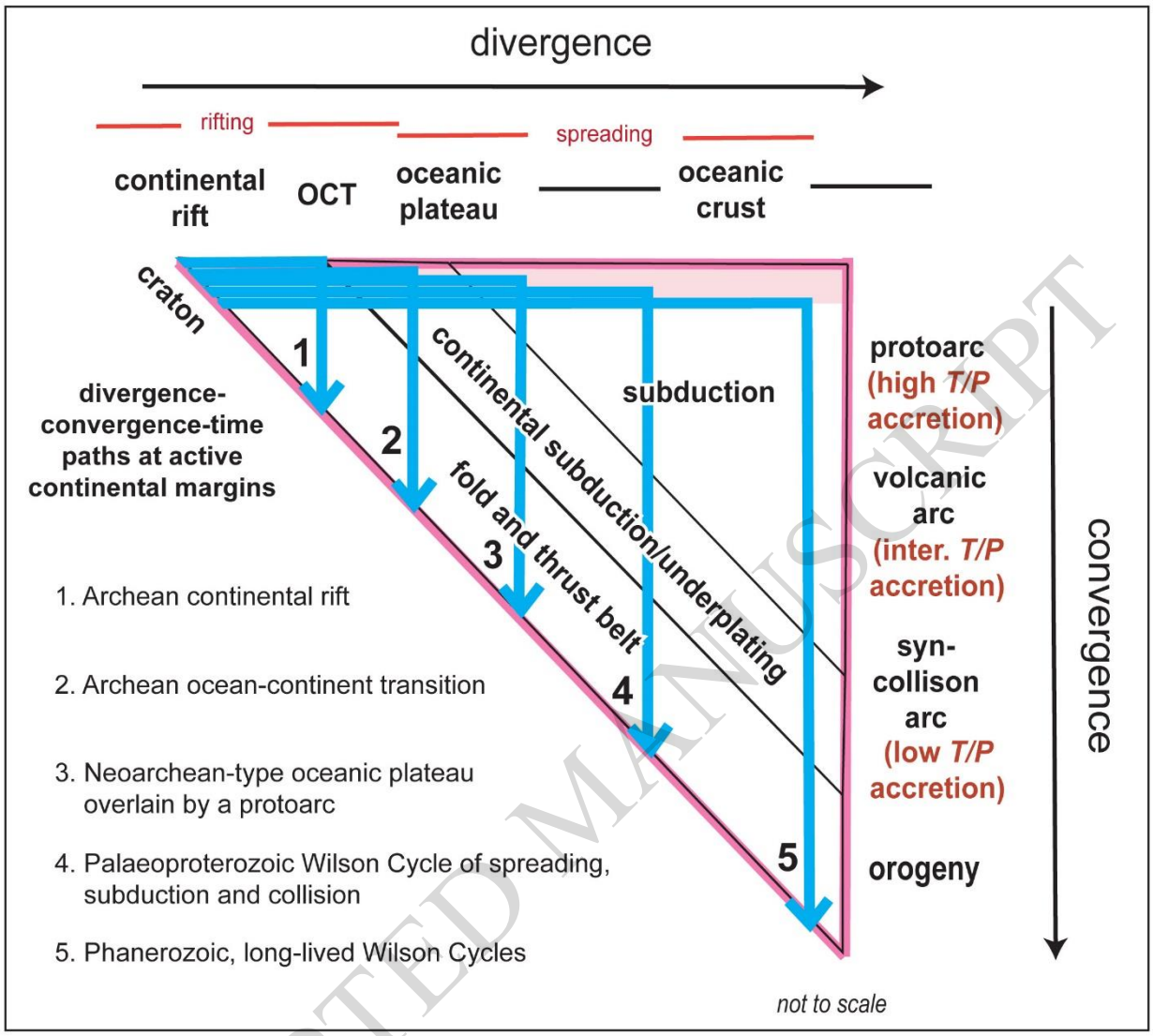

Figure 12

Table 1: Detail on decision points (DP) for identification of plate tectonic signatures as represented in the flow chart in Fig. 1
DP1a. Distinguishes potential subduction from potential intraplate volcanics based on high Th/Nb suites of the former v low-high Th/Nb in the latter (due to Th-enriched mantle source in the former cf. progressive and variable addition of Th due to magma-crust interaction in the latter).
DP1b. Distinguishes potential oceanic crust from potential intraplate volcanics based on low Th/Nb suites of the former v low-high Th/Nb in the latter (due to the crust-absent OcB magmas in the former cf. progressive and variable addition of Th due to magma-crust interaction in the latter).
DP2. Transfers from the potential subduction to potential intraplate route, any volcanic suites that extrapolate back to the OcB array and are thus have low Th/Nb mantle endmembers. May be achieved geochemically by, for example, Th/Nb v MgO plots (not shown here). Aided if necessary by arc v intraplate geological criteria (see the main text) as well as petrologic characteristics such as komatiites (if present) and/or high Tp in the latter.
DP3a. Transfers from the potential intraplate to potential subduction route, any low-high Th/Nb suites that are due to variable subduction input, as in many SSZ ophiolites. Achieved by identifying ophiolite oceanic crust characteristics (see the main text) and checking the geochemical nature of the high and low Th/Nb endmembers.
DP3b. Transfers from the potential intraplate to oceanic crust route, any low-high Th/Nb which represent oceanic crust modified by high-temperature metasomatism. Achieved by checking for significant small-length scale variations in Th/Nb and using careful sample section to back-extrapolate Th/Nb along alteration trends. Also need to identify ophiolite oceanic crust characteristics if possible.
DP4. Transfers from the oceanic crust to intraplate route, any low Th/Nb suites with evidence for a continental setting and therefore representing highly attenuated continental, rather than oceanic, crust. Achieved by further geochemical studies and identification of continental discriminants such as zircon xenocrysts, clastic sediments and autochthonous continental crust.
DP5. Separates the remaining suites in the potential subduction group into active subduction (mantle wedge source) or inherited subduction (SZLM source). Typically, the former has volcanic arc geological characteristics, and the latter has intraplate geological characteristics (see the main text). Isotopic systems such as Re-Os might also distinguish an older lithospheric source from a contemporaneous mantle wedge source while some geochemical features (e.g. enrichment or depletion in Ba, P, Ti) and preence of sanukitoids can indicate a SZLM source.
DP6. Separates the remaining intraplate suites into plume-crust and plume-SZLM interactions. The former can formally be characterised as having no plate tectonic connotation, the latter providing evidence for inherited subduction that requires transfer to the inherited subduction route. Best achieved elementally or isotopically by plotting on projections that fully distinguish whether the high Th/Nb endmember trends has crustal or subduction characteristics.
DP7(a-b). Distinguishes true subduction-based plate tectonic settings from non-uniformitarian settings (e.g. thickened crust delamination; primitive mantle sources) with no plate tectonic connotations. This is a complicated process, not always achievable and discussed in the main text. Ideally, geological reconstructions are needed to pinpoint the precise context of the high Th/Nb component and elemental and isotopic studies are needed to distinguish between subduction and the potential non-uniformitarian options (such as lower crust cumulates).